12-15-2014

Functionalized Graphitic Nanoreinforcement for Cement Composites

Nima Zohhadi
University of South Carolina - Columbia

FUNCTIONALIZED GRAPHITIC NANOREINFORCEMENT FOR CEMENT COMPOSITES

by

Nima Zohhadi

Bachelor of Science
University of Tehran, 2010

Master of Science
University of South Carolina, 2014

Submitted in Partial Fulfillment of the Requirements

For the Degree of Doctor of Philosophy in

Civil Engineering

College of Engineering and Computing

University of South Carolina

2014

Accepted by:

Fabio Matta, Major Professor

Joseph Flora, Committee member

Navid B. Saleh, Committee member

Paul Ziehl, Committee member

Lacy Ford, Vice Provost and Dean of Graduate Studies

DEDICATION

To my parents, for their endless love, support, and encouragement, to Samaneh for her invaluable friendship, and to my professor at University of South Carolina and all my friends

ACKNOWLEDGMENTS

I would like to express my deepest appreciation to my advisor Dr. Fabio Matta for his guidance, patience and support. Your support was essential to my success here.

I would like to thank my committee members, Dr. Paul Ziehl, Dr. Navid Saleh, and Dr. Joseph Flora for their invaluable advice and help throughout my research. My gratitude also extends to my friend and coworker Nirupam Aich. Much of my experimental work would have not been completed without your assistance.

I owe my deepest gratitude to my parents, for their endless love, support, and encouragement. No words can describe my love to you both.

I would like to thank my dearest friend Samaneh Kamali for her invaluable friendship and support in difficult times and my fellow graduate students for their friendship and assistance. I will always remember the great times we had. I would also like to thank my cousin Farzad Saneghi for all his support in difficult time.

At last, I would like to thank the members of my department, Civil and Environmental Engineering Department. The faculty, staff, and students made my stay in Columbia a great experience.

ABSTRACT

Physical and mechanical properties of graphitic nanomaterials, in particular multiwalled carbon nanotubes (MWCNTs) and graphene nano-platelets (GNPs) make them promising candidates for nanoreinforcement of cement composites. The two key challenges associated with the incorporation of MWCNTs and GNPs are to attain uniform dispersion and interfacial bonding within the composite matrix. The effects of three main-stream dispersion techniques (namely, ultrasonication, acid-etching, and surfactant-coating) on the mechanical properties and microstructure of MWCNT- and GNP-cement composites were experimentally studied. Compressive strength tests and different characterization techniques including dynamic light scattering, Raman spectroscopy, Fourier-transform infrared spectroscopy, X-ray photoelectron spectroscopy, scanning electron microscopy, and transmission electron spectroscopy were employed to evaluate the dispersion and embedment of nanoreinforcement in cement mortar and paste.

As a result of significant and consistent compressive strength enhancements, further supported with material characterization results, acid-etching and surfactant-coating were selected as suitable functionalization techniques to manufacture MWCNT- and GNP-cement composites, respectively. The validity of the selected functionalization techniques was further investigated through bending tests on single-edge notched cement paste beams. The results were studied with respect to flexural strength and stiffness. In addition, the effects of incorporating well-dispersed acid-etched MWCNTs on the

fracture behavior of cement paste were studied through bending tests on notched beam samples.

This research contributes to filling the gap in understanding whether dispersibility of MWCNTs and GNPs in aqueous solutions by means of well-known dispersion and functionalization techniques results in good dispersion and embedment (i.e., resulting in consistent and repeatable enhancement in relevant mechanical properties) in cement matrices. This gap is addressed by presenting new experimental evidence on improved mechanical properties as well as supporting evidence from material characterization tests, in particular for the case of GNP-reinforced mortar and cement paste. A novel contribution of this work is offered by the results of digital image correlation measurements aimed at visualizing full-field strain maps from the area surrounding the notch in cement paste beams. These results provide insight into the morphology and evolution of the fracture process zone in nanoreinforced cement paste vis-à-vis unreinforced counterparts, and constitute new evidence on the potential fracture toughening effect of MWCNTs.

TABLE OF CONTENTS

LIST OF TABLES

LIST OF FIGURES

CHAPTER 1

INTRODUCTION

1.1 Background

1.1.1 Fiber reinforcement for cement composite materials

Cement composites (such as concrete, mortar, and grout) are the most widely used class of materials in the world. Their popularity stems from several advantages, most notably: (1) availability of constituents and relatively low cost, (2) high compressive strength, (3) high durability, (4) ease of handling, manufacturing, and maintenance, (5) moldability, and (6) non-combustibility and ability to withstand high temperatures [Mehta 2006].

However, cement composites suffer from a number of shortcomings that limit their efficient use as construction materials. The main shortcomings are the low tensile strength, brittleness, and inevitable cracking due to mechanical and environmental loads (mainly due tensile loads, shrinkage, and freeze and thaw cycles) [Mehta 2006].

Different types of reinforcement are incorporated in cement composites to compensate for the low tensile strength and lack of ductility. Traditionally, steel reinforcing bars are embedded in concrete at the regions subjected to high tensile forces to improve the tensile strength and limit crack widths. In order to improve the load-bearing capacity, limit the deformations under working loads, and control cracking, concrete may also be placed under permanent compressive stresses by pre- or post-tensioning of the steel reinforcement [MacGregor 1997].

These reinforcing methods have long been utilized successfully. However, their efficiency in controlling local cracking (especially at the smaller scales) is limited. Uncontrolled cracks impair the strength and stiffness of cement composites, and provide fast pathways for the ingress of chlorides, thus negatively affecting durability. Well-distributed and randomly-oriented short fibers (e.g., steel and polypropylene fibers) can also be incorporated in cement composites. Such strategy is not as efficient as traditional steel reinforcement to withstand tensile stresses. However, due to their closer spacing, these fibers are more effective in controlling the cracks. Thus the primary use of fibers is to control cracking in cement matrices and provide some post-cracking ductility [Bentur 2007].

Fibers of different sizes are used to control cracks at different scales. Macrofibers, with typical length in the range of 1-10 cm and diameter from 0.1 to 1 mm, control cracks at the millimeter scale. Microfibers having typical lengths from 0.1 to 10 mm and diameters in the range of 1-100 μm are effective in controlling the microcracks [Bentur 2007].

In fiber-reinforced cement composites, fibers bridge cracks at different scales and offset their growth. The effect of fibers in controlling the propagation of cracks is the result of different mechanisms, including: crack-bridging, crack-deflection, fiber pull-out, fiber deformation and breakage, and fiber/matrix debonding. The energy dissipated through these mechanisms during crack propagation contributes to enhancing the energy absorption capacity [Banthia 1996, Zollo 1997, Bentur 2007, and Brandt 2008].

1.1.2 Graphitic nanoreinforcement

Conventional macro- and microfibers are most effective in controlling crack propagation from the millimeter to the micrometer scale. Although microfibers delay the development of microcracks, they hardly contribute to delaying their initiation. Recent advances in the processing and characterization of graphitic nano-sized particles have opened a new field of research on nano-scale reinforcement of cement composites. The successful incorporation of graphitic nanoreinforcement may contribute to mechanical performance by enhancing strength, stiffness and damage-tolerance characteristics at the nano- and micro-scale. Well-dispersed and embedded nanoreinforcements are envisioned to delay the growth of cracks and their coalescence into microcracks. Moreover, due to their small size (diameters <100 nm), nanoreinforcements can contribute to reducing porosity, resulting in a denser microstructure, and thus improving the characteristics of the paste/aggregate interface [Makar 2004, Raki 2010].

1.2 Multiwalled carbon nanotubes and graphene nano-platelets

1.2.1 Multiwalled carbon nanotubes

Graphitic nanomaterials are promising candidates as nanoreinforcement for cement composite materials. Carbon nanotubes (CNTs) can be conceptualized by rolling up a single or multiple sheets of graphene into seamless cylinder(s). Graphene is a two-dimensional sheet of carbon atoms that are bonded with strong covalent bonds in a hexagonal pattern. CNTs are categorized as singlewalled carbon nanotubes (SWCNTs) and multiwalled carbon nanotubes (MWCNTs). SWCNTs are formed by wrapping a single sheet of graphene into a cylinder with an outside diameter smaller than 2 nm and

length in the range of micrometers. MWCNTs are made by wrapping multiple sheets of graphene into concentric tubes, with an outside diameter ranging from 2 to 100 nm, and length in the range of micrometers (typically between 1 and 50 μm) [Hilding 2003]. The atomic structure of graphene, SWCNTs, and MWCNTs is illustrated in Figure 1.1. MWCNTs possess unique physical and mechanical properties such as high Young's modulus (~1 TPa), high tensile strength (65-93 GPa with corresponding tensile strains on the order of 10-20%), high aspect rations (100-2,500,000), high thermal conductivity (two times that of diamond) and electrical conductivity (1,000 times that of copper) [Makar 2004].

Wide application of construction materials is mostly governed by their price. The price of MWCNTs is currently very high (for example, the unit price for the MWCNTs used in this study was 12.5 USD per gram). Advances in the process of MWCNTs is expected to reduce the high cost of MWCNTs over the next few years, but a drastic price reduction such that they are used in routine construction is highly unlikely. Therefore, the most probable applications for MWCNT-cement composites are in high value projects where controlling crack propagation at nanoscale, or additional functionalities such as high thermal or electrical conductivity provide additional benefits.

1.2.2 GNPs

Graphene is a one atom-thick 2D sheet structure consisting of carbon atoms that are densely packed in a regular sp^2-bonded atomic-scale hexagonal pattern. GNPs exhibit unique mechanical properties such as high Young's modulus (~1 TPa), high tensile

strength (130 GPa), light weight (0.77 mg/m^2, about 0.001% of the weight of 1 m^2 of paper), high thermal conductivity (~5000 W.m^{-1}•K^{-1}, about five times higher than copper) and high electrical conductivity (electron mobility of up to 200,000 cm^2.V^{-1}.s^{-1}) [Lee 2008]. In addition, graphene in the form of nano-platelets (GNPs) possesses a high ratio of exposed (chemically active) surface area to weight (see Table 8.1), thus facilitating interfacial bonding mechanism with cement paste.

1.3 State-of-the-art

1.3.1 Dispersion and bonding

The main challenge in the use of MWCNTs and GNPs as nanoreinforcement for cement composites is to achieve a uniform dispersion throughout the matrix [Makar 2004, Stankovich 2006]. Dispersion can be defined as: (1) separating individual MWCNTs (or graphene sheets) from bundles (or GNP stacks) and/or entangled aggregates, and (2) stabilizing the separated MWCNTs (or graphene sheets) to attain a homogeneous distribution in the composite matrix [Vaisaman 2006]. Due to their high specific surface area and strong van der Waals attractive forces, graphitic nanoparticles exhibit a strong self-agglomeration tendency, which makes their dispersion in cement composites a major challenge [Thostenson 2001, Li 2008, and Kuilla 2010].

Another important challenge in the use of GNPs and MWCNTs is to enable bonding with cement hydrates [Thostenson 2001]. The main bonding mechanism is through interfacial chemical interactions. Pristine GNPs and MWCNTs show poor chemical affinity with cement hydration products [Nochaiya 2008], and surface

functionalization techniques are typically utilized to enhance the interfacial bonding [Stankovich 2006, Parveen 2013].

Several methods have been proposed over the past two decades to facilitate the dispersion of graphitic nanomaterials in different media [Saleh 2010, Zaib 2012] and composite matrices [Parveen 2013]. Several methods, especially those used for production of polymer-matrix composite materials, were specifically designed and developed for non-aqueous media and are not compatible with cement hydration chemistry [Makar 2004]. Mechanical mixing methods such as co-grinding have been used [Raki 2010] in metallic or ceramic matrices, but due to the softness of some cement composite constituents (e.g., gypsum), grinding is not suitable for cement composites. Instead, research has focused on dispersion approaches that are compatible with cement hydration chemistry, i.e., introducing nanoparticles into cement mixtures in dispersed phases, e.g., in the form of an aqueous suspension [Makar 2004]. However, in addition to strong van der Waals interactions, MWCNTs and GNPs are highly hydrophobic, which further complicates their homogeneous dispersion in water [Hilding 2003].

1.3.2 MWCNT-cement composites

In this section, the main-stream dispersion techniques used in the production of MWCNT-cement composites, namely, ultrasonication, acid-etching, and surfactant-coating, are introduced and their influence on the mechanical properties and microstructure of MWCNT-cement composites are discussed.

1.3.2.1 Ultrasonication

In this technique, large amounts of sonic energy are released in an ultrasonication bath or through an ultrasonication probe (known as sonicator), providing high local shear forces to the bundles of MWCNTs and resulting in their separation [Wang 2003]. Different factors determine the effectiveness of ultrasonication. These factors can be listed as: type of sonicator used (ultrasonication bath or probe), duration, energy, temperature, and amount and properties of the MWCNTs to be dispersed. A standard sonication procedure has not been established yet; therefore, various sonication procedures have been used [Manzur 2010].

Longer sonication durations are required using an ultrasonication bath (typically 1-4 hours) to achieve a similar level of dispersion obtained by using an ultrasonication probe for shorter durations (typically less than 30 minutes). Excessive sonication may result in breakage of MWCNTs reducing their aspect ratio, and/or excessive damage to their atomic structure [Sobolkina 2012]. Surface functionalization of MWCNTs can reduce the sonication time required to obtain a suitable dispersion level. For example, according to Sobolkina et al. [2012], sonication times less than 30 minutes using a sonication probe were insufficient to produce homogenous aqueous dispersion of sodium dodecyl sulfate (SDS)- and polyoxyethylene(23) Brij35-coated MWCNTs, while Cwirzen et al. [2009] reported that a 2.5-minute sonication in presence of polyacrylic polymer acid (PAAP) was adequate to attain a homogenous MWCNT aqueous dispersion.

1.3.2.2 Pristine MWCNT-cement composites

Some researchers investigated the effects of incorporating pristine MWCNTs in cement composites. Typically, MWCNTs were mechanically dispersed in aqueous solutions with the aid of ultrasonication, and the aqueous dispersions were mixed with other composite constituents to produce MWCNT-cement composites. While some improvements some mechanical properties were noted [Saez de Ibarra 2006, Tyson 2011, and Collins 2012], in other instances it was reported that the addition of pristine MWCNTs impaired the mechanical performance of the cement composites [Musso 2009, Manzur 2010, Luo 2011, and Nochaiya 2011].

Manzur et al. [2010] investigated the effects of different ultrasonication procedures on the compressive strength of pristine MWCNT-mortar cubes. Three different ultrasonication procedures were used to disperse 0.3% of pristine MWCNTs: (1) continuous sonication for 5 minutes, (2) continuous sonication for 15 minutes, and (3) sequential addition of 0.1% of MWCNT loadings followed by 5-minute sonication for each addition. It was found that the sequential addition of MWCNTs and sonication for shorter durations was more effective than the continuous sonication of larger MWCNT amounts for longer durations. The effect of the water/cement (w/c) ratio on the compressive strength of MWCNT-reinforced mortar cubes was also tested. According to Manzur et al. [2010], due to the presence of strong capillary forces between the MWCNTs, MWCNTs may attract water molecules reducing the workability of the fresh mixture. It was found that at a constant MWCNT concentration, increasing the w/c ratio produced an increase in the compressive strength of MWCNT-reinforced mortar. For

example, for mortar having 0.5% of MWCNT, increasing the w/c ratio from 0.485 to 0.60 produced an increase in the average compressive strength at 7- and 28- days by 30% and 44%, respectively. For 0.8% of MWCNTs a similar increase in the w/c ratio resulted in an average of 33% and 45% increase in the 7- and 28-day compressive strength, respectively [Manzur 2010]. Typically, smaller w/c ratios (0.25-0.40) are preferred to obtain a denser microstructure with fewer amounts of voids to facilitate the bonding between MWCNTs and cement matrix [Cwirzen 2009]. Superplasticizers (SPs) may also be used to ensure workability at relatively low w/c ratios [Konsta-Gdoutos et al. 2010].

Nochaiya et al. [2008] showed that pristine MWCNTs are unlikely to chemically bond with cement hydrates. Pristine MWCNTs at 0.5% and 1% concentrations were dispersed in aqueous solutions by sonication for three minutes, and the aqueous dispersions were used to manufacture MWCNT-cement mortar samples. Thermogravimetric analysis curves of unreinforced and nanoreinforced mortar did not show formation of new peaks, or alterations in the peak intensities or the band morphologies suggesting no chemical reactions were formed between pristine MWCNTs and cement hydrates. In spite of poor dispersion of pristine MWCNTs in mortar matrix suggested by SEM analysis of fracture surfaces, addition of 0.5% pristine MWCNTs increased the average 7- and 28-day compressive and flexural strengths of mortar by 34% and 17%, and 24% and 35%, respectively.

Morsy et al. [2011] used nano-metakaolin (NMK) to dispersed pristine MWCNTs in cement mortar. Nanocomposites were produced by dry mixing of cement, sand, NMK,

and MWCNTs, followed by addition of water and hand mixing. According to Morsy et al. due to their small dimensions (200×200×20 nm) NMKs can sit in between MWCNTs and facilitate their dispersion. Replacing Portland cement with NMK at 6% increased the average compressive strength by 18%. The addition of pristine MWCNTs at 0.02% further increased the compressive strength up to 11% but addition of pristine MWCNTs at 0.05% decreased the compressive strength.

1.3.2.3 Acid-etching

Surface functionalization techniques can be divided into two main groups of physical (non-covalent treatment) and chemical (covalent treatment) techniques. In chemical functionalization techniques alterations are made to the atomic structure of MWCNTs whereas in physical technique the atomic structure of MWCNTs remains intact. Acid-etching (or oxidation) is a chemical functionalization technique which is intended to create oxygen-contained compounds on the surface of the MWCNTs. In a typical process, the surfaces of MWCNTs are etched with strong acids resulting in attachment of oxygen-contained functional compounds, mainly carboxyl (-COOH) and hydroxyl (-OH), to their surface [Nagasawa 2000]. Functional groups are water soluble and thus reduce the hydrophobicity of MWCNTs. These compounds are essentially electrically charged and facilitate MWCNTs dispersion through electrostatic repulsions [Datsyuk 2008]. The acid-etching dispersion mechanism is illustrated in Figure 1.2.

Several factors determine the effectiveness of acid-etching technique. These factors can be listed as: type, amount, and weight ratio of the acid(s); duration of

exposure; concentration of MWCNTs processed as well as their morphology; sonication method, temperature, duration and energy; and finally the sequence of the steps. As a general rule, the effectiveness of acid-etching depends on the amount of functional groups created on the surface of MWCNTs. Attachment of these groups calls for presence of "active" carbon atoms on the surface of MWCNTs which are carbon atoms with free electrons capable of forming new covalent reactions. Since the continuous atomic structure of MWCNTs is typically cut at the end caps, active atoms are more frequently found at end caps of MWCNTs. Active carbon atoms can also be found at locations where covalent bonds between adjacent carbon atoms are broken (defects). Exposure to strong acids can also result in breakage of some of C-C bonds increasing the number of active atoms providing more sites for the attachment of the functional groups.

1.3.2.4 Acid-etched MWCNT-cement composites

Etching the surface of MWCNTs with strong oxidants leads to attachment of carboxyl (-COOH) and hydroxyl (-OH) functional groups to the surface of MWCNTs. Functional groups are essentially electrically charged and counterbalance van der Walls attractive forces through electrostatic repulsions. In addition covalent reactions between acid-etched MWCNTs and cement hydrates through these functional groups enable strong bonds between MWCNTs and cement paste. Several researchers investigated the effects of incorporation of acid-etched MWCNTs on mechanical properties and microstructure of MWCNT-cement nanocomposites.

Cwirzen et al. [2009] achieved a good dispersion of MWCNTs in aqueous solutions and cement paste matrix but no improvements with respect to compressive and flexural strength were obtained. MWCNTs at 0.006-0.042% concentrations were dispersed in aqueous solutions containing polyacrylic acid polymer (PAAP) by sonication for 3 minutes. It was noted that incorporation of PAAP resulted in a homogenous MWCNT-aqueous dispersion even before the application of ultrasonication. The aqueous dispersions were stable for 2 hours followed by progressive sedimentation. SEM analysis of cement paste samples containing acid-etched MWCNTs showed a good level of MWCNT dispersion in cement paste matrix. However, frequent encounter of sites in which MWCNTs were pull-off the matrix suggested a weak interfacial bond was obtained. Addition of acid-etched MWCNTs did not improve compressive or flexural strength of the nanocomposites.

Musso et al. [2009] found that incorporation of acid-etched MWCNTs may reduce the amount of tobermorite gel, i.e. an important contributor to cement paste strength. In this study the effects of MWCNTs surface decorations on the compressive and flexural strengths of MWCNT-cement mortar were evaluated. Surface decorations are chemical compounds attached to the surface of MWCNTs during synthesis or functionalization process. Three types of MWCNTs were tested: pristine, annealed, and acid-etched MWCNTs. High temperature annealing was used to remove the lattice defects from the walls of MWCNTs and enhance their atomic structure. MWCNTs were dispersed in acetone by sonication in an ultrasonication bath for 4 hours. The acetone was then allowed to evaporate. The resulting MWCNTs (in the form of dry powder) were

mixed with cement, sand, water, SP, and viscosity enhancing agent. Addition of pristine and annealed MWCNTs at 0.5% concentration increased the average compressive and flexural strengths by 11% and 34%, and 17% and 9%, respectively. However, addition of the same acid-etched MWCNTs amount decreased the compressive and flexural strengths by 2.5 and 6 times, respectively. The thermogravimetric analysis (TGA) curves of cement paste containing acid-etched MWCNTs showed a considerable reduction of the peak intensity at 116oC associated with the tobermorite gel. According to Musso et al. [2009] entrapment of water molecules between hydrophilic acid-etched MWCNTs hindered proper formation of the tobermorite gel reducing the compressive strength of the nanocomposites. It was also shown that increasing the w/c ratio from 0.5 to 0.56 dramatically reduced the compressive strength loss (to only 3%).

As opposed to the findings of Musso et al. [2009], Luo et al. [2011] found that addition of acid-etched MWCNTs at 1% concentration increased the average flexural strength, fracture toughness, and critical CMOD of cement paste by 56%, 119%, and 55%, respectively.

Li et al. [2005] obtained significant enhancements in the compressive and flexural strengths of cement mortar by addition of acid-etched MWCNTs. MWCNTs were dispersed in 0.1 g/ml aqueous solutions of sulfuric and nitric acids (with a 3:1 volume ratio) by sonication for 3 hours in an ultrasonication bath. Aqueous solutions were then diluted to a 1:5 volume ratio and allowed to rest for 24 hours. The top part of the diluted solutions was removed and the procedure was repeated 4 times. Incorporation of 0.5%

acid-etched MWCNTs in cement mortar increased its compressive and flexural strengths by 19% and 25%, respectively. The FT-IR analysis of plain and acid-etched MWCNT-cement paste showed that: (1) The peak at 1756 cm^{-1} assigned to COOH showed a positive shift of 22 cm^{-1}, (2) the peak assigned to OH of $Ca(OH)_2$ at 3643 cm^{-1} disappeared, and (3) the morphology of the curve at 400-1200 cm^{-1} (assigned to cement hydrations products) was altered. The observed changes in the FT-IR absorbance curves suggested formation of chemical reactions between acid-etched MWCNTs and cement hydration products. Figure 1.3 illustrates the reaction scheme between acid-etched MWCNTs and cement hydrates as proposed by the authors. In the proposed scheme the Ca^{2+} ions present in C-S-H undergo covalent reactions with O- of the functional groups attached the surface of acid-etched MWCNTs. The mercury intrusion porosimetry (MIP) tests showed that addition of 0.5% acid-etched MWCNTs reduced the total porosity of cement mortar by 64% and the amount of pores with diameters less than 50 nm by 82%.

Formation of covalent reactions between acid-etched MWCNTs and cement hydrates was also suggested by the findings of Aich et al. [Aich 2012]. Aich et al developed a novel technique for studying the binding mechanisms of acid-etched MWCNTs and cement hydrates using high resolution TEM imaging. Acid-etching was performed by addition of MWCNTs to aqueous solutions containing ammonium persulfate and sulfuric acid. The aqueous suspensions were sonicated and stirred for 10 minutes and 24 hours, respectively. The acid-etched MWCNTs were washed with deionized water to raise the pH level to neutral level and stored in a dessicator cabinet. The obtained dried acid-etched MWCNT powder was introduced to water and sonicated

for 10 minutes before incorporation in cement mixture. TEM analysis of acid-etched MWCNT-cement paste samples showed the attachment of cement hydrates to the chemical active ends of MWCNTs suggesting enhanced interfacial chemical compatibility of acid-etched MWCNTs and cement hydrates.

Formation of covalent reactions between acid-etched MWCNTs and cement hydrates was recently demonstrated by Nasibulina et al. [2012]. Acid-etching was performed by mixing the MWCNTs with nitric and sulfuric acids (at a volume ratio of 1:3) at 80^{o}C for about 4 hours. Addition of $Ca(OH)_2$ to aqueous dispersion of acid-etched MWCNTs resulted in progressive sedimentation of small floccules due to covalent reactions between Ca^{2+} ions and (COO-) and (O-) functional groups attached to the surface of MWCNTs. Addition of $Ca(OH)_2$ to aqueous dispersions of SDS-coated MWCNTs did not result in sedimentation, indicating physical attraction is most likely the predominant bonding mechanism between SDS molecules and cement hydrates. Incorporation of acid-etched MWCNTs (at 0.02-0.09%) in cement paste increased the compressive strength with the highest strength improvement (+97% compared with respect to control group) obtained for 0.03% MWCNTs loading.

1.3.2.5 Surfactant-coating

Surfactant-coating is a physical (non-covalent) functionalization technique commonly used to improve the dispersibility of MWCNTs in aqueous solution. In a typical process, MWCNTs are added to surfactant aqueous solutions and sonicated to facilitate the absorption of surfactant molecules on the surface of MWCNTs. Surfactants

can be highly effective in separating individual MWCNTs from their bundles through an "unzipping mechanism", as illustrated in Figure 1.4. Steric or electrostatic repulsive forces between surfactant molecules counterbalance van der Waals attractive forces between MWCNTs facilitating a thermodynamically stable dispersion [Vaisman 2006]. Surfactant-coating dispersion mechanism is illustrated in Figure 1.5.

Different surfactants have been used to disperse MWCNTs in cement matrices [Luo 2009, Collins 2012]. The dispersive capacity of surfactants depends on their chain length and surface density [Luo 2009]. In addition, a crucial criterion in selection of surfactants for manufacture of MWCNT-cement composite is their compatibility with cement hydration [Sobolkina 2012]. The void formation due to the foaming effects of surfactants may decrease the potential of good bonding between MWCNTs and cement matrix [Luo 2011]. The surfactant amount also plays a vital role in determining the aqueous dispersion quality and the final properties of hardened cement composites. Previous studies showed that surfactants show their highest dispersive capacity at a surfactant/MWCNT weight ratio that lies between 1-10 for a wide range of surfactants [Islam 2003, Luo 2009, and Konsta-Gdoutos 2010]. The use of smaller amounts of surfactant is insufficient to coat all MWCNTs surfaces and using higher surfactant amounts may result in surfactant flocculation or micelle formation.

An extensive research on the effects of surfactant concentration and sonication time on the dispersion of MWCNTs in aqueous solutions was performed by Sobolikna et al. [2012]. The surfactants studied were anionic sodium dodecyl sulfate (SDS) and

nonionic polyoxyethylene(23) (Brij35). UV-Vis analysis showed that at small surfactant concentrations (up to approximately 6 mM for SDS and 1.5 mM for Brij35) the extension of sonication time from 30 to 120 minutes had almost no influence on the degree of dispersion but increasing the surfactant content improved the dispersion. At medium surfactant concentrations (up to 20 mM SDS and 5 mM Brij35) increase in both sonication time and surfactant content increased the dispersion degree. At higher surfactant concentrations, increasing the surfactant concentration did not improve the dispersion but the effect of increasing sonication time remained pronounced. These results show that there exists a threshold for surfactant concentration below which the surfactant amount is not enough to coat all MWCNTs surfaces thus increasing the sonication time is not beneficial. Increasing surfactant amount above this threshold will also have no further effect on the dispersion as all the MWCNTs are coated with surfactants.

1.3.2.6 Surfactant-coated MWCNT-cement composites

Surfactant-coating of MWCNTs can significantly improve their dispersion and may facilitate interfacial bonding [Luo 2009]. Previous studies showed that surfactants show their highest dispersive capacity at a surfactant/MWCNT weight ratio that lies between 1-10 for a wide range of surfactants [Islam 2003, Luo 2009, and Konsta-Gdoutos 2010]. The use of smaller amounts of surfactant is insufficient to coat all MWCNTs surfaces and using higher surfactant amounts may result in surfactant flocculation or micelle formation.

Konsta-Gdoutos et al. [2010], showed that a high dispersion level of MWCNTs coated with a polycarboxylate-based water reducing agent (Glenium 3030) can be achieved in cement paste matrix at a surfactant/MWCNT weight ratio of 4. MWCNTs were dispersed in surfactant-aqueous solutions by 20-sec sonication cycles performed at an energy rate of 1900-2100 J/min. Two types of MWCNTs with same diameters (20-40 nm) and different lengths, short MWCNTs (10-30 μm) and long MWCNTs (10-100 μm) were tested. It was also found that a higher concentration of short MWCNTs (0.08%) is needed to achieve effective reinforcement while a lower concentration of long MWCNTs (0.048%) is required to attain the same level of mechanical performance. Addition of 0.048% surfactant-coated long MWCNTs increased the average fracture load and Young's modulus of cement paste notched beams by 25%, and 45%, respectively. It was also found through nanoindentation tests that the addition of MWCNTs can increase the amount of high-stiffness C-S-H and reduce the nanoporosity in cement paste [Konsta-Gdoutos 2010].

In another study by Konsta-Gdoutos et al. [2010], addition of MWCNTs at 0.025-0.048% in cement paste dispersed following the method described previously, reduced the autogenous shrinkage of prisms by 30-40%. According to Konsta-Gdoutos et al. [2010] addition of highly-dispersed MWCNTs reduced the amount of mesopores and thus the capillary stresses, improving the early-age strain capacity of nanoreinforced prisms.

Luo et al. [2009] and Collins et al. [2012] investigated the dispersive capacity of a wide range of surfactants and their influence on the mechanical properties of MWCNT-cement nanocomposites. Luo et al. [2009] compared the effects of five different surfactants (applied separately or jointly), namely, sodium dodecyl benzene sulfonate (SDBS), sodium deoxycholate (NaDC), Triton X-100 (TX10), Arabic gum (AG), and cetyltrimethyl ammonium bromide (CTAB), on the colloidal stability of MWCNT-aqueous suspensions. MWCNTs were dispersed in aqueous solutions at surfactant/MWCNT weight ratios of 4 and 10, by 90 rounds of 90-second sonication using an ultrasonication tip operated at 40 W. The dispersive capacity of tested surfactants measured as the sedimentation time, decreased in the order of SDBS+TX10, SDBS, NaDC+TX10, NaDC, AG, TX10, and CTAB. The best dispersion was achieved using SDBS+TX10 with a sedimentation time of 80 minutes and 60 days with and without centrifugation, respectively. Cement paste nanocomposites containing NaDC-coated MWCNTs outperformed other groups with respect to compressive and flexural strengths which were higher than those of plain cement paste samples by an average of 37% and 30%, respectively. According to Luo et al. [2009], NaDC-coated MWCNTs form strong bonds with cement hydrates due to the large and rigid backbone of NaDC.

Collins et al. [2012] investigated the effects of seven different dispersants, namely, alkylbenzene sulfonic acid-based air entraining agent, styrene butadiene rubber latex, aliphatic propylene glycol ether containing ethoxylated alkyl phenol (SR), polycarboxylate, calcium naphthalene sulfonate (CNS), naphthalene sulfonic acid derivative (NSAD), and lignosulfonate on the stability of MWCNT-aqueous dispersions

and compressive strength of MWCNT-cement paste. MWCNTs were dispersed in surfactant-aqueous solutions at a surfactant/water weight ratio of 1-3% by sonication for 12 minutes in an ultrasonic bath. The aqueous dispersion prepared using air entraining agent and lignosulfonate outperformed other groups and were stable for more than 9 days. The only improvement in the average compressive strength was obtained for cement mortar containing pristine MWCNTs at 0.5% which was higher compared with control samples by 200%. SEM analysis showed poor dispersion of MWCNTs in cement matrix for all the tested dispersants.

In some cases, the use of the same surfactant for manufacture of MWCNT-cement nanocomposites has resulted in inconsistent and in some cases contradictory outcomes between different studies [Saez de Ibarra 2006, Cwirzen 2008, and Wang 2013]. For example, contradictory effects of incorporation of GA-coated MWCNTs on microstructure and mechanical properties of MWCNT-cement nanocomposites were reported by the three following studies.

Wang et al. [2013] dispersed MWCNTs in aqueous solutions containing GA (GA/MWCNT weight ratio of 6) by sonication for 30 minutes. In this study incorporation of 0.05% and 0.08% MWCNTs increased the average fracture toughness by 5% and 510%, respectively. In another study, Saez de Ibarra et al. [2006] investigated the effects of incorporation of SWCNTs and MWCNTs (at 0.05-2%) dispersed with and without the use of GA on the Young's modulus and hardness of cement paste. The details of dispersion procedure were not reported. Incorporation of pristine SWCNTs (0.1%) and

MWCNTs (0.2%) decreased the average hardness and relative content of high-density C-S-H by 80% and 58%, and 66% and 25%, respectively. On the other hand, incorporation of GA-coated SWCNTs and MWCNTs increased the hardness and Young's modulus of low- and high-density C-S-H compared with control samples. For example, addition of 0.1% GA-coated SWCNTs increased the Young's modulus of high-density C-S-H. The reported improvements in the mechanical properties of the nanocomposite tested in these studies indicate that an effective dispersion of MWCNTs was achieved with the use of GA as surfactant.

As opposed to the findings of Wang et al. [2013] and Saez de Ibarra et al. [2006], Cwirzen et al. [2008] obtained sever drops in compressive and flexural strength of cement paste with incorporating GA-coated MWCNTs. 0.023-0.14% MWCNTs were dispersed in aqueous solutions containing 2.1% (with respect to water content in weight) GA. The GA-coated MWCNT-aqueous dispersions were stable for 2 hours and their incorporation in cement paste resulted in dramatic decrease in compressive and flexural strengths.

1.3.3 GNP-cement composites

Very little work has been documented on the use of graphene as nanoreinforcement for cement composites [Lv 2013, Alkhateb 2014, Sedaghat 2014,]. Lv et al. [2013] investigated the effect of acid-functionalized GNPs on the compressive and flexural strength of mortar beams and tensile strengths of mortar dumbbell-like specimens. The GNPs were functionalized by exposure to sulfuric acid (H_2SO_4),

potassium permanganate ($KMnO_4$), sodium nitrate ($NaNO_3$), and hydrogen peroxide (H_2O_2), which increased the relative oxygen content of GNPs by 30%. Acid-functionalized GNPs were dispersed in water by ultrasonication for one hour. The tensile and flexural strength of nanocomposites increased by increasing GNP concentrations between 0.01% and 0.03% but further increase in GNPs to 0.04% and 0.05% decreased the strength. Addition of 0.03% GNPs increased the average 28-day tensile and flexural strength by 78.6% and 60.7%, respectively. The compressive strength increased with increasing the GNP concentration up to 0.05% such that addition of 0.05% GNPs increased the average 28-day compressive strength by 47.9%.

Sedaghat et al. studied the effects of pristine GNPs on electrical conductivity and thermal diffusivity characteristics of cement paste [Sedaghat 2014]. GNPs were incorporated in cement paste by simple mechanical mixing for 3 minutes. It was found that addition of 1% and 10% pristine GNPs increased the electrical conductivity of the nanocomposites by 3 and 6 orders of magnitude, respectively, changing the electrical behavior of cement paste from insulating to semiconducting. In addition, incorporation of 10% GNPs increased the average thermal diffusivity of the nanocomposites by about 75% and 60% at 25_oC and 400_oC, respectively.

Alkhateb et al. [2014] investigated the effects of pristine and acid-functionalized GNPs on the microstructure and elastic and shear modulus of cement paste. Pristine and acid-etched GNPs at 0.5% concentration were dispersed in water by three-minute ultrasonication, and the resulting suspensions were used to fabricate 2-cm GNP-cement

paste cubes. Molecular Dynamics (MD) analysis showed that the attachment of carboxyl (-COOH) and hydroxyl (-OH) groups (assuming that the functional groups cover 18.18 % of GNP surface) increase the interfacial bond strength between GNPs and C-S-H by about 10 times. Resonant Ultrasound Spectroscopy (RUS) analysis of nanocomposites showed that the addition of 0.5% pristine and acid-treated GNPs resulted in an increase in the elastic and shear modulus of cement paste on average by 6% and 21%, and 23% and 37%, respectively.

1.3.4 Importance of dispersion technique

The major influence of the dispersion technique on the properties of MWCNT-cement nanocomposites was discussed in Section 1.3.2. It was shown that the use of very similar dispersion techniques may result in inconsistent and sometimes contradictory outcomes. In the case of ultrasonication, while several researchers found it ineffective in dispersing MWCNTs [Saez de Ibarra 2006, Tyson 2011, and Collins 2012], others reported successful outcomes [Musso 2009, Manzur 2010, Luo 2011, Nochaiya 2011]. Manzur and Yazdani [2010] used ultrasonication to disperse 0.3% of MWCNTs (all MWCNT concentrations are reported as weight ratio of cement) and obtained up to a 29% increase in the compressive strength of mortar. In another study, the use of 0.5% of MWCNTs resulted in increased flexural strength of mortar on average by 35% [Nochaiya 2008]. According to Musso et al. [2009], the average modulus of rupture of cement paste was 35% higher for a 0.5%-MWCNT addition. But the opposite result was obtained by [Collins 2012], where the addition of 0.5% and 1% of MWCNT produced a decrease in the average compressive strength of cement paste by 29% and 59%, respectively. In

[Tyson 2011] 0.1% nanotubes reduced the flexural strength of cement paste by 50% but 0.2% enhanced it by 39%.

Even in case of surface functionalized MWCNTs the published findings are highly inconsistent. Li et al. [2005] reported up to 19% and 25% enhancements in the compressive and flexural strengths of mortar with the addition of acid-treated MWCNTs at 0.5%. The same concentration and functionalization approach resulted in 86% and 1.6 times decrease in the compressive strength and the modulus of rupture of cement paste [Musso 2009]. Konsta-Gdoutos et al. 2010] employed surfactant-treatment technique to disperse MWCNTs in cement paste and attained 25% and 45% increase in the fracture load and Young's modulus at 0.048%, respectively. Luo et al. [2009] compared dispersive effects of SDBS, NaDC, CTAB, TX10 and Arabic gum, and found higher compressive and flexural strength for all cases. Sobolkina et al. [2012] observed no distinct change in the compressive and tensile strengths of cement paste at 0.025% and 0.05% MWCNTs treated with SDS and Brig 35. In another study [Nasibulina 2012] the use of SDS surfactant resulted in 65% drop in the compressive strength.

1.4 Objective

The main objectives of this study are:

(1) Identify a suitable dispersion technique to manufacture MWCNT-cement paste and mortar.

(2) Identify a suitable dispersion technique to manufacture of GNP-cement paste and mortar.

(3) Study the effects of incorporating well-dispersed and well-embedded MWCNTs and GNPs on salient strength and stiffness properties of cement paste and mortar.

(4) Understand the potential of incorporating well-dispersed and well-embedded MWCNTs in enhancing the fracture toughness of cement matrices.

1.5 Methodology

The research methodology followed in this study is illustrated in the flow chart presented in Figure 1.6. In this chapter, the influence of three main-stream dispersion techniques [Saleh 2008, Saleh 2010, Zaib 2012, Khan 2013], namely, ultrasonication, acid-etching, and surfactant-coating, on the microstructure and mechanical properties of MWCNT- and GNP-reinforced cement composites was overviewed. The effective formation of functional groups on the surface of MWCNTs and GNPs under the acid-etching protocol was verified using Raman spectroscopy, FT-IR spectroscopy, and XPS analysis. Dispersion in aqueous solutions was assessed through DLS analysis, while compressive strength characterization served as an indirect measure of dispersion and chemical affinity. Dispersion and bonding states of MWCNTs and GNPs in the composite matrix were evaluated using SEM analysis of fracture surfaces of the failed samples. Based on experimental evidence obtained in compression tests and SEM analysis, acid-etching and surfactant-coating were selected as the most suitable

techniques for MWCNTs and GNPs, respectively. TEM analysis was performed to investigate the interfacial compatibility of a-MWCNTs with cement paste. The selected functionalization techniques were verified by investigating the effect of acid-etched MWCNTs and surfactant-coated GNPs on flexural strength and stiffness cement paste notched beams.

The effect of highly-dispersed and well-bonded acid-etched MWCNTs on the fracture characteristics of cement paste was studied by means of three-point bend tests on single-edge notched beams. Different fracture parameters obtained from load-CMOD data were used to describe the effects of acid-etched MWCNTs on fracture behavior of cement paste. Digital image correlation (DIC) technique was used to obtain full-field displacement data around the notch. The principal tensile strain maps extracted from DIC displacement data were used to study the effects of acid-etched MWCNTs on the characteristics of fracture process zone (FPZ) at different stages of loading.

1.6 Significance

The research presented herein contributes to filling the gap in understanding whether dispersibility of MWCNTs and GNPs in aqueous solutions by means of well-known, main-stream dispersion and functionalization techniques results in good dispersion and embedment (i.e., resulting in consistent and repeatable enhancement in relevant mechanical properties) in cement matrices. These techniques include ultrasonication, acid-etching, and surfactant-coating.

This knowledge gap is addressed through new experimental evidence on improved mechanical properties as well as supporting evidence from material characterization tests, in particular for the case of GNP-reinforced mortar and cement paste. The supporting material characterization results include those from including dynamic light scattering, Raman spectroscopy, Fourier-transform infrared spectroscopy, X-ray photoelectron spectroscopy, scanning electron microscopy, and transmission electron spectroscopy analysis. A novel contribution of this work is provided by the results of digital image correlation measurements, which succeeded in visualizing in high resolution full-field strain maps from the area surrounding the mid-span notch in cement paste beams. Specifically, these results provide insight into the morphology and evolution of the fracture process zone in nanoreinforced cement paste vis-à-vis unreinforced counterparts, and constitute new evidence on the potential fracture toughening effect of MWCNTs.

1.7 References

Aich N., Zohhadi N., Khan I.A., Matta F., Ziehl P., and Saleh N.B., Applied TEM approach for micro/nanostructural characterization of carbon nanotube reinforced cementitious composites. Journal of Research Updates in Polymer Science 2012; 1: 14-23.

Banthia N., and J. Sheng. Fracture toughness of micro-fiber reinforced cement composites. Cement and Concrete Comp 1996: 18(4): 251-269.

Bentur A., and Mindess S., Fiber reinforced cementitious comp. CRC Press, 2006.

Brandt A.M., Fiber reinforced cement-based (FRC) composites after over 40 years of development in building and civil engineering. Compos Struct 2008: 86(1): 3-9.

Collins F., Lambert J., and Duan W.H., The influences of admixtures on the dispersion, workability, and strength of carbon nanotube–OPC paste mixtures. Cement Concrete Comp 2012; 34(2): 201-207.

Cwirzen A., Habermehl-Cwirzen K., and Penttala V., Surface decoration of carbon MWCNTs and mechanical properties of cement/carbon nanotube composites. Adv Cem Res 2008; 20(2): 65-73.

Cwirzen A., Habermehl-Cwirzen K., Nasibulin A.G., Kaupinen E.I., Mudimela P.R., and Penttala V., SEM/AFM studies of cementitious binder modified by MWCNT and nano-sized Fe needles. Mater Charact 2009; 60(7): 735-740.

Datsyuk V., Kalyva M., Papagelis K., Parthenios J., Tasis D., Siokou A., Kallitsis I., and Galiotis C., Chemical oxidation of multi-walled carbon MWCNTs. Carbon 2008; 46(6): 833-840.

Hilding J., Grulke E.A., Zhang Z.G., and Lockwood F. Dispersion of carbon MWCNTs in liquids. J Disper Sci Technol 2003; 24(1): 1-41.

Ishibashi A., and Nakashima N., Individual Dissolution of Single-Walled Carbon Nanotubes in Aqueous Solutions of Steroid or Sugar Compounds and Their Raman and Near-IR Spectral Properties. Chem-Eur J 2006: 12(29): 7595-7602.

Islam M.F., Rojas E., Bergey D.M., Johnson A.T., and Yodh A.G., High weight fraction surfactant solubilization of single-wall carbon MWCNTs in water. Nano Lett 2003; 3(2): 269-273.

Khan I.A., Afrooz A.N., Flora J.R.V., Schierz P.A., Ferguson P.L., Sabo-Attwood T., and Saleh N.B., "Chirality affects aggregation kinetics of single-walled carbon nanotubes. Environ. Sci. Technol. 2013: 47(4): 1844-1852.

Konsta-Gdoutos M.S, Metaxa Z.S., and Shah S.P., Multi-scale mechanical and fracture characteristics and early-age strain capacity of high performance carbon nanotube/cement nanocomposites. Cement and Concrete Comp 2010: 32(2): 110-115.

Konsta-Gdoutos M.S., Metaxa Z.S., and Shah S.P., Highly dispersed carbon nanotube reinforced cement based materials. Cement Concrete Res 2010; 40(7): 1052-1059.

Kuilla T., Bhadra S., Yao D., Kim N.H., Bose S., and Lee J.H., Recent advances in graphene based polymer composites. Prog Polym Sci 2010: 35(11): 1350-1375.

Lee C., Wei X., Kysar J.W., and Hone J., Measurement of the elastic properties and intrinsic strength of monolayer graphene, SCIENCE 2008: 321: 385-388.

Li D., Müller M.B., Gilje S., Kaner R.B., and. Wallace G.G, Processable aqueous dispersions of graphene nanosheets, Nat. Nanotechnol. 2008: 3: 101-105.

Li G.Y., Wang P.M., and Zhao X., Mechanical behavior and microstructure of cement composites incorporating surface-treated multi-walled carbon MWCNTs. Carbon 2005; 43(6): 1239-1245.

Luo J., Duan Z., and Li H., The influence of surfactants on the processing of multi-walled carbon MWCNTs in reinforced cement matrix composites. Phys Status Solidi (a) 2009; 206(12): 2783-2790.

Luo J.L., Duan Z., Xian G., Li Q., and Zhao T., Fabrication and fracture toughness properties of carbon nanotube-reinforced cement composite. Eur Phys J Appl Phys 2011; 53: 30402.

Lv S., Ma Y., Qiu C., Sun T., Liu J., and Zhou Q., Effect of graphene oxide nanosheets of microstructure and mechanical properties of cement composites, Const. Build. Mats. 2013: 49: 121-127.

MacGregor B., Grierson J., Wight J.K., Teng S., and Irawan P.. Reinforced concrete: mechanics and design. Vol.3. Upper Saddle River, NJ: Prentice Hall, 1997.

Makar J.M., and Beaudoin J.J., Carbon MWCNTs and their application in the construction industry. Special Publication-Royal Society of Chemistry 2004; 292: 331-342.

Manzur T., and Yazdani N., Strength Enhancement of Cement Mortar with Carbon MWCNTs. Transp Res Record: Journal of the Transportation Research Board 2010; 2142(1): 102-108.

Mehta P.K., and Monteiro P.J.M., Concrete: microstructure, properties, and materials. Vol.3. New York: McGraw-Hill, 2006.

Mi Y., Zhang X., Zhou S., Cheng J., Liu F., Zhu H., Dong X., and Jiao Z., Morphological and mechanical properties of bile salt modified multi-walled carbon nanotube/poly (vinyl alcohol) nanocomposites. Composites Part A: Applied Science and manufacturing 2007: 38(9): 2041-2046.

Morsy M.S., Alsayed S.H., and Aqel M., Hybrid effect of carbon nanotube and nano-clay on physico-mechanical properties of cement mortar. Constr Build Mater 2011: 25(1): 145-149.

Musso S., Tulliani J.M., Ferro G., and Tagliaferro A., Influence of carbon MWCNTs structure on the mechanical behavior of cement composites. Compos Sci Technol 2009: 69(11): 1985-1990.

Nagasawa S., Yudasaka M., Hirahara K., Ichihashi T., and Iijima S., Effect of oxidation on single-wall carbon MWCNTs. Chem Phys Lett 2000: 328(4): 374-380.

Nasibulina L.I., Anoshkin I.V., Nasibulin A.G., Cwirzen A., Penttala V., and Kauppinen E.I., Effect of carbon nanotube aqueous dispersion quality on mechanical properties of cement composite. J Nanomater 2012: 169262.

Nochaiya T., and Chaipanich A., Behavior of multi-walled carbon MWCNTs on the porosity and microstructure of cement-based materials. Appl Surf Sc 2011: 257(6): 1941-1945.

Nochaiya T., Tolkidtikul P., Singjai P., and Chaipanich A., Microstructure and characterizations of Portland-carbon MWCNTs pastes. Adv Mat Res 2008: 55: 549-552.

Parveen S., Rana S., and Fangueiro R., A review on nanomaterial dispersion, microstructure and mechanical properties of carbon nanotube and nanofiber reinforced cementitious composites, J. Nanomater. 2013: 80.

Raki L., Beaudoin J., Alizadeh R., Makar J., and Sato T., Cement and concrete nanoscience and nanotechnology. Materials 2010: 3(2): 918-942.

Rastogi R., Kaushal R., Tripathi S.K., Sharma A.L., Kaur I., and Bharadwaj L.M., Comparative study of carbon nanotube dispersion using surfactants. J Colloid Interf Sci 2008: 328(2): 421-428.

Saez de Ibarra Y., Gaitero J.J., Erkizia E., and Campillo I., Atomic force microscopy and nanoindentation of cement pastes with nanotube dispersions, Phys Status Solidi (a): 2006: 203: 1076-1081.

Saleh N.B., Pfefferle L.D., and Elimelech M., Aggregation kinetics of multiwalled carbon nanotubes in aquatic systems: measurements and environmental implications, Environ Sci Technol 2008: 42(21): 7963-7969.

Saleh N.B., Pfefferle L.D., and Elimelech M., Influence of biomacromolecules and humic acid on the aggregation kinetics of single-walled carbon nanotubes. Environ Sci Technol 2010: 44(7), 2412-2418.

Sanchez F., and Sobolev K., Nanotechnology in concrete – A review, Constr Build Mater 2010: 24: 2060-2071.

Sedaghat A., Ram M.K., Zayed A., Kamal R., and Shanahan N., Investigation of physical properties of graphene-cement composite for structural applications, Open J Comp Mats 2014: 4:12-21.

Sobolkina A., Mechtcherine V., Khavrus V., Maier D., Mende M., Ritschel M., and Leonhardt A., Dispersion of carbon MWCNTs and its influence on the mechanical properties of the cement matrix. Cement Concrete Comp 2012: 34:1104-1113.

Stankovich S., Dikin D.A., Dommett G.H.B., Kohlhaas K.M., Zimney E.J., Stach E.A., Piner R.D., Nguyen S.T., and Ruoff R.S., Graphene-based composite materials. Nature 2006: 442(7100): 282-286.

Strano M.S., Moore V.C., Miller M.K., Allen M.J., Haroz E.H., Kittrell C., Hauge R.H., and Smalley R.E., The role of surfactant adsorption during ultrasonication in the dispersion of single-walled carbon MWCNTs. J Nanosci Nanotechno 2003: 3(1-2): 81-86.

Thostenson E.T., Ren Z., and Chou T.W., Advances in the science and technology of carbon MWCNTs and their composites: a review. Compos Sci Technol 2001: 61(13): 1899-1912.

Tyson B.M., Abu Al-Rub R.K., Yazdanbakhsh A., and Grasley Z., Carbon MWCNTs and carbon nanofibers for enhancing the mechanical properties of nanocomposite cementitious materials. J Mater Civil Eng 2011: 23(7): 1028-1035.

Vaisman L., Wagner H.D., and Marom G., The role of surfactants in dispersion of carbon MWCNTs. Adv Colloid Interfac 2006: 128: 37-46.

Wang B., Han Y., and Liu S., Effect of highly dispersed carbon MWCNTs on the flexural toughness of cement-based composites. Constr Build Mater 2013: 42: 8-12.

Wang Y., Wu J., and Wei F., A treatment method to give separated multi-walled carbon MWCNTs with high purity, high crystallization and a large aspect ratio. Carbon 2003: 41(15): 2939-2948.

Yang Y., Grulke A., Zhang G.Z., Wu G., Thermal and rheologic al properties of carbon nanotube-in-oil dispersions, J. Appl. Phys. 2006: 99(11): 114307.

Zaib Q., Khan I.A., Yoon Y., Flora J.R.V., Park Y.G., and Saleh N.B., Ultrasonication study for suspending single-walled carbon nanotubes in water, J. Nanosci Nanotechno. 2012: 12(5): 3909-3917.

Zollo R.F., Fiber-reinforced concrete: an overview after 30 years of development. Cement and Concrete Comp 1997: 19(2): 107-122

1.8 Figures

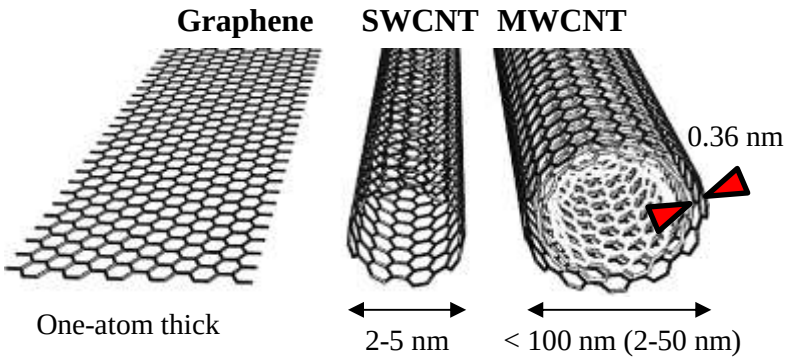

Figure 1.1 - Atomic structure of graphene, SWCNTs, and MWCNTs

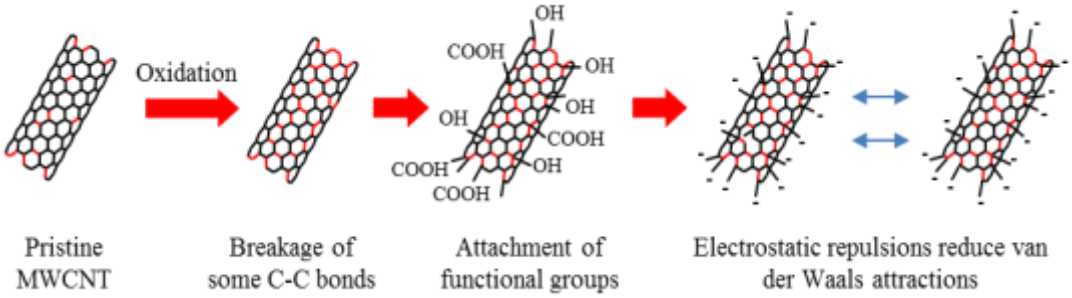

Figure 1.2 - Acid-etching dispersion mechanism

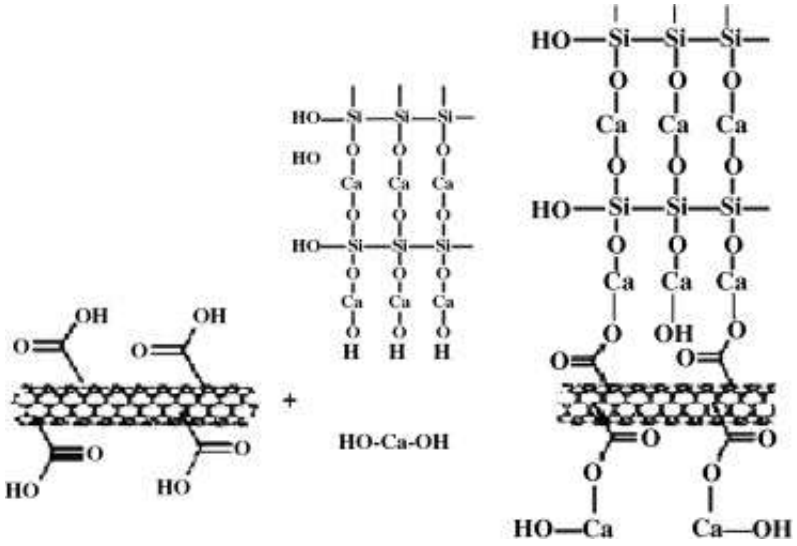

Figure 1.3 - Covalent reaction scheme between acid-etched MWCNTs and cement hydrates as proposed by Li et al. [Li 2005]

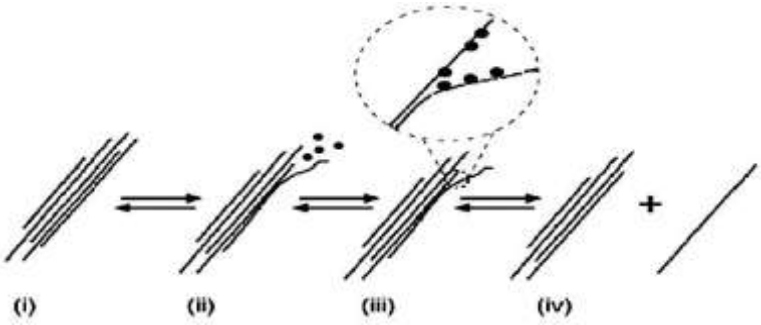

Figure 1.4 - "Unzipping" effect of surfactants [Strano 2003]

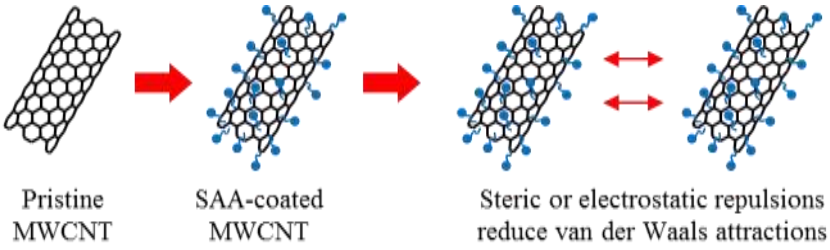

Figure 1.5 - Surfactant-coating dispersion mechanism.

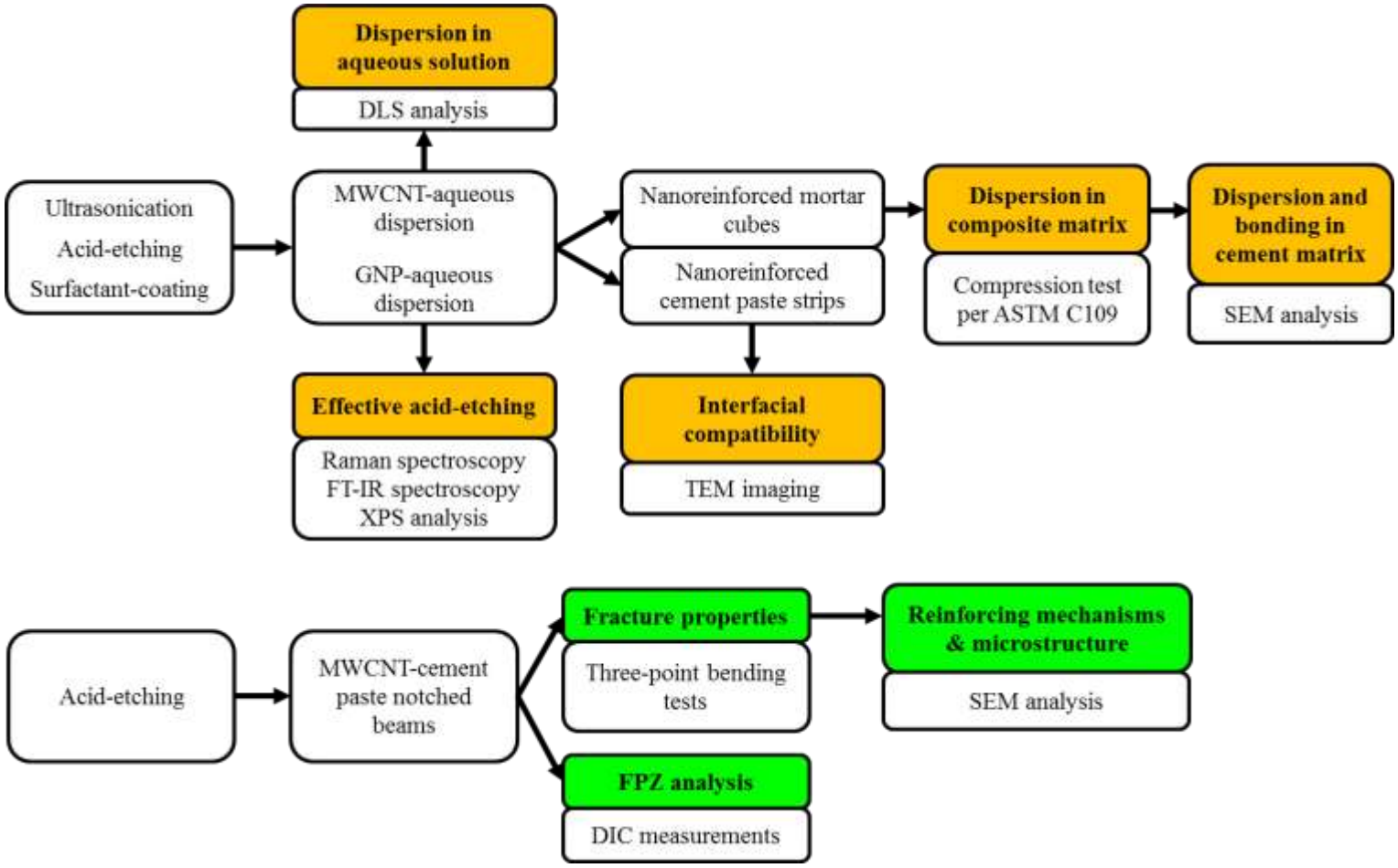

Figure 1.6 - Flowchart of the research methodology

CHAPTER 2

EFFECT OF FUNCTIONALIZATION TECHNIQUE ON MECHANICAL PROPERTIES AND MICROSTRUCTURE OF MWCNT-REINFORCED CEMENTITIOUS COMPOSITES

ABSTRACT

The two prerequisites for incorporation of MWCNTs as nanoreinforcement for cement composites are uniform dispersion and effective bonding in composite matrix. In this chapter the influence of three MWCNT dispersion techniques, namely, ultrasonication, acid-etching, and surfactant-coating on the microstructure and mechanical properties of MWCNT-reinforced cement composites was studied. Effective formation of necessary functional groups on the surface of MWCNTs under the acid-etching protocol was verified using Raman spectroscopy, FT-IR spectroscopy, and XPS analysis. Dispersion in aqueous solutions was assessed through DLS analysis, while compressive strength characterization served as an indirect measure of dispersion and chemical affinity. Dispersion and bonding states of MWCNTs in the composite matrix were evaluated using SEM analysis of fracture surfaces of the failed samples. Acid-etching was selected as the most suitable technique based on experimental evidence obtained in compression tests and SEM analysis. TEM analysis was performed to investigate the interfacial compatibility of a-MWCNTs with cement paste. Addition of 0.05% acid-etched MWCNTs (by weight of cement) increased the average compressive strength of mortar cubes by 25%. The selected acid-etching technique was verified by investigating the effect of acid-etched MWCNTs on strength, stiffness, and fracture energy of cement paste notched beams tested under three-point bending. Addition of 0.05% MWCNTs increased the average flexural strength, stiffness, and fracture energy by 26%, 75%, and 33%, respectively.

2.1 Introduction

Remarkable physical and mechanical properties of MWCNTs [Hilding 2003] have drawn much interest in their use as nanoreinforcement for cementitious composites [Makar 2004, Raki 2010, and Parveen 2013]. The key challenge is to attain a uniform distribution of the MWCNTs throughout the composite matrix [Thostenson 2001]. MWCNTs are typically introduced to cement mixtures in dispersed phase in the form of an aqueous suspension. Due to their high hydrophobicity and strong van der Waals interactions a stable and homogenous aqueous dispersion of the MWCNTs cannot be easily achieved [Hilding 2003]. Another major challenge in the use of MWCNTs as reinforcement is to obtain an effective bonding between the MWCNTs and the cement hydrates [Thostenson 2001]. Bonding becomes a challenge as: (1) due to their small size (see Table 6.1) traditional anchorage for this type of reinforcement is not feasible, and (2) MWCNTs have poor chemical affinity with cement hydration products [Nochaiya 2008].

To overcome these drawbacks, dispersion techniques [Saleh 2008, Saleh 2010, Zaib 2012] are employed to enhance the dispersibility and enable interfacial bonding. Three main-stream dispersion techniques in fabrication of MWCNT-cement composites are (1) ultrasonication, (2) acid-etching, and (3) surfactant-coating [Parveen 2013]. In (1) a large amount of energy is released during the process producing high local shearing forces within the MWCNT bundles resulting in their temporary separation [Wang 2003]. In (2) mechanical dispersion is coupled with surfactant-coating. The accumulation of amphiphilic surfactant compounds on MWCNT surfaces reduces the surface tension between water and MWCNTs and improves their solubility [Nagasawa 2000]. Surfactant

also benefits MWCNTs debundling by adsorbing on the small spaces between the MWCNTs in a MWCNT aggregate, thereby facilitating separation through an "unzipping mechanism" [Strano 2003]. Steric or electrostatic repulsive forces between surfactant molecules counterbalance the van der Waals attractive forces between MWCNTs and result in a thermodynamically stable dispersion [Vaisman 2006]. In (3) mechanical dispersion is coupled with acid-etching where the surface of MWCNTs is modified by creating carboxyl (-COOH) and hydroxyl (-OH) compounds [Nagasawa 2000]. The functional groups are water-soluble and reduce the hydrophobicity of the MWCNTs. These compounds are essentially electrically charged and once attached to the MWCNTs, facilitate their dispersion through electrostatic repulsive forces [Datsyuk 2008].

Previous research reported the use of these dispersion techniques in production of MWCNT-cement nanocomposites and documented inconsistent and in some cases contradictory findings. In case of ultrasonication while many researchers found it ineffective in dispersing MWCNTs [Saez 2006, Tyson 2011, and Collins 2012], others reported successful use of the method [Musso 2009, Manzur 2010, Luo 2011, and Nochaiya 2011]. Manzur and Yazdani [2010] used ultrasonication to disperse 0.3% pristine MWCNTs (all MWCNTs concentrations are reported herein with respect to the cement content in weight) and obtained up to 29% increase in the compressive strength of mortar cubes. In another study the incorporation of 0.5% pristine MWCNTs increased the flexural strength of mortar beams by 35% (all improvement and reduction values are herein reported as average value unless otherwise noted) [Nochaiya 2008]. According to Musso et al. [2009] the modulus of rupture of cement paste beams was 35% higher for

0.5% pristine MWCNTs addition. But the opposite result was obtained by Collins et al. [2012] where 0.5% and 1% pristine MWCNTs addition decreased the compressive strength of cement paste cylinders by 29% and 59%, respectively. Tyson et al. [2011] reported 0.1% pristine MWCNTs reduced the flexural strength of cement paste beams by 50% but 0.2% enhanced it by 39%. Even in case of surface functionalized MWCNTs the published findings are inconsistent. Li et al. [2005] reported up to 19% and 25% enhancements in the compressive and flexural strengths of mortar with the addition of acid-etched MWCNTs at 0.5%. The same concentration and similar functionalization approach resulted in 86% and 1.6 times decrease in the compressive strength (of fragments of beam specimens) and the modulus of rupture of cement paste beams [Musso 2009]. Konsta-Gdoutos et al. [2010] employed surfactant-coating technique to disperse MWCNTs in cement paste and attained 25% and 45% increase in the fracture load and Young's modulus of notched beam samples at 0.048%, respectively. Luo et al. [2009] compared dispersive effects of sodium dodecyl benzene sulfonate (SDBS), sodium deoxycholate (NaDC), cetyltrimethyl ammonium bromide (CTAB), Triton X-100 (TX10), and Arabic gum (AG), and found higher compressive (tested fragments of beam samples) and flexural strength (tested beam samples) for all cases. Sobolkina et al. [2012] observed no distinct change in the compressive and tensile strengths of cement paste dumbbell-shaped cylinders at 0.025% and 0.05% MWCNTs coated with sodium dodecyl sulfate (SDS) and polyoxyethylene(23) lauryl ether (Brig 35). In another study the use of SDS surfactant resulted in 65% drop in the compressive strength of prism specimens [Nasibulina 2012]. These finding highlight the need for a better understanding of the

effect of the dispersion technique on the properties of MWCNT-reinforced cement composites.

In this chapter the influence of the dispersion technique on salient mechanical properties and microstructure of MWCNT-reinforced cement mortar and paste was studied. Ultrasonication, acid-etching, and surfactant-coating were considered. Since the effectiveness of the acid-etching technique depends on the successful formation of carboxyl and hydroxyl functional groups on the surface of MWCNTs, material characterization methods including Raman spectroscopy, Fourier transform infrared (FTIR) spectroscopy, and X-ray photoelectron spectroscopy (XPS) were employed to verify the effective attachment of the functional groups. Transmission electron microscopy (TEM) analysis was used to study the cluster morphology of MWCNTs and to investigate the a-MWCNT-cement paste interfacial compatibility. MWCNT aqueous dispersions were produced using different dispersion techniques and characterized based on the average hydrodynamic radius (AHR) obtained from DLS analysis. The aqueous solutions were then used to fabricate MWCNT-cement mortar cubes that were tested in compression. The results of compression tests and SEM analysis on fracture surfaces were used to evaluate the effectiveness of the dispersion techniques. Acid-etching was selected as the most suitable technique for fabrication of MWCNT-cement paste notched beams, which were tested in flexure to investigate the effect of highly-dispersed and well-bonded MWCNTs on flexural strength, stiffness, and fracture energy.

2.2 Materials and methods

2.2.1 Materials

Ordinary Portland cement (OPC) type I was used to fabricate mortar and paste for the specimens used in this research. The sand for the cement mortar was standard silica sand. MWCNTs (Cheap Tubes Inc., cat# sku-030101, Brattleboro, VT) were used as-received. Specifications of MWCNTs (reported by the supplier) are listed in Table 6.1. However, pristine MWCNTs have shown to have diameters in tens of nm [Thostenson 2001, Datsyuk 2008]. Figure 2.1 presents a TEM micrograph of an entangled aggregate of MWCNTs highlighting the agglomeration of as-received MWCNTs.

2.2.2 Preparation of aqueous suspensions

MWCNTs were dispersed in water using different techniques and the resulting suspensions were then mixed with cement (and sand for preparation of mortar mixtures) according with ASTM C305 [ASTM C305 2013]. The three dispersion techniques used are described in the following three sections.

2.2.2.1 Ultrasonication

MWCNTs were sonicated in deionized (DI) water at an energy rate of 22-25 W at amplitude of 50% for 20 minutes using an ultrasonic processor (S-4000 Ultrasonic Processor, Misonix, Inc., Farmingdale, NY). MWCNTs prepared by this technique are herein referred to as u-MWCNTs.

2.2.2.2 Acid-etching

Acid-etching was performed following the procedure used by Aich et al. [2012]. MWCNTs were soaked in an aqueous solution containing ammonium persulfate, $(NH_4)_2S_2O_8$ (Sigma Aldrich, cat# 215589) and sulfuric acid, H_2SO_4 (Sigma Aldrich, cat# 339741) and the resulting suspension was stirred for 24 hours using a magnetic stirrer (VWR stirrer, Henry Troemner LLC., Thorofare, NJ). The aqueous suspensions were then sonicated for 10 minutes to mechanically separate the nanotube clusters to facilitate the penetration of oxidants along the innermost MWCNTs. The aqueous suspensions were then stirred for another 24 hours. At this point, MWCNTs have a pH of about 1 and are not suitable for mixing with cement. Therefore, the acid-etched MWCNTs were washed with DI water and filtered through a 0.45 μm PVDF membrane filter (Millipore, Billerica, MA) to raise the pH level to a value of 7.0. Each batch of 500 mg of MWCNTs was washed with 2 liters of DI water and then dried and stored as dry powder. The dried acid-etched MWCNT powder was added to water and sonicated for 20 minutes before incorporating them in the cement mixtures. Acid-etched MWCNTs are herein referred to as a-MWCNTs.

2.2.2.3 Surfactant-coating

Surfactant was added to DI water and stirred with a magnetic stirrer at 1200 rpm until a clear solution was achieved. MWCNTs were then added to the solution and the resulting suspension was sonicated for 20 minutes following the procedure described previously. The surfactant used was an anionic surfactant sodium deoxycholate, NaDC (Sigma Aldrich, cat# D6750) and was selected based on the findings of Luo et al. [2011]

who compared the colloidal stability of MWCNT-aqueous dispersions for five commonly used surfactants of different chemical nature (including anionic, cationic, and non-ionic surfactants) and their combinations. NaDC outperformed SDBS, TX10, Arabic gum, and CTAB by delaying the sedimentation time of MWCNTs in water by 42 days compared to pristine MWCNTs. In addition, samples reinforced with NaDC-coated MWCNTs showed the highest compressive and flexural strengths among the surfactants considered.

Previous studies suggest that a suitable surfactant/MWCNT weight ratio exists at which MWCNTs dispersion is maximized [Islam 2003, Konsta-Gdoutos 2010, and Nasibulina 2012]. The most suitable NaDC/MWCNT weight ratio was estimated by comparing the average hydrodynamic radius (AHR) of MWCNT-aqueous suspensions containing the same amount of MWCNTs and different amounts of surfactant. Surfactant concentrations were selected based on the work done by Islam et al. [2003] which showed the most suitable surfactant/SWCNT weight ratio for different surfactant types to be between 5 and 10. Similar findings were reported by Wang et al. [2013]. Results of DLS analysis are presented in Figure 2.2. The best dispersion, associated with least average hydrodynamic radius (AHR) and scattering intensity, was achieved at NaDC/MWCNT weight ratio of 10. Therefore, this ratio was used in fabrication of mortar cubes for compression strength characterization. Surfactant-coated MWCNTs are herein referred to as s-MWCNT.

2.2.3 Methods

2.2.3.1 DLS analysis

MWCNT-aqueous suspensions were characterized using DLS analysis. DLS analysis can be used to obtain the average size of MWCNTs in water as AHR and is widely used to evaluate the level of dispersion [Hilding 2003]. DLS measurements were conducted using an ALV/CGS-3 compact goniometer system (ALV-Laser Vertriebsgesellschaft m-bH, Langen/Hessen, Germany). The DLS system was equipped with a 22 mW HeNe Laser at 632 nm wavelength and high QE APD detector with photomultipliers of 1:25 sensitivity. A cleaned borosilicate glass vial was filled with 2 mL MWCNT-aqueous suspension and vortex mixed prior to insertion to the DLS vat chamber. Data were collected at a 90° scattering at 15-second intervals for up to 10 minutes with the laser operating at full exposure level. Each measurement was the average of 50 runs.

2.2.3.2 Raman spectroscopy

Raman spectroscopy analysis was used to verify creation of active carbon sites (defects) on the surface of a-MWCNTs. Raman spectroscopy analysis was performed using a LabRam confocal Raman spectrophotometer (JY Horiba, HORIBA Instruments Inc., CA), equipped with a liquid nitrogen-cooled CCD detector and a He/Ne laser operating at 632 nm. Presented Raman spectra are average of 5 scans with integration times of 90 seconds.

2.2.3.3 FT-IR spectroscopy analysis

FT-IR analysis was used to verify the attachment of functional groups on the surface of a-MWCNTs. For FT-IR analysis pristine and a-MWCNT were ground and mixed with FT-IR grade KBr to obtain a homogeneous powder and was subsequently pressed to make a pellet. The pellet was placed in the sample holder of a Nicolet Nexus 470 spectrometer equipped with a MCT-B detector for FT-IR analysis. A wavenumber range of 4000 to 1200 cm^{-1} was used at transmission mode. Spectra were obtained at 4 cm^{-1} resolution with 16 scans per collection.

2.2.3.4 XPS analysis

XPS analysis was used to quantify the amount of functional groups attached to the surface of a-MWCNTs. XPS measurements were taken using Kratos Axis Ultra spectrometer (Kratos Analytical Ltd., Tokyo, Japan) equipped with a hemispherical energy analyzer and monochromatic Al Kα source. The takeoff angle for the source to the sample was maintained at 90° and the applied voltage was 15 keV corresponding to 150 W (10 mA) of power or current. A base pressure of 1.2×10^{-8} Torr was maintained for the performance of the analyses [Kohn 2003]. At least three spectra were collected to obtain the representative spectra for each sample which were later analyzed with CasaXPS software to extract relevant information.

2.2.3.5 SEM analysis

SEM analysis was performed to investigate the dispersion and incorporation of MWCNTs in the cement matrix based on visual evidence. SEM micrographs were

acquired using a Zeiss Ultra Plus Field Emission Scanning Electron Microscope. All samples were oven-dried for 24 hours at 60°C and gold-sputtered prior to being tested.

2.2.3.6 TEM analysis

TEM analysis was used to characterize the cluster morphology of MWCNTs and to investigate the a-MWCNT/cement paste interfacial compatibility. Cement paste samples with w/c ratio of 0.485 containing a-MWCNTs at 0.1% concentration were prepared, grounded, and examined via TEM (Hitachi High Technologies America, Inc, Pleasanton, CA). The details of the TEM analysis methodology is described elsewhere [Aich 2012].

2.2.3.7 Compression tests

MWCNT-aqueous suspensions were mixed with cement and sand following ASTM C305 [ASTM C305] with mixing proportions of cement:sand:water of 1:2.75:0.5. Three reinforcement contents of 0.05%, 0.5%, and 1% were used and three replications were made per group. For ultrasonication technique only 0.05% was considered since at higher concentrations u-MWCNTs appeared mainly as large agglomerates in water. Specimens were moist-cured for 24 hours and then demolded and kept under saturated lime water until the age of 28 days. Compression tests were performed using a test frame (MTS 810 Material Testing System, MTS systems Inc., Eden Prairie, Minnesota) under displacement control mode with a displacement rate of 0.625 mm/minute. Compression test setup is shown in Figure 2.3

2.2.3.8 Notched beam tests

As presented in the discussion of results, based on the experimental evidence obtained through compression tests and SEM analysis, acid-etching was selected as the most suitable functionalization technique. The selected functionalization technique was further studied to understand the effect of highly-dispersed and well-bonded MWCNTs on flexural strength, stiffness, and fracture energy of MWCNT-reinforced cement paste beams. Three-point bend tests were performed on 20×20×80 mm single-edge notched beam specimens. Three specimens per group were made following the mixing protocol described previously. Specimens were moist-cured for 24 hours and then demolded and kept under saturated lime water until the age of 28 days. A water-cooled diamond saw was used to make a 6×2 μm at the mid-span section of each beam sample. A clip gage was used to measure the crack mouth opening displacement (CMOD). Three point bending tests were performed under displacement rate of 0.01 mm/minute. Figure 2.4 illustrates the test frame setup for three-point bend with beam specimen in place.

2.3 Results and discussion

First, the formation of necessary functional groups on the surface of MWCNTs is verified by experimental evidence obtained through Raman spectroscopy, FT-IR spectroscopy, and XPS analysis. The dispersion quality of MWCNTs in aqueous dispersions prepared by different dispersion techniques is then compared based on AHR values. The compression test results for different dispersion technique are discussed separately and representative SEM micrographs illustrating the dispersion and incorporation of MWCNTs in cement mortar are presented. Based on this experimental

evidence, acid-etching was selected as the most suitable functionalization technique. The results of notched beam tests are then presented and the effects of a-MWCNTs on flexural strength, stiffness, and fracture energy of cement paste are discussed.

2.3.1 Formation of functional groups on a-MWCNTs

Several factors determine the effectiveness of acid-etching. These factors can be listed as: type, amount, and weight ratio of the acid(s); duration of exposure; concentration of MWCNTs processed as well as their morphology; sonication method, temperature, duration and energy; and finally the sequence of the steps. As a general rule, the effectiveness of acid-etching depends on the amount of carboxyl and hydroxyl groups created on MWCNT surface. Attachment of these groups calls for "active" carbon atoms on surface of MWCNTs which are carbon atoms with free electrons capable of forming new reactions. Active atoms are mostly concentrated at ends of MWCNTs and at locations where covalent bonds between adjacent carbon atoms are broken (defects). Combination of ultrasonication and exposure to strong acids can also result in breakage of some of C-C bonds and increase the number of active atoms providing more sites for attachment of functional groups. Formation of "active" carbon atoms, attachment of functional groups, and amount of the attached groups were examined using Raman spectroscopy, FT-IR spectroscopy, and XPS analysis, respectively.

Raman spectra of pristine MWCNTs and a-MWCNTs are presented in Figure 2.5. The peaks near 1350 cm^{-1} (D-band) and 1580 cm^{-1} (G-band) represent C-O and C=C stretches, respectively; and the ratio between the intensities of the two provides a

quantitative value of the amount of defects or active carbons [Osswald 2007]. This ratio increased from 0.200 for pristine MWCNTs to 0.402 for a-MWCNTs. Attachment of functional groups to a-MWCNTs was verified using FT-IR technique. Figure 2.6 compares the absorbance spectra of pristine and a-MWCNT. The peak near 1580 cm^{-1} appearing in both cases represents C-C stretches [Musso 2009] and the peak near 1725 cm^{-1} is assigned to C-O stretches of functional groups [Osswald 2007]. XPS analysis of pristine and a-MWCNT showed that the relative oxygen content increased from 3.14% to 7.06% due acid-etching. It is concluded that acid-etching enabled the formation of the necessary functional groups on the surface of MWCNTs.

2.3.2 DLS characterization of MWCNT-aqueous suspensions

The effectiveness of different functionalization techniques was evaluated by DLS characterization of MWCNT-aqueous suspensions. Figure 2.7 illustrates the average MWCNTs agglomerate size measured as AHR. Before the application of ultrasonication the majority of agglomerates were larger than the largest particle detectable by the DLS machine. Thus u-MWCNT was considered as benchmark. The AHR values for u-MWCNTs, a-MWCNTs, and s-MWCNTs were 215 ± 50 nm (average ± standard deviation), 97 ± 5 nm, and 51 ± 1 nm, respectively. The highest level of dispersion was achieved by means of surfactant-coating. Comparing the standard deviations highlights the effect of surface functionalization and especially surfactant-coating in improving the homogeneity of the MWCNT-aqueous dispersions. Figure 2.8 illustrates a debundled aggregate of MWCNTs after the application of acid-etching.

2.3.3 Compressive strength and microstructure of cement mortar

2.3.3.1 Ultrasonication

The effect of dispersion technique and MWCNTs amount on the compressive strength of cement mortar was investigated via compression tests on 50-mm cubes made of plain and MWCNT-reinforced mortar. The test results are presented in Figure 2.9. The test results for all specimens of different groups are shown in Table 6-2. The incorporation of u-MWCNTs consistently resulted in a decrease in the average compressive strength by 29%. Fracture surfaces of failed specimens were also examined under SEM. A representative micrograph showing the dispersion state of u-MWCNTs in cement matrix is presented in Figure 2.10. u-MWCNTs were mostly found as entangled bundles with diameters two orders of magnitude larger than the outside diameter for an individual nanotube as reported by the supplier (<8 nm). u-MWCNT bundles exhibited larger diameters in cement matrix (in the range of 200-600 nm) even compared with their AHR of 215 ± 50 nm in aqueous suspension (Figure 2.7), suggesting a relatively low dispersion stability. The surface of u-MWCNTs was typically free of cement hydrates showing little incorporation in cement hydrates, thus indicating poor affinity. In addition, bundles of u-MWCNTs were frequently found throughout the fracture surfaces, which may suggest that u-MWCNTs facilitate the formation of defect sites. Strength reduction may also be partially attributed to a decrease in workability specific to u-MWCNTs, as reported by Manzur and Yazdani [2010].

2.3.3.2 Acid-etching

All samples reinforced with a-MWCNTs exhibited higher compressive strength than plain mortar samples. The average compressive strength for nanoreinforced mortar cubes containing 0.05%, 0.5%, and 1% a-MWCNTs was 39.31 ± 0.85, 44.42 ± 4.93, and 40.50 ± 1.79 MPa, which was higher than that of counterpart plain mortar cubes by 25%, 41%, and 28%, respectively (Figure 2.9). The standard deviation parameter is used as a measure of data variations between the samples of each group. Standard deviation values for all MWCNT-reinforced cubes were close to that of unreinforced specimens. The microstructure of mortar reinforced with 0.05%, 0.5% and 1% of a-MWCNTs concentration is illustrated in the representative SEM micrographs in Figures 2.11-2.13, respectively. For 0.05%, a-MWCNTs were mostly found as individual MWCNTs with diameters below 20 nm (Figure 2.11) indicating that an effective dispersion was achieved. The number of MWCNTs with larger diameter increased at increasing concentration of MWCNTs but the majority were still below 20-30 nm. The dispersion state for 0.5% and 1% concentrations can be seen in Figure 2.12 and 2.13, respectively. A representative area where bundles with larger diameters were found is presented in Figure 2.13. Even in this case a-MWCNTs formed a net-like arrangement showing good incorporation in the cement matrix, though it is noted that even when relatively high levels of dispersion are achieved the formation of some agglomerates is inevitable [Sanchez 2009].

a-MWCNTs showed enhanced bonding with the surrounding matrix. In fact, MWCNTs were typically embedded in or coated with cement hydrates, suggesting that

enhanced bonding with cement hydrates was enabled by acid-etching. Strong covalent bonding between (-COOH) and (-OH) and cement hydrates has been proposed by other researchers [Li 2005] and was recently experimentally shown by Nasibulina et al. [Nasibulina 2012]. Functional groups take part in reactions of ion exchange, replacing protons by metal ions like Ca^{2+}, Mg^{2+}, Al^{3+}, and Fe^{3+}, present in cement hydrates. Covalent reactions bind MWCNTs and cement paste and facilitate load transfer. A TEM micrograph of a-MWCNTs in cement paste is presented in Figure 2.14. Attachment of cement hydrates at the end caps where carboxyl (-COOH) and hydroxyl (-OH) groups are expected to be concentrated supports the hypothesis of formation of covalent reactions with cement hydrates through functional groups.

Increasing a-MWCNTs content above 0.5% resulted in smaller strength gains compared with that observed for a-MWCNTs concentration of 0.05%. Smaller gains for higher reinforcement loadings was observed also in previous studies [Yu 2007, Nochaiya 2008, Cwirzen 2008, and Cwirzen 2009] and may result from difficulty in dispersing MWCNTs at higher concentrations [Yu 2007, Cwirzen 2008, and Luo 2011].

To the best of knowledge of the writer, only one study in the open literature reported the unsuccessful incorporation of a-MWCNTs [Musso 2009], although evidence suggesting the formation of COOH and OH groups (or lack thereof) was not reported. The strength enhancements can be attributed to a combination of mechanisms. Higher strength can be contributed to porosity reduction as a result of MWCNTs incorporation. MWCNTs fill in pores and provide some mechanical continuity throughout the cement

matrix (see Figures 2.13 and 2.20). The effect of well-dispersed MWCNTs with respect to porosity reduction has been reported in the literature [Li 2005, Nochaiya 2011, Sobolkina 2012, and Wang 2013]. In particular Li et al. [2005] reported a 64% reduction in porosity with 0.5% addition of a-MWCNTs. Pores with d<50 nm and d>50 nm were reduced by 82% and 33%, respectively. Strength enhancements can also be a result of composite action [Konsta-Gdoutos 2010] and matrix modification (i.e. formation of stronger and stiffer hydration products) [Ibarra 2006, Konsta-Gdoutos 2010]. In addition a-MWCNTs may have a crack-arrest effect as a result of reduced porosity and nano-scale crack-bridging of well-bonded a-MWCNTs.

2.3.3.3 Surfactant-coating

Samples containing surfactant-coated MWCNTs exhibited lower compressive strength than plain mortar (Figure 2.9). The average compressive strength at 0.05, 0.5, and 1% s-MWCNTs was 24.90 ± 2.18 MPa, 13.34 ± 1.81 MPa, and 7.86 ± 0.72 MPa, which was lower than that of counterpart plain mortar cubes by 21%, 58%, and 75%, respectively. Increasing the s-MWCNT content resulted in higher strength drops, even well below the strength of u-MWCNT-reinforced samples. Representative fracture surfaces were examined via SEM. Typical dispersion state of s-MWCNTs in cement matrix at 0.05%, 0.5%, and 1% are shown in Figures 2.15-2.17, respectively. At 0.05% and 0.5%, s-MWCNTs were uniformly dispersed (Figure 2.15 and 2.17). Representative examples for the s-MWCNTs bundle diameters at 0.05% concentration are shown in Figure 2.15. Comparing bundle thickness values for s-MWCNTs (in the range of 30-90 nm) with u-MWCNTs (in the range of 200-600 nm) indicates that debundling was

significantly improved by surfactant-coating. However, larger aggregates more frequently found at 1% indicate that surfactant-coating was less effective for higher concentrations (Figure 2.17). s-MWCNTs showed a good affinity with cement hydrates, as suggested by Figure 2.16 which shows numerous s-MWCNTs coated by cement hydrates.

The strength loss observed for s-MWCNT-reinforced samples was further investigated by evaluating the sole effect of surfactant on the compressive strength of mortar cubes. Test results are shown in Figure 2.18. The surfactant amounts of 2.5, 25 and 50 g correspond to the absolute amount of surfactant used in preparation of 0.05, 0.5 and 1% s-MWCNT suspensions, respectively. In the absence of MWCNTs, the addition of surfactant led to strength drops similar to those exhibited by the samples containing s-MWCNTs. The observed strength losses can be attributed to the excessive amount of surfactant present in these samples. Although the surfactant/MWCNT weight ratio was constant at all s-MWCNT concentrations, but compared with s-MWCNT at 0.05%, the absolute amount of surfactant introduced to the mixture increased by 10 and 20 times for 0.5% and 1% s-MWCNT concentrations, respectively. The negative effect of surfactant is attributed in part to the reduced workability of surfactant-containing mortar. It was noted during the fabrication of cube specimens that the addition of surfactant decreased the workability of fresh mixtures such that a proper compaction was hardly achieved for 1% s-MWCNTs.

2.3.4 Effect of a-MWCNTs on flexural strength, stiffness, and fracture energy

The effect of highly-dispersed and well-bonded a-MWCNTs on the flexural strength, stiffness, and fracture energy of cement paste was evaluated by performing three-point bending tests on notched beams. Flexural strength was defined as the fracture load. Stiffness was defined as the slope of the linear portion of the load-CMOD curves. The fracture energy was calculated as the area under load-CMOD curve. Salient test results are summarized in Table 2-1. The notched beam test results for all specimens of different groups are shown in Table 6-3. The average failure load (flexural strength) for a-MWCNT concentrations of 0.0, 0.05, and 0.5%, were 110.86 ± 3.33 N, 139.37 ± 19.81 N, and 134.94 ± 14.27 N, respectively. Addition of 0.05% and 0.5% a-MWCNTs increased the failure load by 26% and 22%, respectively. Stiffness was defined as the slope of the linear portion of the load-CMOD curves. Stiffness was more affected by addition of a-MWCNTs. The stiffness for 0.0, 0.05%, and 0.5% a-MWCNTs concentrations was 5476 ± 560 N/mm, 9599 ± 1531 N/mm, and 9246 ± 1660 N/mm. Incorporation of 0.05% and 0.5% a-MWCNTs increased the stiffness by 75%, and 69%, respectively. Representative examples of load-CMOD curves for plain and nanoreinforced samples are presented in Figure 2.19. The plain samples experienced a sudden drop in load upon reaching the peak load where the reinforced samples exhibited a higher level of progressive fracture. The average fracture energy for 0.0, 0.05, and 0.5% a-MWCNTs was 1.62 ± 0.06, 2.14 ± 0.86, and 2.09 ± 0.66 N.mm respectively. Addition of 0.05% and 0.5% a-MWCNTs increased the fracture energy by 33% and 29%, respectively (Table 2-1).

The improvements in flexural strength, stiffness, fracture energy and post-peak behavior of a-MWCNT-reinforced cement paste notched beams can be partially attributed to the effect of MWCNTs incorporation in reducing the matrix porosity. As stated earlier, incorporation of well-dispersed MWCNTs can significantly reduce the total and meso-porosity of cement mortar [Li 2005] and cement paste [Konsta-Gdoutos 2010]. Porosity reduction increases the Young's modulus, flexural strength, and fracture toughness of the cement composites and improves the crack propagation resistance of the matrix [Kendal 1983]. The observed improvements can also be attributed in part to incorporation of high-stiffness and strength MWCNTs in cement matrix. Due to their high tensile strength (65-135 GPa) and Young's modulus (~ 1TPa) addition of small MWCNTs concentrations (even smaller than 0.05%) can increase the flexural strength and Young's modulus of the MWCNT-cement nanocomposite [Konsta-Gdoutos 2010]. It was also shown that incorporation of MWCNTs may increase the relative amount of high-stiffness C-S-H [Konsta-Gdoutos 2010] and promote formation of stiffer cement paste [Ibarra 2006].

In addition MWCNTs may control the propagation of cracks at nanoscale and mitigate their coalescence into large cracks. The crack-arrest effect of MWCNTs occurs through several distinct mechanisms similar to those observed for conventional fibers at larger scale [Makar 2004, Raki 2010]. Figure 2.20 illustrates potential crack-bridging mechanism of a-MWCNTs as a contributor to improvements observed in notched beam tests. Energy dissipated through crack-arrest mechanism improves the energy absorption

capacity of the nanoreinforced notched beams increasing their fracture energy. Further research is needed to verify and evaluate the contribution of these mechanisms.

2.4 Conclusions

The following conclusions are drawn from the research presented in this chapter:

(1) Ultrasonication in absence of proper surface functionalization leads to poor dispersion of MWCNTs in cement matrix. Poorly dispersed MWCNTs have poor affinity with cement paste and introduce defect sites in cement matrix reducing the compressive strength.

(2) Acid-etching created carboxyl (-COOH) and hydroxyl (-OH) groups on the surface of MWCNTs which are necessary to obtain a uniform dispersion and interfacial covalent bonds between a-MWCNTs and cement hydrates.

(3) Acid-etched MWCNTs were uniformly dispersed in mortar irrespective of their concentration and showed enhanced chemical affinity with cement hydrates. However, the number of MWCNT clusters increased at increasing MWCNT concentrations. The incorporation of acid-etched MWCNTs at 0.5% concentration consistently increased the average compressive strength of mortar by 41%. The a-MWCNT-reinforced mortar cubes had comparable standard deviation with respect to control samples.

(4) Surfactant-coating of MWCNTs leads to their uniform dispersion at a concentration of 0.05%. However, an increase in the amount of MWCNTs negatively affects dispersion.

(5) It was found that in addition to the surfactant/MWCNT weight ratio the absolute amount of surfactant introduced to the mixture of mortar affects final properties and microstructure of the nanocomposites. Incorporation of excessive NaDC reduced the workability of the mixture and resulted in significant drops in compressive strength.

(6) Incorporation of a-MWCNTs in cement paste improved the flexural strength, stiffness, fracture energy, and post-peak behavior of notched beams. The obtained improvements may be attributed to a set of distinct mechanisms including porosity reduction, composite action, crack-arrest, and matrix modification (i.e. formation of stronger and stiffer cement hydrates). The incorporation of 0.05% of highly-dispersed acid-etched MWCNTs resulted in an increase in flexural strength, stiffness, and fracture energy of cement paste by 26%, 75%, and 33%, respectively.

2.5 References

Aich N., Zohhadi N., Khan I.A., Matta F., Ziehl P., and Saleh N.B., Applied TEM approach for micro/nanostructural characterization of carbon nanotube reinforced cementitious composites. Journal of Research Updates in Polymer Science 2012; 1: 14-23.

ASTM Standard C305, 2013, "Standard practice for mechanical mixing of hydraulic cement pastes andmortars of plastic consistency" ASTM International, West Conshohocken, PA, 2013, DOI: 10.1520/C0305, www.astm.org

Chengdong Z., Luo S., and Chen W., Activity of catalase adsorbed to carbon MWCNTs: Effects of carbon nanotube surface properties. Talanta (2013).

Collins F., Lambert J., and Duan W.H., The influences of admixtures on the dispersion, workability, and strength of carbon nanotube–OPC paste mixtures. Cement Concrete Comp 2012: 34(2): 201-207.

Cwirzen A., Habermehl-Cwirzen K., and Penttala V., Surface decoration of carbon MWCNTs and mechanical properties of cement/carbon nanotube composites. Adv Cem Res 2008: 20(2): 65-73.

Cwirzen A., Habermehl-Cwirzen K., Nasibulin A.G., Kaupinen E.I., Mudimela P.R., and Penttala V., SEM/AFM studies of cementitious binder modified by MWCNT and nano-sized Fe needles. Mater Charact 2009: 60(7): 735-740.

Datsyuk V., Kalyva M., Papagelis K., Parthenios J., Tasis D., Siokou A., Kallitsis I., and Galiotis C., Chemical oxidation of multi-walled carbon MWCNTs. Carbon 2008: 46(6): 833-840.

Hilding J., Grulke E.A., Zhang Z.G., and Lockwood F., Dispersion of carbon MWCNTs in liquids. J Disper Sci Technol 2003: 24(1): 1-41.

Islam M.F., Rojas E., Bergey D.M., Johnson A.T., and Yodh A.G., High weight fraction surfactant solubilization of single-wall carbon MWCNTs in water. Nano Lett 2003: 3(2): 269-273.

Kohn T., Kane S.R., Fairbrother D.H., and Roberts A.L., Investigation of the inhibitory effect of silica on the degradation of 1, 1, 1-trichloroethane by granular iron. Environ Sci Technol 2003: 37(24): 5806-5812.

Konsta-Gdoutos M.S., Metaxa Z.S., and Shah S.P., Highly dispersed carbon nanotube reinforced cement based materials. Cement Concrete Res 2010: 40(7): 1052-1059.

Kowald T., and Trettin R., Influence of surface-modified carbon MWCNTs on ultrahigh performance concrete. In Proceedings of the International Symposium on Ultra High Performance Concrete 2004: 195-202.

Li G.Y., Wang P.M., and Zhao X., Mechanical behavior and microstructure of cement composites incorporating surface-treated multi-walled carbon MWCNTs. Carbon 2005: 43(6): 1239-1245.

Luo J., Duan Z., and Li H., The influence of surfactants on the processing of multi-walled carbon MWCNTs in reinforced cement matrix composites. Phys Status Solidi (a) 2009: 206(12): 2783-2790.

Luo J.L., Duan Z., Xian G., Li Q., and Zhao T., Fabrication and fracture toughness properties of carbon nanotube-reinforced cement composite. Eur Phys J Appl Phys 2011: 53: 30402.

Makar J.M., and Beaudoin J.J., Carbon MWCNTs and their application in the construction industry. Special Publication-Royal Society of Chemistry 2004: 292: 331-342.

Manzur T., and Yazdani N., Strength Enhancement of Cement Mortar with Carbon MWCNTs. Transp Res Record: Journal of the Transportation Research Board 2010: 2142(1): 102-108.

Musso S., Tulliani J.M., Ferro G., and Tagliaferro A., Influence of carbon MWCNTs structure on the mechanical behavior of cement composites. Compos Sci Technol 2009: 69(11): 1985-1990.

Saleh N.B., Pfefferle L.D., and Elimelech M., Influence of biomacromolecules and humic acid on the aggregation kinetics of single-walled carbon nanotubes. Environ. Sci. Technol. 2010: 44(7), 2412-2418.

Saleh N.B., Pfefferle L.D., and Elimelech M., Aggregation kinetics of multiwalled carbon nanotubes in aquatic systems: measurements and environmental implications, Environ. Sci. Technol. 2008: 42(21): 7963-7969.

Nagasawa S., Yudasaka M., Hirahara K., Ichihashi T., and Iijima S., Effect of oxidation on single-wall carbon MWCNTs. Chem Phys Lett 2000: 328(4): 374-380.

Nasibulina L.I., Anoshkin I.V., Nasibulin A.G., Cwirzen A., Penttala V., and Kauppinen EI. Effect of carbon nanotube aqueous dispersion quality on mechanical properties of cement composite. J Nanomater 2012: 169262.

Nochaiya T., and Chaipanich A., Behavior of multi-walled carbon MWCNTs on the porosity and microstructure of cement-based materials. Appl Surf Sc 2011: 257(6): 1941-1945.

Nochaiya T., Tolkidtikul P., Singjai P., and Chaipanich A., Microstructure and characterizations of Portland-carbon MWCNTs pastes. Adv Mat Res 2008: 55: 549-552.

Osswald S., Havel M., and Gogotsi Y., Monitoring oxidation of multi-walled carbon MWCNTs by Raman spectroscopy. J Raman Spectrosc 2007: 38(6): 728-736.

Parveen S., Rana S., and Fangueiro R., A review on nanomaterial dispersion, microstructure and mechanical properties of carbon nanotube and nanofiber reinforced cementitious composites. J Nanomater 2013: 710175.

Raki L, Beaudoin J, Alizadeh R, Makar J, and Sato T. Cement and concrete nanoscience and nanotechnology. Materials 2010: 3(2): 918-942.

Saez de Ibarra Y., Gaitero J.J., Erkizia E., and Campillo I., Atomic force microscopy and nanoindentation of cement pastes with nanotube dispersions. Phys Status Solidi (a) 2006: 203(6): 1076-1081.

Sanchez F., and Ince C., Microstructure and macroscopic properties of hybrid carbon nanofiber/silica fume cement composites. Compos Sci Technol 2009: 69(7): 1310-1318.

Sobolkina A., Mechtcherine V., Khavrus V., Maier D., Mende M., Ritschel M., and Leonhardt A., Dispersion of carbon MWCNTs and its influence on the mechanical properties of the cement matrix. Cement Concrete Comp 2012: 34:1104-1113.

Strano M.S., Moore V.C., Miller M.K., Allen M.J., Haroz E.H., Kittrell C., Hauge R.H., and Smalley R.E., The role of surfactant adsorption during ultrasonication in the dispersion of single-walled carbon MWCNTs. J Nanosci Nanotechno 2003: 3(1-2): 81-86.

Thostenson E.T., Ren Z., and Chou T.W., Advances in the science and technology of carbon MWCNTs and their composites: a review. Compos Sci Technol 2001: 61(13): 1899-1912.

Tyson B.M., Abu Al-Rub R.K., Yazdanbakhsh A., and Grasley Z., Carbon MWCNTs and carbon nanofibers for enhancing the mechanical prope rties of nanocomposite cementitious materials. J Mater Civil Eng 2011: 23(7): 1028-1035.

Vaisman L., Wagner H.D., and Marom G., The role of surfactants in dispersion of carbon MWCNTs. Adv Colloid Interfac 2006: 128: 37-46.

Wang B., Han Y., and Liu S., Effect of highly dispersed carbon MWCNTs on the flexural toughness of cement-based composites. Constr Build Mater 2013: 42: 8-12.

Wang Y., Wu J., and Wei F., A treatment method to give separated multi-walled carbon MWCNTs with high purity, high crystallization and a large aspect ratio. Carbon 2003: 41(15): 2939-2948.

Yu J., Grossiord N., Koning C.E., and Loos J., Controlling the dispersion of multi-wall carbon MWCNTs in aqueous surfactant solution. Carbon 2007: 45(3): 618-623.

Zaib Q., Khan I.A., Yoon Y., Flora J.R.V., Park Y.G., and Saleh N.B., Ultrasonication study for suspending single-walled carbon nanotubes in water, J. Nanosci Nanotechno 2012: 12(5): 3909-3917.

2.6 Tables

Table 2.1 - Notched beam test results for all groups

Specimen	Failure load [N]	Stiffness [N/mm]	Fracture energy [N-mm]
Control	110.86 ± 3.33	5476 ± 560	1.62 ± 0.06
a-MWCNT 0.05%	139.37 ± 19.81	9599 ± 1531	2.14 ± 0.86
a-MWCNT 0.5%	134.94 ± 14.27	9246 ± 1660	2.09 ± 0.66

2.7 Figures

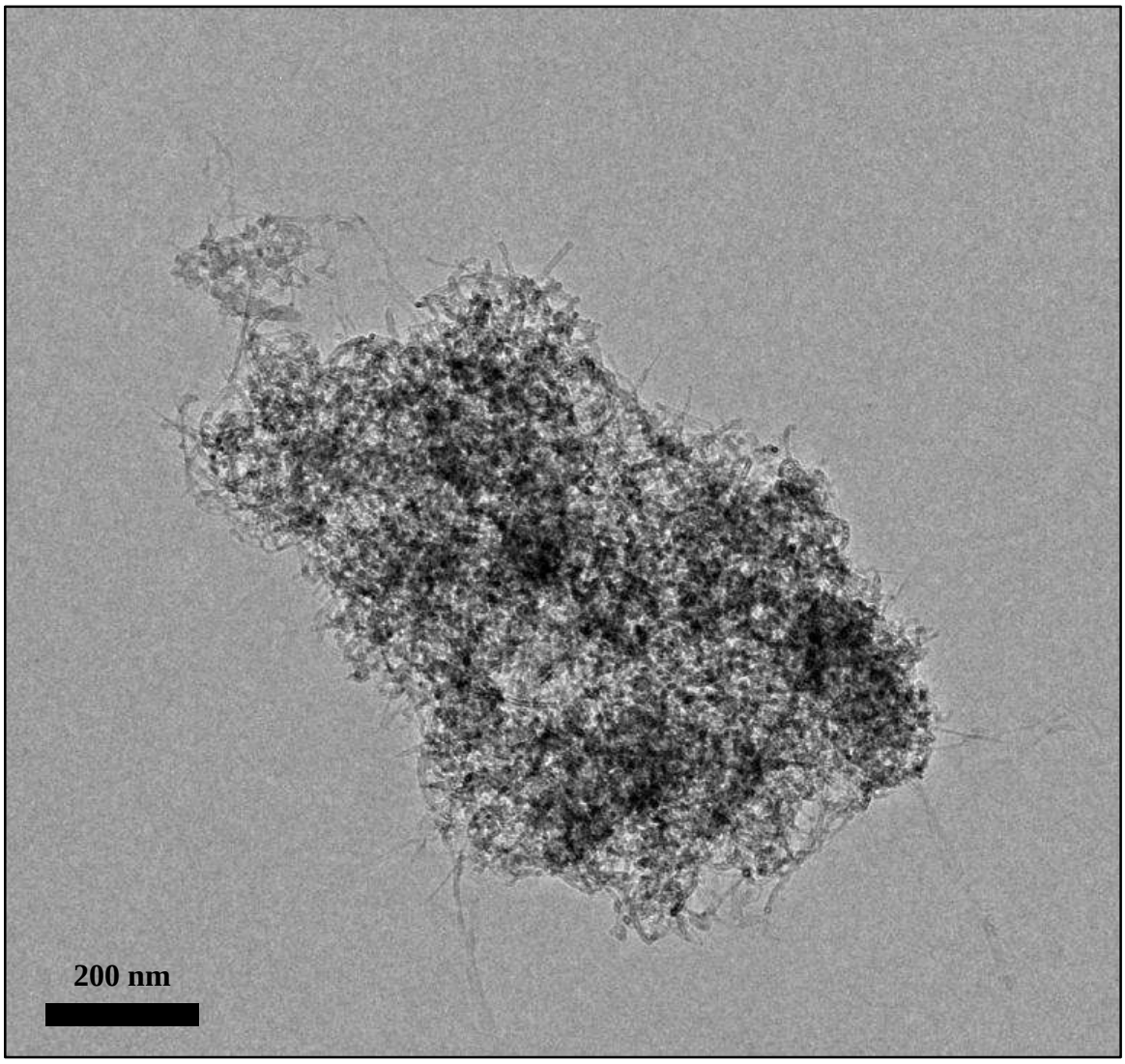

Figure 2.1 - TEM micrograph of entangled MWCNTs (as-received sample)

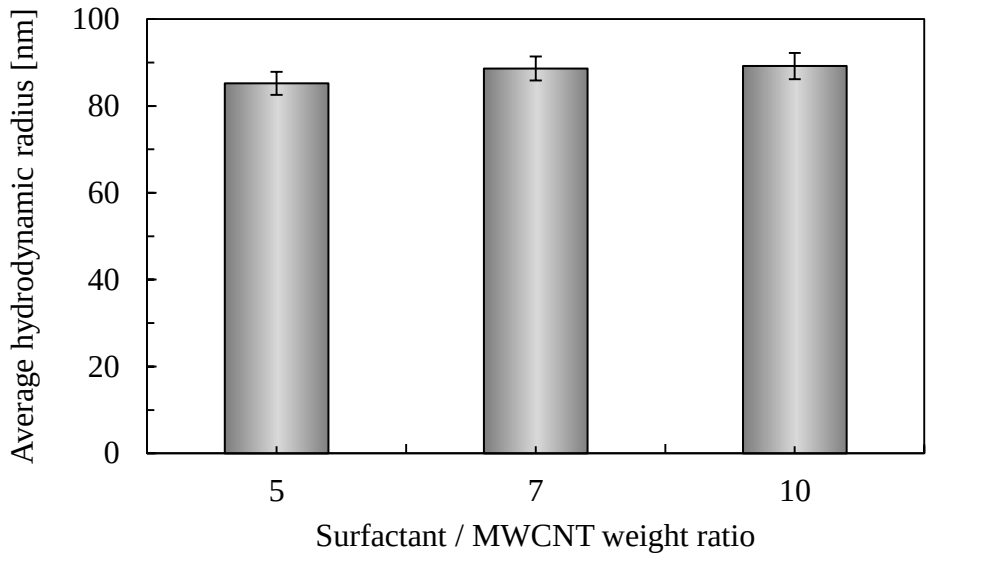

(a)

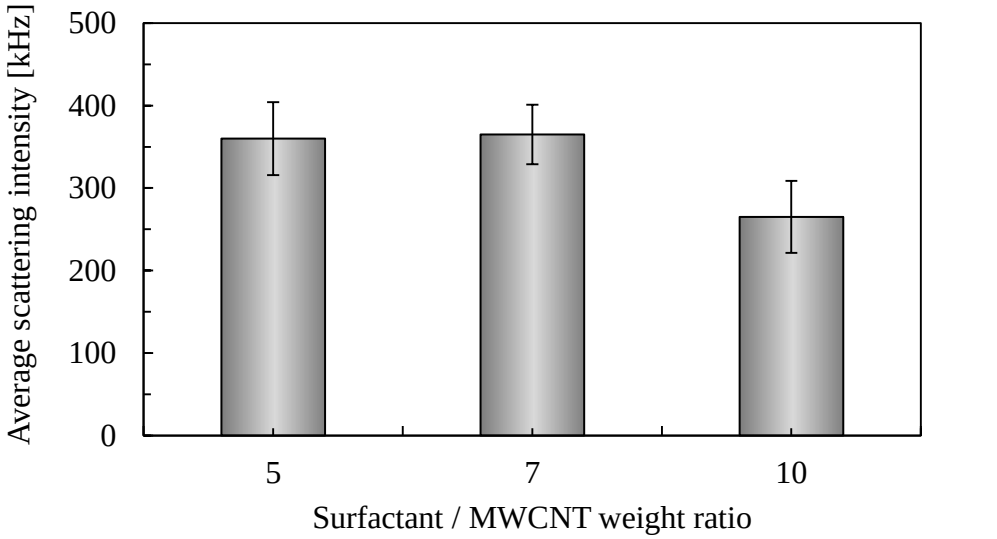

(b)

Figure 2.2 - Effect of surfactant concentration on DLS characteristics of MWCNT-aqueous suspensions, (a) average hydrodynamic radius (AHR), and (b) average scattering intensity

Figure 2.3 - Compression tests setup – Tests were performed in displacement control using a 810 MTS Material Testing System

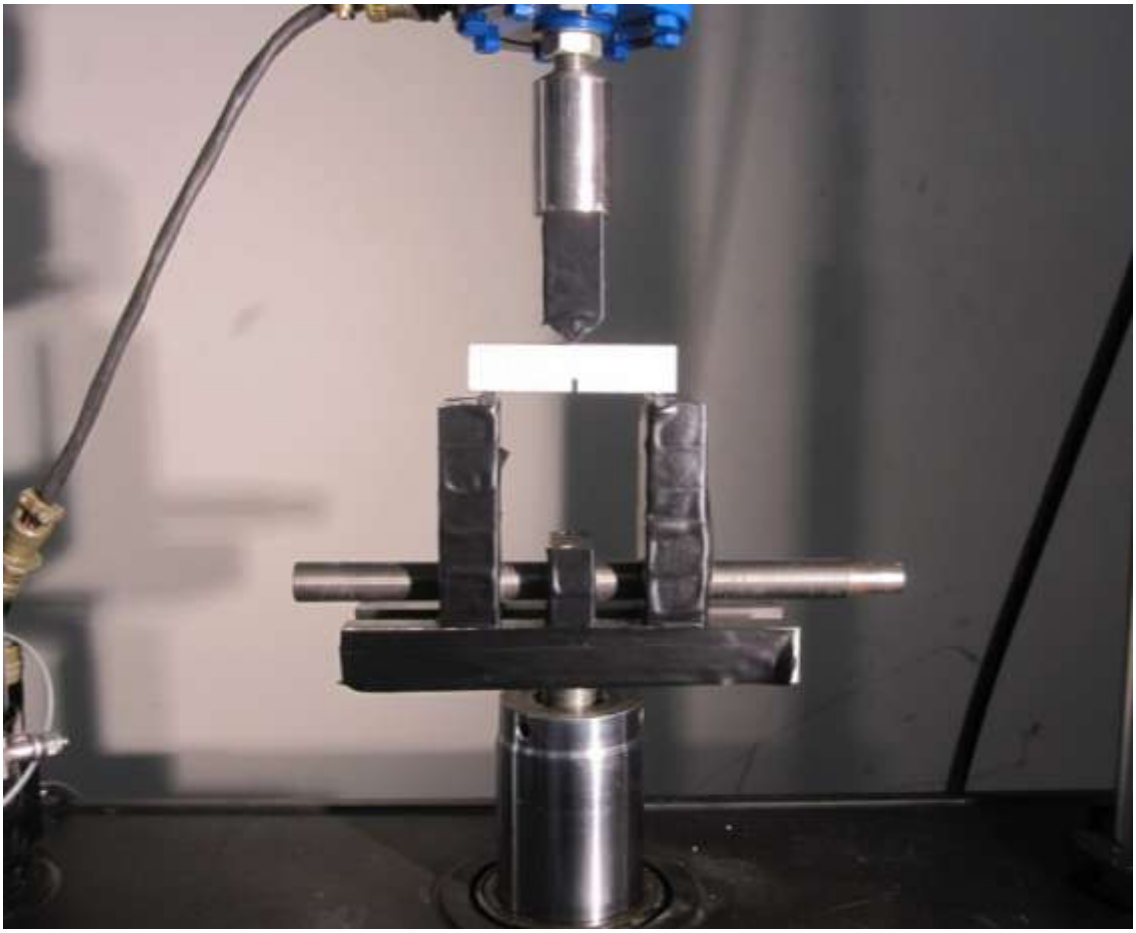

Figure 2.4 - Test frame setup for three-point bend with beam specimen in place – Tests were performed in displacement control using a MTS 810 Material Testing System

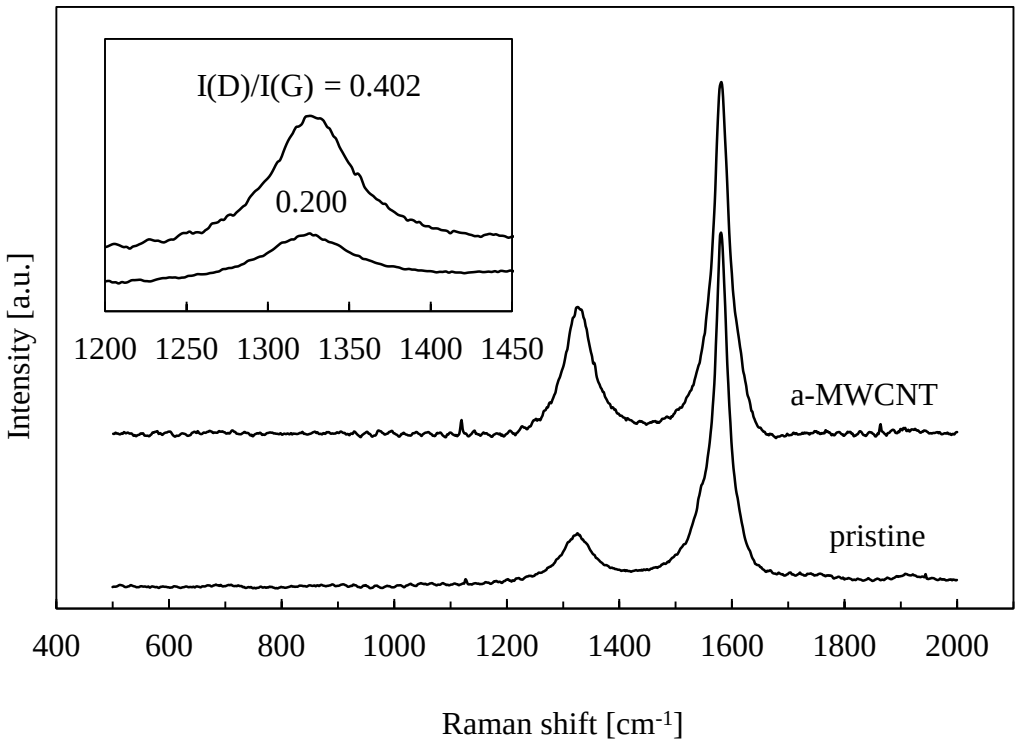

Figure 2.5 - Raman spectra of pristine and a-MWCNT

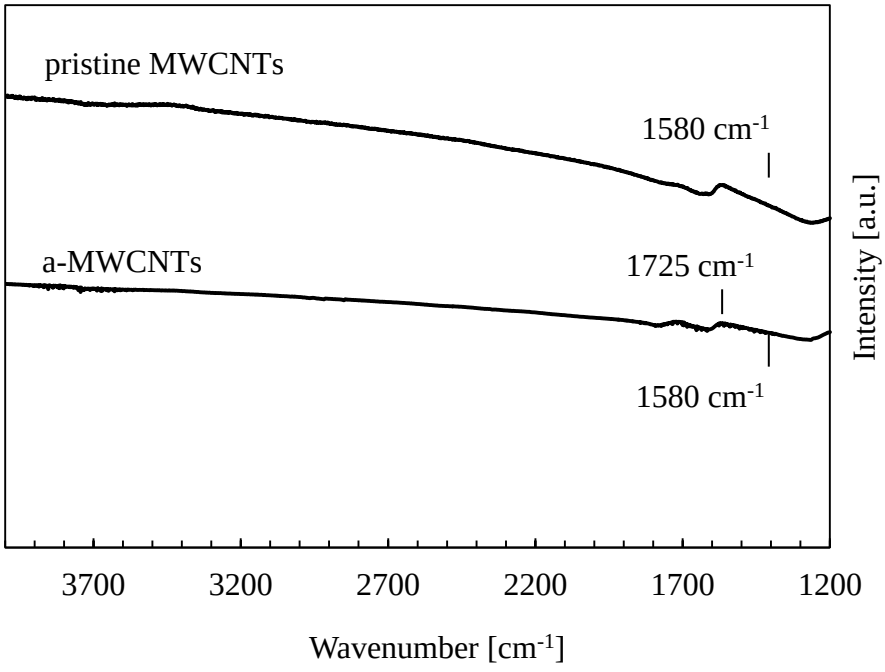

Figure 2.6 - FT-IR absorption spectra for pristine and a-MWCNT

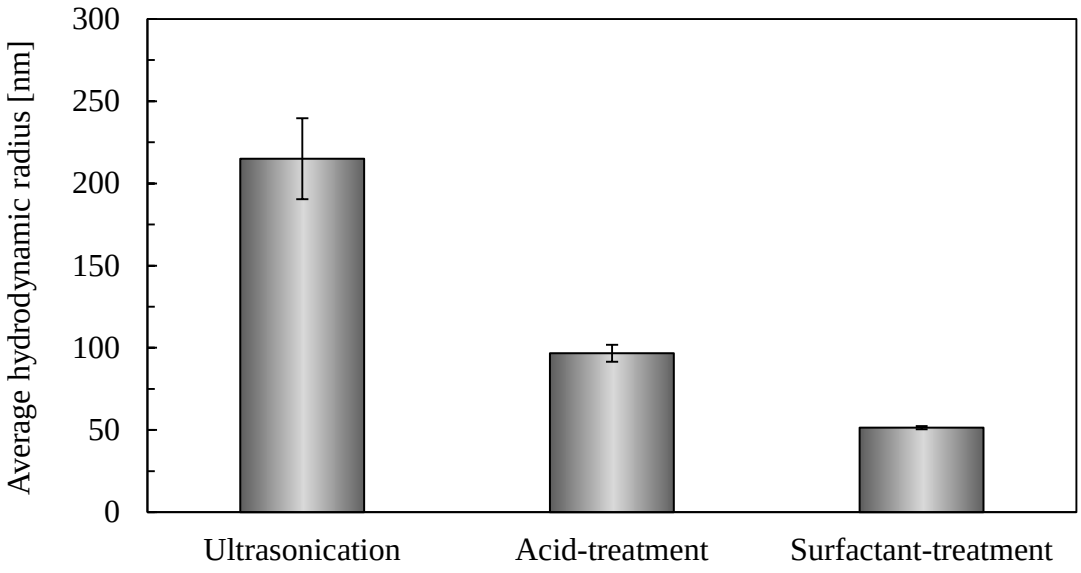

Figure 2.7 - Effect of dispersion technique on the average hydrodynamic radius of MWCNTs in aqueous suspension

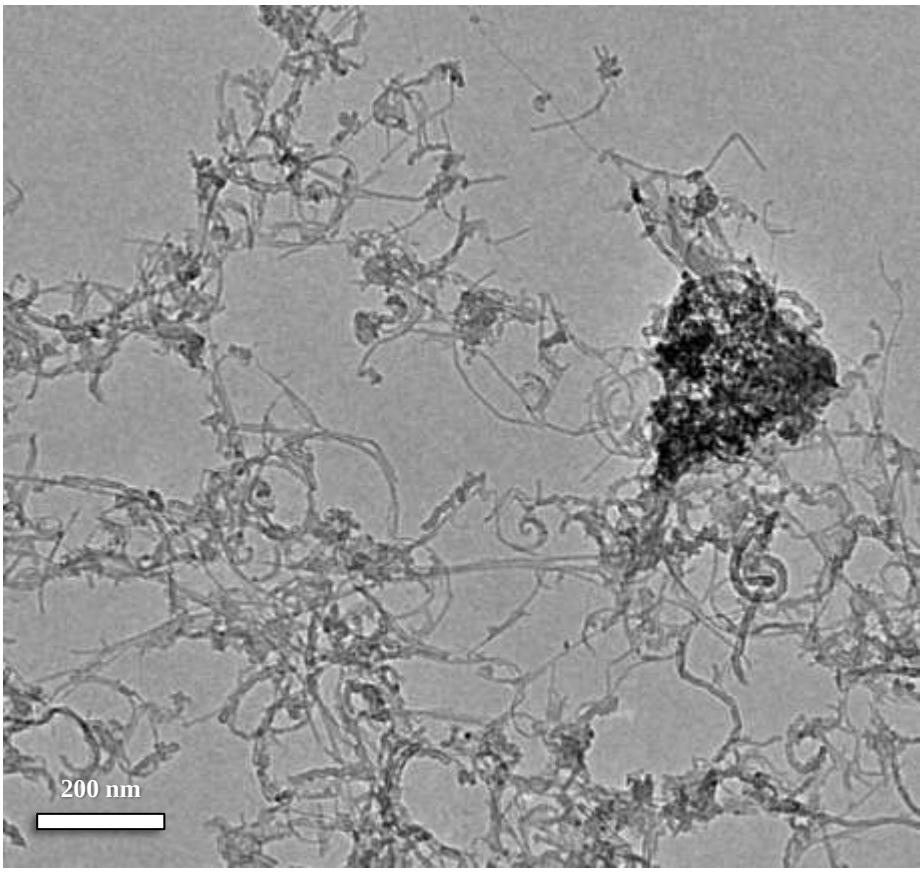

Figure 2.8 - TEM micrograph illustrating debundled a-MWCNTs

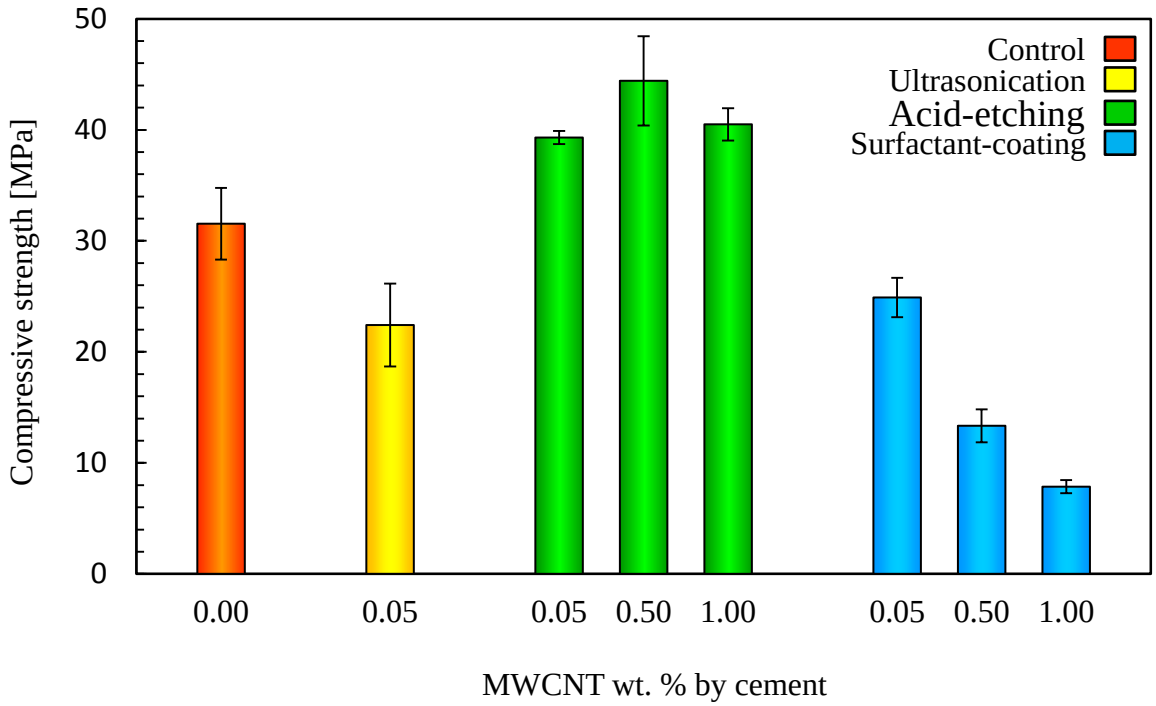

Figure 2.9 - Compression test results for plain and nanoreinforced mortar cubes

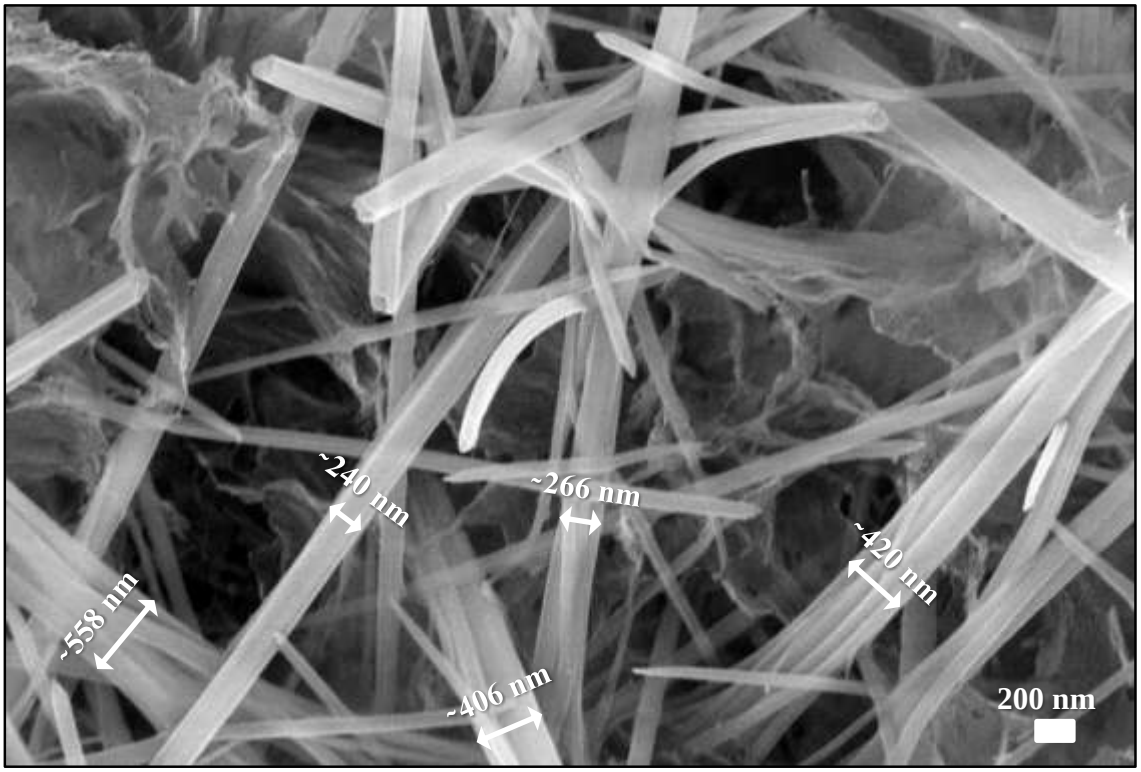

Figure 2.10 - Typical dispersion state of u-MWCNT at 0.05% in mortar matrix

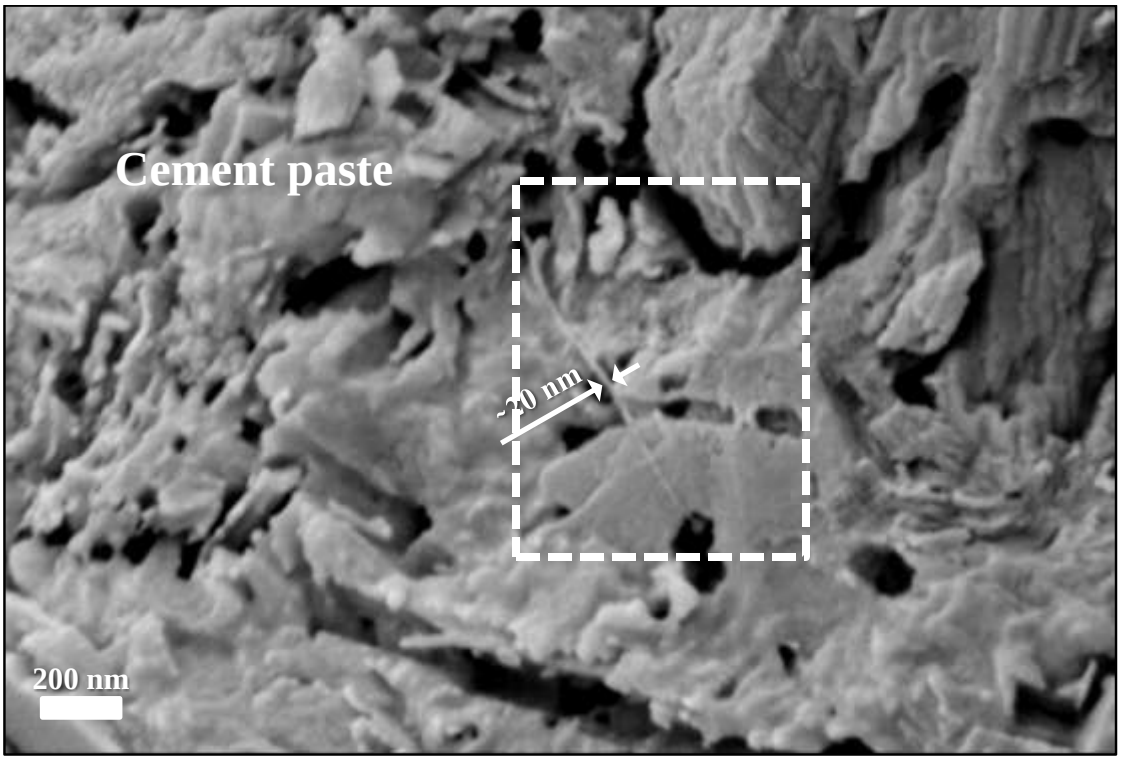

Figure 2.11 - Typical dispersion state of a-MWCNTs in mortar matrix at 0.05%

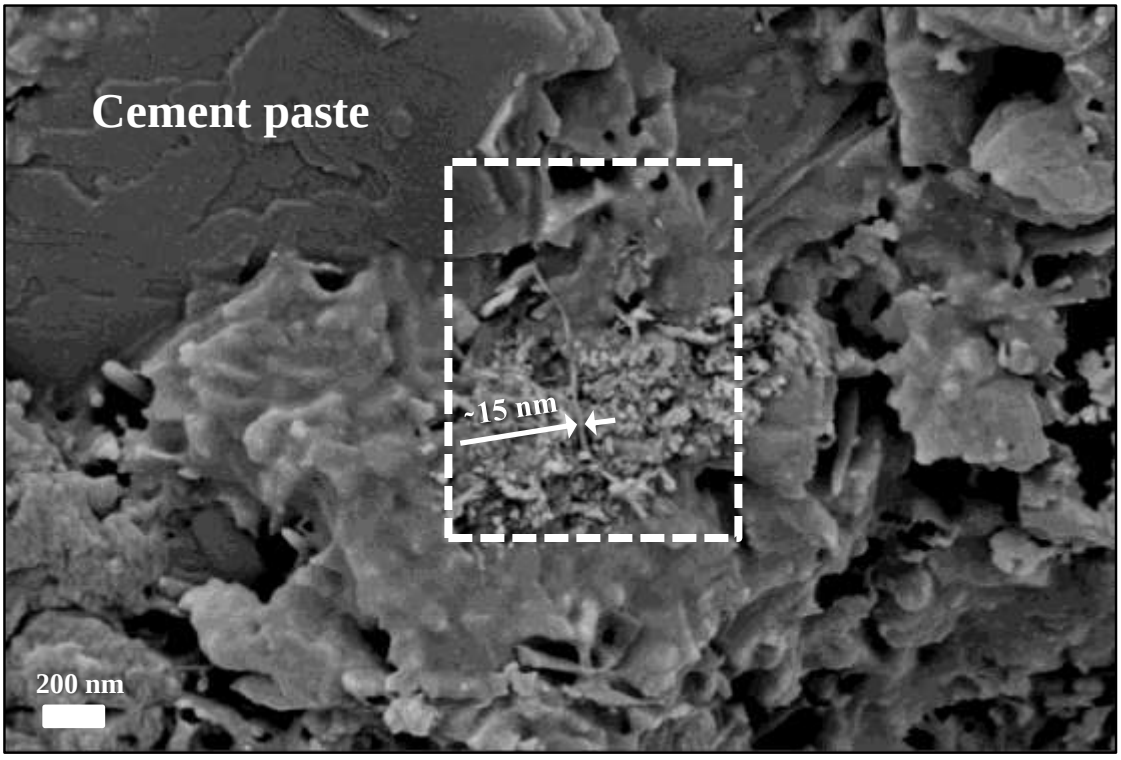

Figure 2.12 - Typical dispersion state of a-MWCNTs in mortar matrix at 0.5%

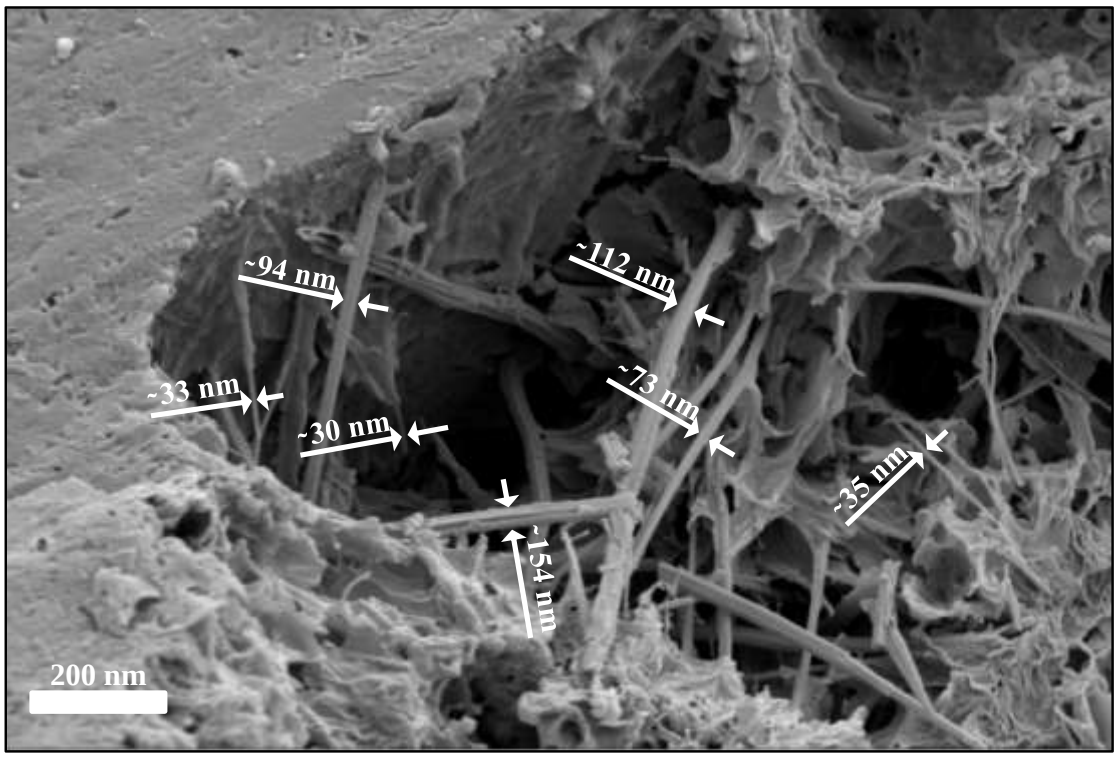

Figure 2.13 - Typical dispersion state of a-MWCNTs in mortar matrix at 1%

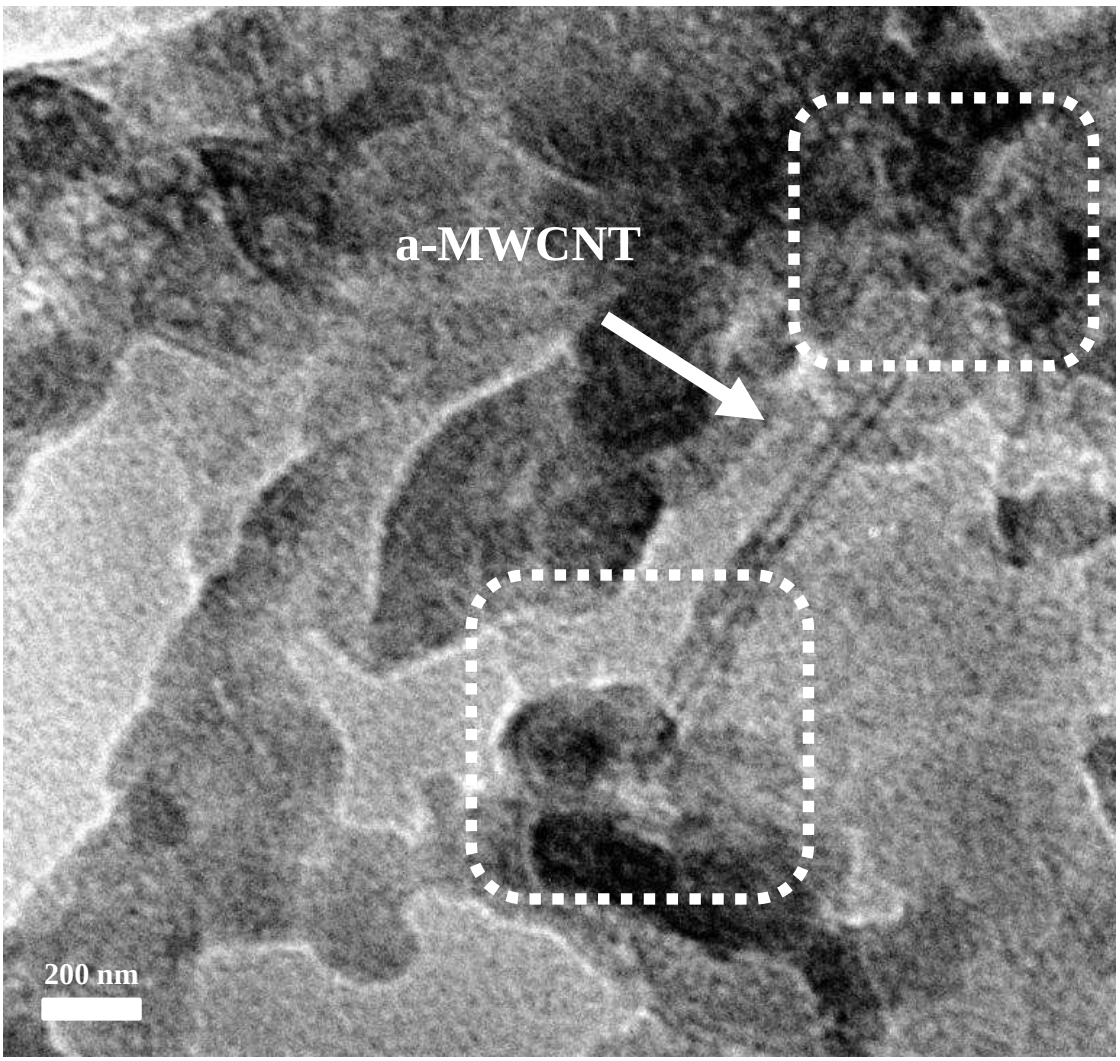

Figure 2.14 - TEM micrograph illustrating interfacial compatibility of a-MWCNTs and cement hydrates

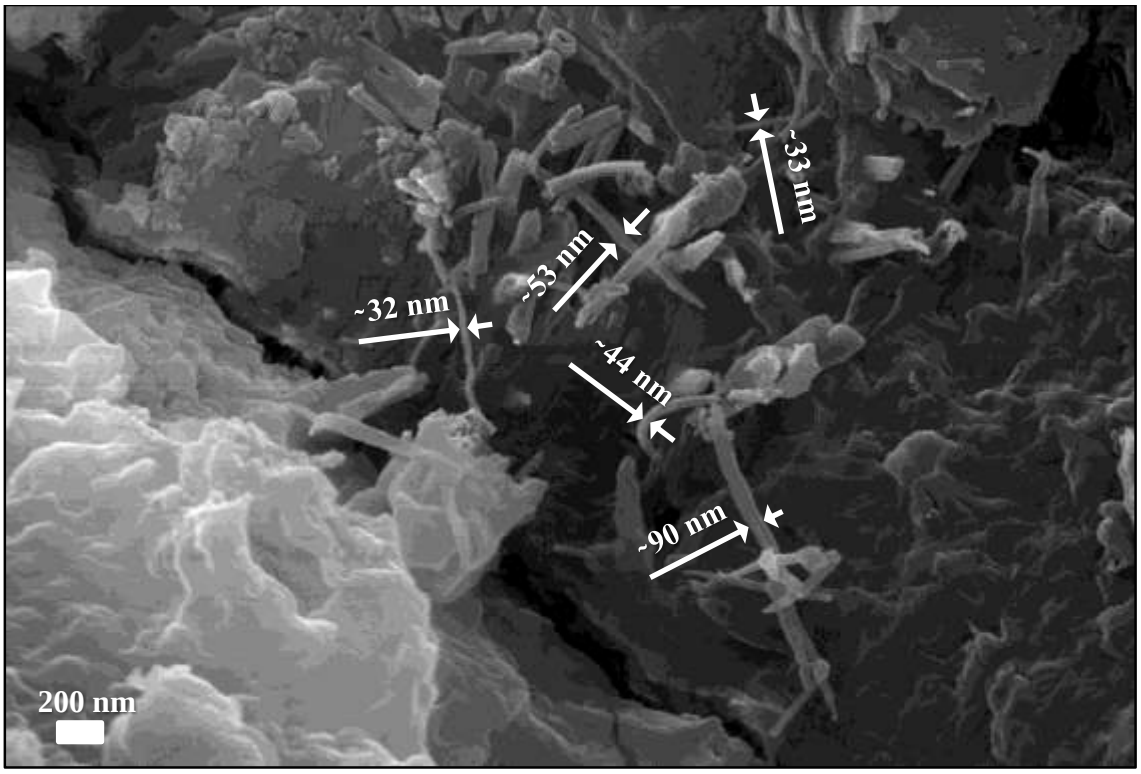

Figure 2.15 - Typical dispersion state of s-MWCNTs in mortar matrix at 0.05%

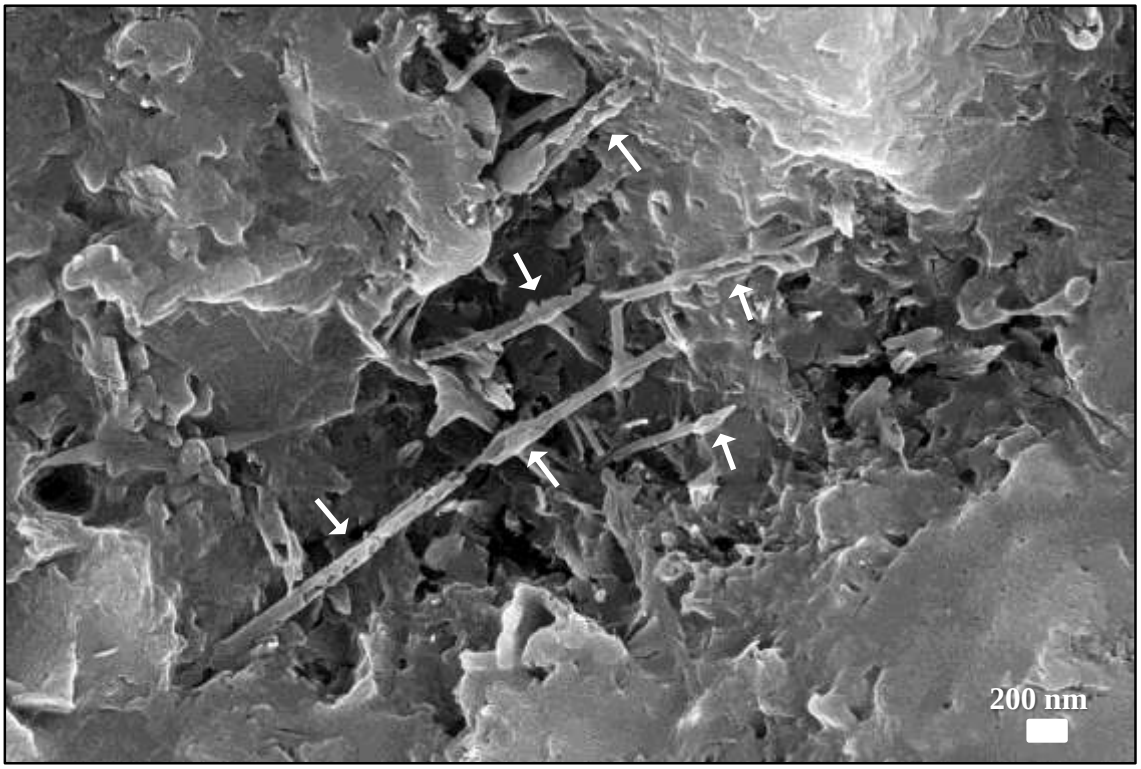

Figure 2.16 - Typical dispersion state of s-MWCNTs in mortar matrix at 0.5%

Figure 2.17 - Typical dispersion state of s-MWCNTs in mortar matrix at 1%

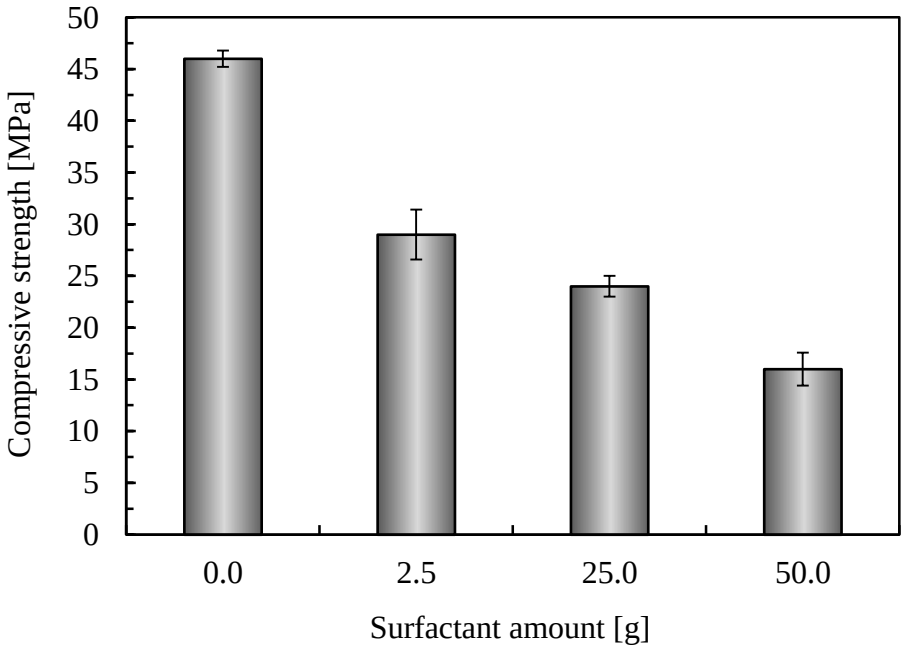

Figure 2.18 - Effect of surfactant amount on compressive strength of s-MWCNT-reinforced mortar

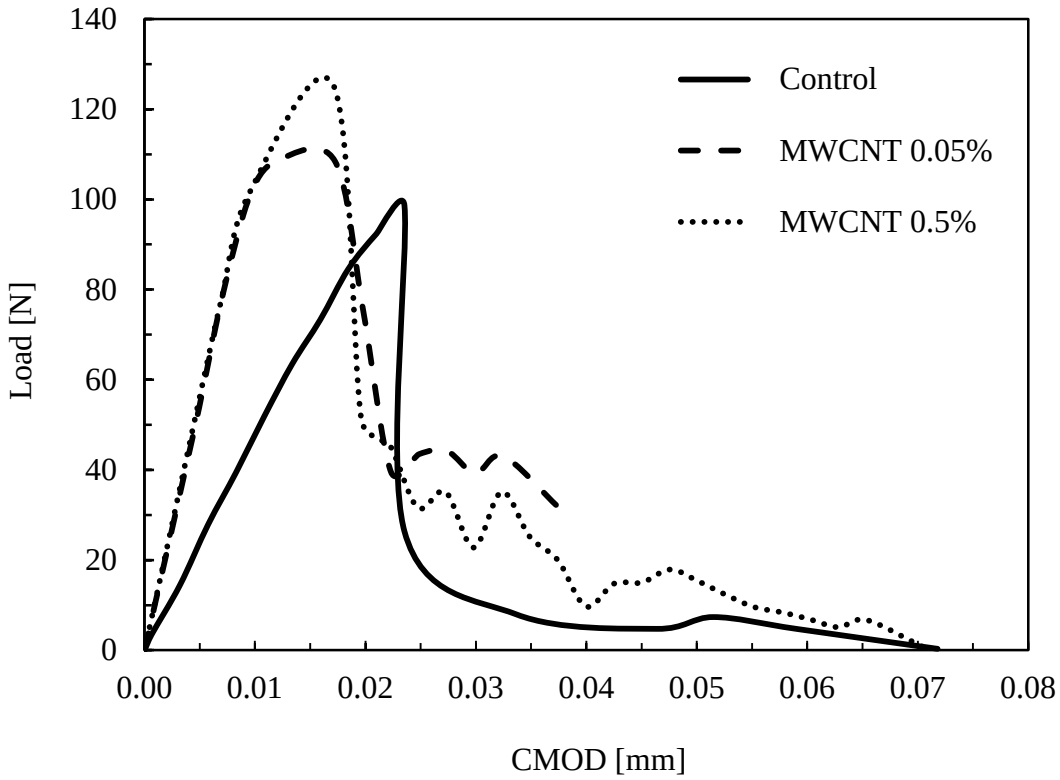

Figure 2.19 - Representative load-CMOD response curves for one specimen per type of plain cement paste samples and nanoreinforced samples at 0.05% and 0.5% a-MWCNTs

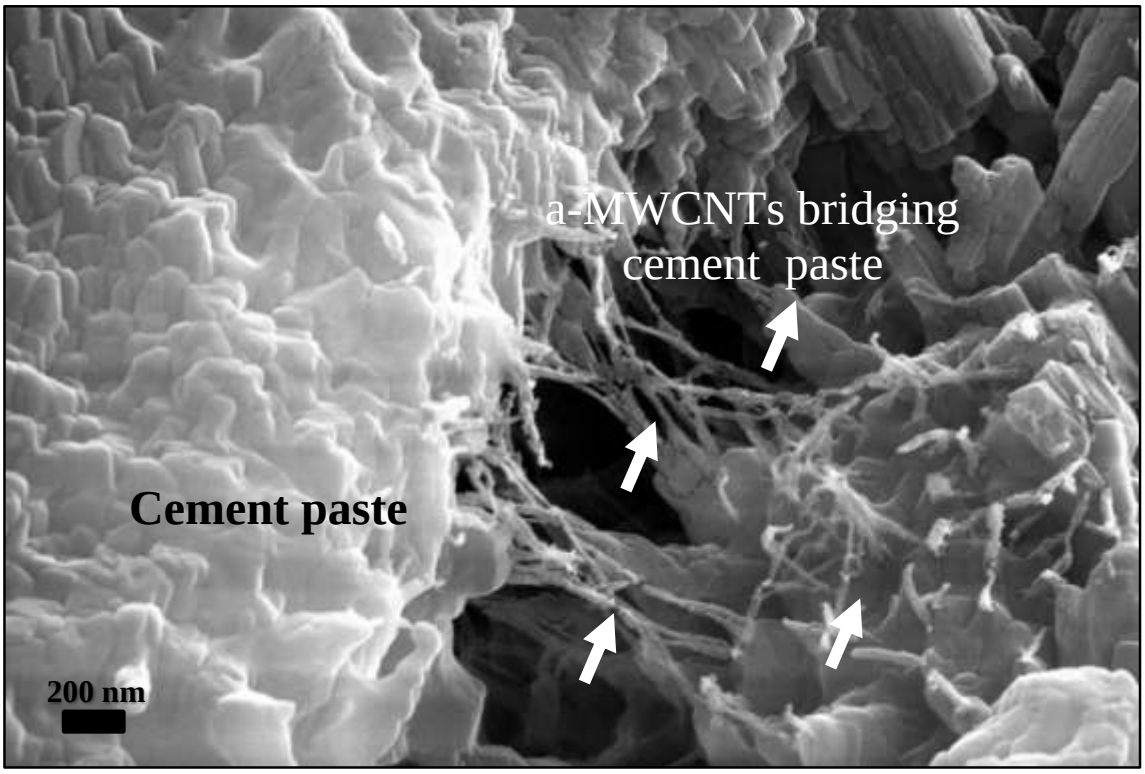

Figure 2.20 - Potential crack-bridging action of MWCNTs - 0.05% a-MWCNTs

CHAPTER 3

EFFECT OF HIGHLY-DISPERSED ACID-ETCHED MWCNTS ON FRACTURE BEHAVIOR OF CEMENT PASTE

ABSTRACT

The fundamental prerequisites for incorporation of MWCNTs in cement composites are good dispersion and effective interfacial bonding with cement hydrates. Based on the evidence presented in chapter 2, acid-etching was selected as a suitable functionalization technique. In this chapter, the effect of well-dispersed acid-etched MWCNTs on the fracture behavior of cement paste is studied with the support of results of three-point bending tests on single-edge notched beam specimens. Digital image correlation (DIC) measurements were used to obtain full-field strain maps around the notch. In particular, principal tensile strain maps were used to gain an insight into the morphology and evolution of the fracture process zone (FPZ) at different stages of loading. It was found that addition of 0.05% acid-etched MWCNTs results in an increase in average stiffness, fracture load, and fracture energy of 108%, 37%, and 13%, respectively. The FPZ for unreinforced samples was visualized via DIC maps as areas of concentrated damage around the crack tip, whereas the FPZ for nanoreinforced beams consisted of larger areas of distributed damage.

3.1 Introduction

The possibility of processing and using extremely high-strength and -stiffness MWCNTs as nanoreinforcement has opened a new field of research to create stronger and more damage tolerant cement composites. MWCNTs are nano-size fibers with exceptional mechanical properties, i.e., Young's modulus of ~1 TPa, tensile strength of 65-135 GPa, and corresponding strain of 10-20% [Hilding 2003, Liu 2007]. The incorporation of MWCNTs is expected to enhance the mechanical properties of cement

composites at the micro- and nano-scale through mechanisms that resemble those provided with conventional synthetic or metallic micro-fibers on a larger scale, such as stress transfer, composite action, and crack-arrest mechanisms [Raki 2010]. In addition, due to their small size (diameter < 100 nm), MWCNTs can fill in meso-pores and meso-defects, thereby reducing and refining porosity [Li 2005, Nochaiya 2011]. Reductions in porosity may result in increased Young's modulus, compressive strength, flexural strength, and fracture toughness [Kendall 1983], and improved durability due to the associated decrease in permeability [Powers 1958]. In addition, MWCNTs can be dispersed at small spacings [Raki 2010], and their high aspect ratio (100-2,500,000) facilitates crack-bridging and -arrest mechanisms provided that the nanoreinforcement is well-incorporated in the cement matrix [Makar 2004, Makar 2005].

The two prerequisites to exploit the reinforcing capabilities of MWCNTs in cement composites are: (1) to obtain a uniform distribution throughout the cement matrix; and (2) to ensure chemical affinity with the surrounding cement hydrates [Sanchez 2010]. Previous research has focused primarily on devising suitable dispersion and functionalization techniques [Saleh 2008, Saleh 2010, Zaib 2012, Khan 2013] to facilitate a uniform distribution of nanoreinforcement and provide chemical affinity [Makar 2004, Sanchez 2010, Raki 2010, and Parveen 2013]. Main-stream techniques are based on the modification of the surface chemistry of MWCNTs to mitigate the attractive van der Waals forces and thus reduce the self-agglomeration tendency, and improve the chemical affinity between the MWCNTs and cement hydrates [Parveen 2013]. Amongst different available techniques, acid-etching and surfactant-coating have gained most popularity

due to their efficiency and compatibility with cement hydration chemistry [Raki 2010]. Acid-etching and surfactant-coating facilitate the debundling of entangled MWCNTs, reduce their hydrophobicity, and promote interfacial bonding [Parveen 2013]. In particular, acid-etching enables the formation of strong bonds through covalent reactions between carboxyl (-COOH) and hydroxyl (-OH) functional groups and positive ions in the cement paste [Aich 2012, Nasibulina 2012]. Conversely, the links between surfactant-coated MWCNTs and cement hydrates, irrespective of the type of surfactant used, tend to be weaker as they rely primarily on the physical attraction between MWCNTs and surfactant molecules [Vaisman 2006].

Previous research showed that, provided that MWCNTs are well dispersed, the associated modifications of cement matrices can result in significantly improved mechanical properties. For example, the addition of small amounts of MWCNTs (in the range of 0.05-1% by the weight of cement; it is noted that all MWCNT concentrations are reported herein with respect to the weight of cement in the composite) has been reported to lead to reduce the autogenous shrinkage strain, Young's modulus, and compressive and flexural strengths, as well as reduced porosity. For example, Konsta-Gdoutos et al. [2010] found that the addition of 0.025-0.048% of well-dispersed surfactant-coated MWCNTs resulted in reduced autogenous shrinkage strain of cement paste prisms up to near 40%. Konsta-Gdoutos et al. [2010] showed that the Young's modulus of cement paste notched beams reinforced with 0.048% of surfactant-coated MWCNTs increased by an average of 45% compared with unreinforced counterparts. Nasibulina et al. [2012] reported an average 97% increase in the compressive strength of 10×10×60 mm cement

paste blocks by adding 0.03% of acid-etched MWCNTs. Luo et al. [2009] obtained an average 30% increase in the flexural strength of cement paste beams with 0.2% of surfactant-coated MWCNTs. Li et al. [2005] reported that the addition of 0.5% of acid-etched MWCNTs resulted in a reduction of porosity of cement mortar of by an average of 64%. Limited evidence has been reported on the effects of MWCNT reinforcement on the fracture behavior of cement composites. Luo et al [2011] showed that addition of 1% acid-etched MWCNTs increased the average fracture toughness of cement paste notched beams by 119%.

In chapter 2, a candidate functionalization technique was identified to manufacture prototype MWCNT-nanoreinforced cement composites. Acid-etching was selected as a suitable technique to attain good dispersion of MWCNTs in cement matrix. Acid-etched MWCNTs exhibited chemical affinity with surrounding cement hydrates, likely facilitated by the formation of covalent bonds with the carboxyl (-COOH) and hydroxyl (-OH) functional groups that were created on the surface of MWCNTs as a result of acid-etching. Preliminary results of notched beam bending tests showed promising effects with respect to flexural strength, stiffness, and damage tolerance of cement paste. These results supported further research by the writer to better understand the effects of acid-etched MWCNT nanoreinforcement on the fracture behavior of cement paste.

As presented in this chapter, the effects of well-dispersed acid-etched MWCNTs on the fracture behavior of cement paste was investigated by means of three-point bending tests on single-edge notched beam specimens. The study is based on data extracted from

load-crack opening displacement curves. The dispersion and incorporation of different concentrations of acid-etched MWCNTs in cement paste were studied by means of SEM analysis of fracture surfaces. Digital image correlation (DIC) measurements were used to obtain full-field strain maps throughout the fracture process zone (FPZ) in the vicinity of the notch. In particular, the principal tensile strain maps were used to study the morphology and evolution of the FPZ in unreinforced and nanoreinforced cement paste.

3.2 Materials and methods

3.2.1 Materials

Type I Ordinary Portland Cement was used in all experiments reported in this chapter. The MWCNTs (Cheap Tubes Inc., cat# SKU-030101, Brattleboro, VT) were used as-received. Salient properties of MWCNTs are shown in Table 6.1.

3.2.2 Functionalization method

Acid-etching was performed following the procedure used by Aich et al. [2012]. The MWCNTs were introduced in an aqueous solution containing ammonium persulfate, $(NH_4)_2S_2O_8$ (Sigma Aldrich, cat# 215589) and sulfuric acid, H_2SO_4 (Sigma Aldrich, cat# 339741). The resulting suspension was stirred for 24 hours using a magnetic stirrer (VWR stirrer, Henry Troemner LLC., Thorofare, NJ). To facilitate the penetration of oxidants along the innermost MWCNTs, the suspensions were sonicated for 10 minutes and stirred for 24 hours. Then, the MWCNTs have a pH value of about 1 and are not suitable for cement mixtures. Therefore, the acid-etched MWCNTs were washed with DI water and filtered through 0.45 μm PVDF membrane filter (Millipore, Billerica, MA) to

raise the pH level to 7. Each batch of 500 mg of MWCNTs was washed with 2 liters of DI water and then dried and stored as dry powder. The dried powder of acid-etched MWCNTs was added to DI water and sonicated for 20 minutes before incorporating it in the cement mixtures. Acid-etched MWCNTs are herein referred to as a-MWCNTs.

3.2.3 Fracture mechanics tests

The fracture mechanics tests consisted of three-point bending tests on single-edge notched beam samples having dimensions of 20×20×80 mm. The test fixtures with a specimen in place are shown in Figure 3.1. a-MWCNTs were incorporated in 0.05 and 0.5% concentrations, fabricating five specimens per group. A w/c ratio of 0.5 was used in the cement paste, which was prepared in accordance with ASTM C305 [ASTM 2013]. A custom-made vibrating table was used to facilitate compaction. The specimens were moist-cured for 24 hours, demolded, and then kept under saturated lime water for 27 days. A water-cooled diamond saw was used to cut 6-mm long and 2-mm wide notches at the mid-span section of each specimen (Figure 3.2). A clip gage was used to measure the crack mouth opening displacement (CMOD). The three-point bending tests were performed in displacement-control mode at a rate of 0.01 mm/minute.

3.2.4 Digital image correlation measurements

Digital image correlation (DIC) is an optical method used to measure full-field deformations on a target planar or curved surface where a high-contrast speckle pattern is painted [Sutton 2009]. Digital images are acquired at different load levels. To calculate the displacement field at any point, the gray value pattern within a small area of interest

(called subset) in the reference image is used to track its corresponding location in the image of a deformed object. In 2D-DIC, a single camera is used to measure in-plane displacement fields, whereas 3D-DIC enlists a stereo-vision system to take into account the out-of-plane deformations and measure displacement fields for 3D objects [Sutton 2009]. 3D-DIC was used in this study.

A thin layer of white wash was applied on the surface of the specimens and a dark speckle pattern was spray-painted on the white-washed background (Figure 3.2). A pair of 5 MP cameras (Grasshopper GRAS-50S5M-C, Point Grey, Richmond, Canada) equipped with 35-mm lenses was used to acquire images at a rate of 5 frames per second. The fracture mechanics and DIC test setup is shown in Figure 3.3. The DIC analysis was performed using the software Vic-3D (v7, Correlated Solutions Inc., Columbia, SC) using a subset size of 49×49 pixels with a step of 15 pixels to analyze an area of 600×600 pixels covering the full height of the beams and extending about 300 pixels to the sides of the notch. The subset size as illustrated in Figure 3.4, was selected to reduce the noise contribution in the calculated strains to an acceptable value (< 20 με).

3.2.5 SEM analysis

SEM micrographs were acquired using a Zeiss Ultra Plus Field Emission Scanning Electron Microscope. All samples were oven-dried for 24 hours at 60°C and gold-sputtered prior to being tested.

3.3 Results and discussion

In this section, the load-CMOD response curves of unreinforced and nanoreinforced beams are presented. Different parameters obtained from load-CMOD data are used to study the effects of a-MWCNTs on the fracture behavior of cement paste. Potential mechanisms contributing to the observed enhancements are discussed, and SEM micrographs obtained from fracture surfaces of failed MWCNT-nanoreinforced beams illustrating the corresponding mechanisms are presented. The effects of a-MWCNTs on the morphology and evolution of the FPZ in the vicinity of the notch at different stages of loading were studied using DIC principal tensile strain maps since cracks form where maximum principal tensile strains are measured.

3.3.1 Load-CMOD response

Two representative load-CMOD curves for each group are presented in Figure 3.5. The load-CMOD curves for all specimens are presented in Figure A.1-A.3. The parameters obtained from load-CMOD data that were used to study the effects of a-MWCNTs on the fracture behavior of nanoreinforced cement paste are summarized in Table 3-1. These parameters for all specimens of different groups are shown in Table 7-1.

3.3.1.1 Stiffness

The flexural stiffness was estimated as the slope of the linear (elastic) portion of the load-CMOD curves. The flexural stiffness for 0.0, 0.05, and 0.5% a-MWCNTs concentration was 5476 ± 561 (average ± standard deviation) N/mm, 11364 ± 2857 N/mm, and 10589 ± 2751 N/mm, respectively. The addition of 0.05 and 0.5% of a-

MWCNTs resulted in an average increase in the flexural stiffness of the notched beams of 108 % and 93%, respectively. Nanoreinforced beams had considerably higher standard deviation values compared with those for unreinforced beams. The high data variations between the nanoreinforced beams can be reasonably attributed to the higher sensitivity of cement paste to MWCNTs dispersion compared with cement mortar.

Stiffness enhancement has been reported by other researchers who used different functionalization methods [Konsta-Gdoutos 2010], and can be attributed to composite action between low-stiffness cement paste and embedded high-stiffness MWCNTs [Konsta-Gdoutos 2010], porosity reduction [Li 2005, Nochaiya 2001], and possibly matrix modification (i.e., a more extensive formation of stronger and stiffer C-S-H phases) [Ibarra 2006, Konsta-Gdoutos 2010]. Due to their high Young's modulus (~ 1TPa), the addition of small concentrations of MWCNTs (even smaller than 0.05%) can lead to significant increases in the Young's modulus of MWCNT-reinforced cement composites. For example, the addition of 0.048% of surfactant-coated MWCNTs produced an average increase in the Young's modulus of cement paste notched beams of 45% [Konsta-Gdoutos 2010]. The greater increase obtained in this study may be attributed to the formation of stronger covalent bonds between acid-etched MWCNTs and cement hydrates compared with surfactant-coated MWCNTs. In fact, the formation of covalent bonds between a-MWCNTs and cement hydrates has been hypothesized [Li 2005, Aich 2012] and shown experimental [Nasibulina 2012]. It was also shown theoretically that covalent bonding between acid-etched GNPs (which have a comparable atomic structure to MWCNTs) and C-S-H can increase the interfacial bond strength

compared with pristine GNPs and C-S-H by nearly 10 times [Alkhateb 2014]. Further research is needed to experimentally evaluate the effect of covalent reactions on the interfacial bond strength of a-MWCNTs and cement hydrates.

In addition, due to their small size (see Table 6.1), MWCNTs can fill in nano- and meso-pores and reduce and refine the porosity of the cement matrix [Nochaiya 2011]. For example, Li et al. [2005] showed that the addition of 0.5% of acid-etched MWCNTs produced a decrease in total porosity and amount of meso-pores (pores with diameters of 2-50 nm) by 64% and 82%, respectively. A decrease in porosity can result in a significant increase in the Young's modulus of cement paste. For example, Kendall et al. [1983] showed that reducing the porosity from 25% to 7.5% (in volume) nearly doubled the Young's modulus of cement paste. The SEM micrographs in Figures 3.6 and 3.7, which were taken from fracture surfaces in the notched beam samples tested by the writer, show a-MWCNTs filling in voids, possibly bridging across the surrounding cement paste, for a-MWCNT concentrations of 0.05 and 0.5%, respectively. Another example from the notched beams containing 0.5% of a-MWCNTs is also presented in Figure 3.8.

Another relevant implication of incorporating well-dispersed MWCNTs is the modification of the cement matrix. Specifically, results of nanoindentation tests showed that the relative amount of high-stiffness C-S-H [Konsta-Gdoutos 2010] and the stiffness of both low-density and high-density C-S-H increased as a result of adding MWCNTs [Ibarra 2006]. More research is needed to understand this phenomenon.

The formation of higher quality cement hydrates (i.e. denser and stiffer) may be a consequence of enhanced hydration conditions due to presence of MWCNTs. In a study by Nasibulina et al. [2012], transmission electron microscopy (TEM) analysis of MWCNTs in hydrating cement at early stage of hydration (1.0 and 5.5 hours after mixing) showed the precipitation of nano-size (10-50 nm) hydration products on the surface of MWCNTs. This observation suggested that MWCNTs may act as nucleation sites for cement hydration, which may lead to the formation of higher quality (i.e., denser and stiffer) C-S-H. Another study on GNP-nanoreinforced cement paste showed that GNPs may produce a "heat sink" effect during cement hydration, leading to the formation of higher-quality cement paste [Sedaghat 2014]. Thermal diffusivity measurements of GNP-nanoreinforced cement paste showed that the addition of GNPs (in the range of 1-10% by the weight of cement) produced an increase in the thermal diffusivity. SEM analysis suggested that an enhanced thermal diffusivity was associated with the formation of a denser microstructure. It was hypothesized that due to their relatively high thermal conductivity (~5000 $W.m^{-1}.K^{-1}$, about five times greater than copper), the presence of GNPs may produce a reduction of the local thermal gradients during cement hydration, and facilitate the formation of denser cement hydrates as well as less defect (void) sites. Since GNPs and MWCNTs have a comparable thermal conductivity, a similar phenomenon may also take place in MWCNT-reinforced cement composites. Further research is needed to test this hypothesis.

3.3.1.2 Flexural strength

The incorporation of well-dispersed a-MWCNTs increased the flexural strength of cement paste beams. The fracture load for specimens containing 0.0, 0.05 and 0.5% of a-MWCNTs was 96.49 ± 2.99 (average ± standard deviation), 132.55 ± 21.11, and 119.29 ± 8.80 N, respectively. The addition of 0.05 and 0.5% of a-MWCNTs produced an average increase in the fracture load of 37% and 24%, respectively. This effect may be attributed to composite action between cement paste and well-incorporated high-stiffness MWCNTs [Konsta-Gdoutos 2010], porosity reduction [Li 2005], and matrix modification in the form of denser cement hydrates [Ibarra 2006, Konsta-Gdoutos 2010]. The smaller improvement in fracture load with respect to stiffness may be due to a greater effect of a denser microstructure (e.g., because of porosity reduction) on stiffness compared with flexural strength. According to Kendall et al. [1983], the flexural strength of cement paste is primarily affected by the presence of macro-defects (i.e., large pores around 1 mm in size) that are inevitably introduced during the mixing process. Therefore reduction of meso-porosity due to incorporation of a-MWCNTs should affect the stiffness to a greater extent than flexural strength. The contribution of porosity reduction in increasing the stiffness is the result of filling in voids (with zero stiffness) with MWCNTs (with Young's modulus ~ 1TPa) as previously shown in Figures 3.6-3.8.

The increase in flexural strength can also be partially attributed to a crack-arrest effect. In fact, MWCNTs may improve the matrix resistance to cracking by offsetting the coalescence of smaller cracks into larger micro-cracks, with a positive effect in terms of damage tolerance. As a result, a higher load is required to grow the critical crack in the a-

MWCNT-reinforced beams, thus resulting in higher failure loads. The SEM micrographs in Figure 3.9, obtained from cement paste beams reinforced with 0.05% of a-MWCNTs, illustrate the likelihood of crack-bridging action of acid-etched MWCNTs. This mechanism was also observed for the a-MWCNT-cement mortar at 0.05% concentration which is shown in Figure 2.19.

3.3.1.3 Post-peak behavior

Incorporation of a-MWCNTs also improved the post-peak behavior of the nanocomposites (Figure 3.5). While unreinforced beams experienced a sudden decrease in strength upon reaching the peak load, nanoreinforced beams exhibited a higher post-peak residual strength. However, the improved post-peak behavior was not observed for all nanoreinforced beams. As a matter of fact, some samples underwent a sudden rupture upon or shortly after reaching the peak load (see Figures 1-3 in appendix A). As a result the average CMOD $_{\text{Rupture}}$ values for nanoreinforced beams were smaller than that of unreinforced beams. The average CMOD at rupture at 0.0, 0.05, and 0.5% a-MWCNT concentrations were 0.070 ± 0.013, 0.024 ± 0.012, and 0.036 ± 0.030 mm (Table 3-1), respectively. It is noted that nanoreinforced beams exhibited a high level of inconsistency with respect to failure mode, fracture load, stiffness, and fracture energy which is reflected in load-CMOD response curves (Figure 3.5) and the large values of standard deviation for different parameters reported in Table 3-1. This level of inconsistency most likely originates from the dispersion-sensitive behavior of nanocomposites.

3.3.1.4 Fracture energy

The fracture energy of the notched beams was calculated as the area under the load-CMOD curves. The average fracture energy of the notched beams at 0.0, 0.05, and 0.5% a-MWCNTs concentration was 1.62 ± 0.06, 1.84 ± 0.78, and 1.61 ± 0.83 N.mm, respectively. The Addition of 0.05% of a-MWCNTs increased the average fracture energy by 13%, whereas the addition of 0.5% a-MWCNTs had a negligible effect. To better describe the effects of a-MWCNTs addition on the fracture energy, the fracture energy values for all specimens are plotted in Figure 3.10. The effect of a-MWCNTs on fracture energy may be missed by only considering the average values. As a matter of fact, for individual specimens, the addition of 0.05 and 0.5% a-MWCNTs increased the fracture energy up to 79% and 56%, respectively.

Improvements in fracture energy can be attributed to porosity reduction [Kendall 1983], crack-arrest effect [Luo 2011], and potential matrix modification mechanisms [Konsta-Gdoutos 2010]. The energy dissipated from debonding or breakage of a-MWCNTs contributes to higher energy adsorption capacity of nanoreinforced beams. Figures 3.8 and 3.9 illustrate the potential crack- and defect-bridging effect of a-MWCNTs. Figures 3.11 and 3.12 illustrate long MWCNTs passing through cement phases acting as long and stiff nano-ropes binding the cement paste phases tightly.

Due to their dimensions (see Table 6.1) MWCNTs can be most effective in controlling the propagation of cracks at the nanoscale. Therefore incorporation of MWCNTs may enhance the non-linear pre-peak behavior of cement composites where

significant inelastic deformations occur due to formation and growth of smaller cracks [Jenq and Shah 1985]. The average load and CMOD corresponding to the beginning of the non-linear pre-peak portion of the load-CMOD curves ($P_{Non\text{-}linear}$ and $CMOD_{Non\text{-}linear}$) for different groups are presented in Table 3-1. The beginning of non-linearity was marked as the first point of visual deviation from linearity, which corresponds to a minimum 20% reduction in the slope of the linear elastic portion of a given curve. The non-linear pre-peak region of load-CMOD curves is shown in Figure 3.13. The average $P_{Non\text{-}linear}$ for beams containing 0.0, 0.05%, and 0.5% of a-MWCNTs was 84.91 ± 5.25, 111.59 ± 26.52, and 103.37 ± 13.53 N, respectively. The addition of 0.05 and 0.5% of a-MWCNTs produced an average increase in $P_{Non\text{-}linear}$ by 31% and 21%, respectively. The $CMOD_{Non\text{-}linear}$ for a-MWCNTs concentration of 0.0, 0.05%, and 0.5% were 0.018 ± 0.001, 0.011 ± 0.004, and 0.011 ± 0.003, respectively. The $CMOD_{Non\text{-}linear}$ for nanoreinforced beams was smaller by 40% and 37%, respectively. The smaller $CMOD_{Non\text{-}linear}$ values can be attributed to higher stiffness of nanoreinforced beams.

Figure 3.14 compares the amount of energy absorbed by specimens of different groups during the non-linear stage of loading prior to reaching the peak load. The amount of energy absorbed for nanoreinforced samples with 0.05 and 0.5% of a-MWCNTs was higher than that of the control samples by an average of 96% and 27%, respectively. This may be attributed to the effect of MWCNTs in controlling the propagation of the nano- and micro-cracks formed at this stage (see Figures 3.8, 3.9, 3.11, and 3.12). As a result of energy dissipation through crack-arrest mechanisms, higher amounts of energy are stored in the nanoreinforced beams. Subsequently, higher amounts

of energy are released upon fracture of these specimens, which contributes to explain the sudden rupture observed for some nanoreinforced beams.

3.3.2 Microstructure

The dispersion and embedment states of a-MWCNTs in cement paste were investigated using SEM analysis of fracture surfaces. The typical microstructure of nanoreinforced beams containing 0.05 and 0.5% of a-MWCNTs are illustrated in Figures 3.15 and 3.16, respectively. At both concentrations, a-MWCNTs were mostly found as individual MWCNTs or in bundles with small diameters (<50 nm), thus showing that a good dispersion was achieved by means of acid-etching. In addition, a-MWCNTs were mostly embedded in or coated by cement hydrates. In the majority of the areas inspected, only a small length of a-MWCNTs was exposed (compare the small length of a-MWCNTs in Figures 3.15 and 3.16 with the long MWCNTs in Figures 3.11 and 3.12). The presence of a-MWCNTs clusters for both 0.05 and 0.5% concentrations were also noted. An example of cluster of a-MWCNTs obtained from beams containing 0.05% of a-MWCNTs is shown in Figure 3.17. MWCNTs clusters have minimal contact with cement hydrates and produce sites of discontinuity (i.e., defects). Note the crack formed in the vicinity of the MWCNTs cluster. The presence of a-MWCNTs clusters even at a 0.05% concentration may explain the high variability in different fracture parameters observed for the nanoreinforced beams. The MWCNTs clusters could be more frequently found on the fracture surfaces of beams containing 0.5% a-MWCNTs. The smaller improvement in different fracture parameters at 0.5% can be reasonably attributed to the higher number of defects introduced into the matrix.

3.3.3 DIC measurements

The damage area ahead of the traction-free crack tip during fracture of cement composites is defined as the fracture process zone (FPZ) [Jenq and Shah 1985]. In the meso-porous microstructure of cement paste, well-bonded MWCNTs can transfer stress between the adjacent phases of cement paste, thus facilitating stress distribution near the notch and influencing the morphology and evolution of the FPZ as damage propagates. The effects of adding a-MWCNTs on the FPZ of cement paste were studied by comparing the DIC principal tensile strain maps of unreinforced and nanoreinforced beams at different stages of loading (Figures 3.18-3.23). In the DIC strain maps, the area of maximum principal tensile strain, ε_1, is marked in red. The areas in yellow, green, light blue, and dark blue, mark the areas where ε_1 is 80%, 60%, 40%, and 20% of the maximum value (in red), respectively.

The evolution of the FPZ in plain cement paste specimens are illustrated in Figure 3.18 and 3.19. The FPZ remained confined in a well-defined and narrow damage zone around and ahead of the crack tip (marked with color red). For nanoreinforced beams containing 0.05% (Figure 3.20 and 3.21) and 0.5% (Figure 3.22 and 3.23) of a-MWCNTs, in the non-linear pre-peak stage of loading (prior to fracture), the FPZ extends to an irregular and larger zone of distributed damage (marked with colors green and light blue). These contours show a smoother transition between the zones of larger and smaller deformation, supporting the hypothesis that a-MWCNTs contribute to damage tolerance. Such enhanced damage tolerance prior to reaching the peak load also helps explain the

high amount of energy stored in the nanoreinforced beams during the non-linear pre-peak stage of loading as shown in Figure 3.12.

3.4 Conclusions

In this chapter, the effects of the incorporation of well-dispersed acid-etched MWCNTs on the fracture behavior of cement paste were investigated by means of three-point bending tests on single-edge notched beams. DIC measurements were used to better understand the morphology and evolution of the fracture process zone. The following conclusions are drawn:

(1) Incorporation of 0.05% and 0.5% of a-MWCNTs resulted in an increase in the average stiffness of cement paste of 108% and 93%, respectively.

(2) Incorporation of 0.05% and 0.5% of a-MWCNTs resulted in an increase in the average flexural strength of notched beams of 37% and 24%, respectively.

(3) The fracture energy was also improved. Due to high variability observed among nanoreinforced specimens, the average fracture energy value did not reflect the potential effect of a-MWCNTs on the fracture energy. The incorporation of a-MWCNTs resulted in an increase in the fracture energy for individual specimens at 0.05% and 0.5% up to 79% and 56% for 0.05 and 0.5% a-MWCNT concentrations, respectively.

(4) Incorporation of 0.05% and 0.5% a-MWCNTs improved the post-peak behavior of notched beams. Nanoreinforced beams had higher post-peak residual strength compared with unreinforced beams.

(5) SEM analysis of fracture surfaces showed uniform dispersion and effective interfacial bonding of a-MWCNTs in cement paste matrix. a-MWCNTs clusters were more frequently found at 0.5% which can explain the smaller improvements in the fracture properties at this concentration.

(6) The FPZ for unreinforced samples consisted of zones of concentrated damage around and ahead the crack tip, with a sharp transition between higher and smaller deformation areas. The FPZ for nanoreinforced beams consisted of larger zones of distributed damage at the vicinity of the notch, with a smoother transition between higher and smaller deformation areas, supporting the hypothesis that well-dispersed and embedded a-MWCNTs contribute to damage tolerance .

3.5 References

Aich N., Zohhadi N., Khan I.A., Matta F., Ziehl P., and Saleh N.B., Applied TEM apprach for micro/nanostructural characterization of carbon nanotube reinforced cementitious composites, Journal of Research Updates in Polymer Science 1 2012: 14-23.

ASTM Standard C305, 2013, "Standard practice for mechanical mixing of hydraulic cement pastes and mortars of plastic consistency" ASTM International, West Conshohocken, PA, 2013, DOI: 10.1520/C0305, www.astm.org

Hilding J., Grulke E.A., Zhang Z.G., and Lockwood F., Dispersion of carbon nanotubes in liquids, J. Disper. Sci. Technol 2003: 24: 1-41.

Jenq Y., and Shah S.P., Two parameter fracture model for concrete, J Eng Mech 19885: 111: 1227-1241.

Kendall K., Howard A.J., and Brichall J.D., The relation between porosity, microstructure and strength, and the approach to advanced cement-based materials, Phil Trans R Soc Lond A 1983: 310: 139-153.

Khan I.A., Afrooz A.N., Flora J.R.V., Schierz P.A, Ferguson P.L, Sabo-Attwood T., and Saleh N.B., Chirality affects aggregation kinetics of single-walled carbon nanotubes. Environ Sci Technol 2013: 47(4): 1844-1852.

Konsta-Gdoutos M.S., Metaxa Z.S., and Shah S.P., Highly dispersed carbon nanotube reinforced cement based materials, Cement Concrete Res. 2010: 40: 1052-1059.

Konsta-Gdoutos M.S., Metaxa Z.S., and Shah S.P., Multi-scale mechanical and fracture characteristics and early-age strain capacity of high performance carbon nanotube/cement nanocomposites, Cement Concrete Comp. 2010: 32: 110-115.

Li G.Y., Wang P.M., and Zhao X., Mechanical behavior and microstructure of cement composites incorporating surface-treated multi-walled carbon nanotubes, Carbon 2005: 43: 1239-1245.

Luo J., Duan Z., and Li H., The influence of surfactants on the processing of multi-walled carbon nanotubes in reinforced cement matrix composites, Phys. Status Solidi (a) 2009: 206: 2783-2790.

Luo J.L., Duan Z., Xian G., Li Q., and Zhao T., Fabrication and fracture toughness properties of carbon nanotube-reinforced cement composite, Eur Phys J Appl Phys 2011: 53: 30402.

Makar J.M., and Beaudoin J.J., Carbon nanotubes and their application in the construction industry, Special Publication-Royal Society of Chemistry: 2004: 292: 331-342.

Makar J.M., Margeson J.C., and Luh J., Carbon nanotube/cement composites-early results and potential applications, 2005: 1-10.

Nasibulina L.I., Anoshkin I.V., Nasibulin A.G., Cwirzen A., Penttala V., and Kauppinen E.I., Effect of carbon nanotube aqueous dispersion quality on mechanical properties of cement composite, J. Nanomater. 2012: 169262.

Nochaiya T., and Chaipanich A., Behavior of multi-walled carbon nanotubes on the porosity and microstructure of cement-based materials, Appl. Surf. Sc 2011: 257: 1941-1945.

Parveen S., Rana S., and Fangueiro R., A review on nanomaterial dispersion, microstructure and mechanical properties of carbon nanotube and nanofiber reinforced cementitious composites, J. Nanomater. 2013: 80.

Powers T.C., Structure and physical properties of hardened Portland cement paste, J Amer Cer Soc 1958: 41: 1-6.

Raki L., Beaudoin J., Alizadeh R., Makar J., and Sato T., Cement and concrete nanoscience and nanotechnology, Materials 2010: 3: 918-942.

Saez de Ibarra Y., Gaitero J.J., Erkizia E., and Campillo I., Atomic force microscopy and nanoindentation of cement pastes with nanotube dispersions, Phys Status Solidi (a) 2006: 203: 1076-1081.

Saleh N.B., Pfefferle L.D., and Elimelech M., Aggregation kinetics of multiwalled carbon nanotubes in aquatic systems: measurements and environmental implications, Environ Sci Technol 2008: 42(21): 7963-7969.

Saleh N.B., Pfefferle L.D., and Elimelech M., Influence of biomacromolecules and humic acid on the aggregation kinetics of single-walled carbon nanotubes. Environ. Sci. Technol. 2010: 44(7), 2412-2418.

Sanchez F., and Sobolev K., Nanotechnology in concrete – A review, Constr Build Mater 2010: 24: 2060-2071.

Sedaghat A., Ram M.K., Zayed A., Kamal R., and Shanahan N., Investigation of physical properties of graphene-cement composite for structural applications, Open J Comp Mats 2014: 4:12-19.

Sutton M.A., Orteu J.J., and Schreier H.W., Image correlation for shape, motion and deformation measurements, Springer, New York, doi 10 (2009): 978-0.

Vaisman L., Wagner H.D., and Marom G., The role of surfactants in dispersion of carbon nanotubes, Adv Colloid Interfac 2006: 128: 37-46.

Zaib Q., Khan I.A., Yoon Y., Flora J.R.V., Park Y.G., and Saleh N.B., Ultrasonication study for suspending single-walled carbon nanotubes in water, J. Nanosci Nanotechno 2012: 12(5): 3909-3917.

3.6 Tables

Table 3.1 - Fracture parameters for different groups

Group	Fracture load [N]	Stiffness [N/mm]	$P_{Non\text{-}linear}$ [N]	CMOD Non-linear [mm]	CMOD Rupture [mm]
Control	96.49 ± 2.99	5476 ± 561	84.91 ± 5.25	0.018 ± 0.001	0.070 ± 0.013
a-MWCNT-0.05%	132.55 ± 21.11	11364 ± 2857	111.59 ± 26.52	0.011 ± 0.004	0.024 ± 0.012
a-MWCNT-0.5%	119.29 ± 8.80	10589 ± 2751	103.37 ± 13.53	0.011 ± 0.003	0.036 ± 0.030

3.7 Figures

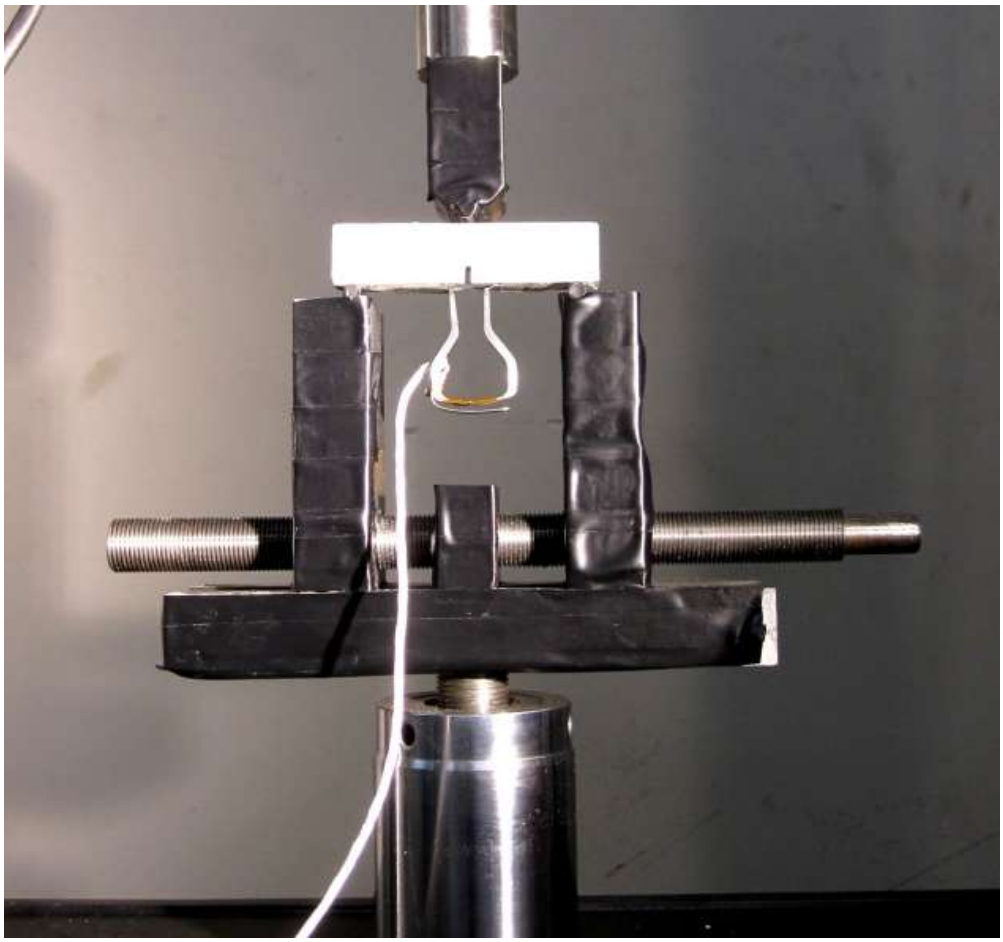

Figure 3.1 - Support fixtures for three-point bend tests with notched beam specimen in place - Tests were performed in displacement control using a MTS 801 Material Testing System

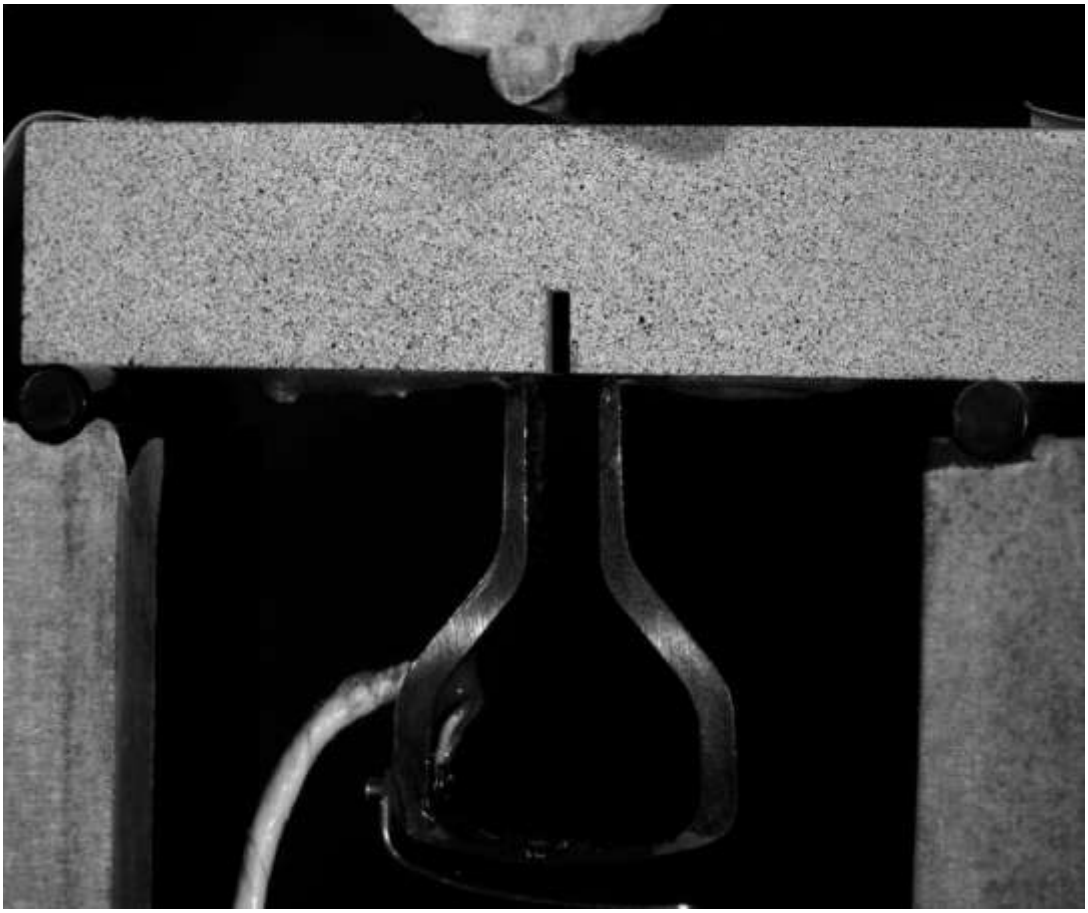

Figure 3.2 - Close-up photograph of notched beam specimen with DIC speckle pattern

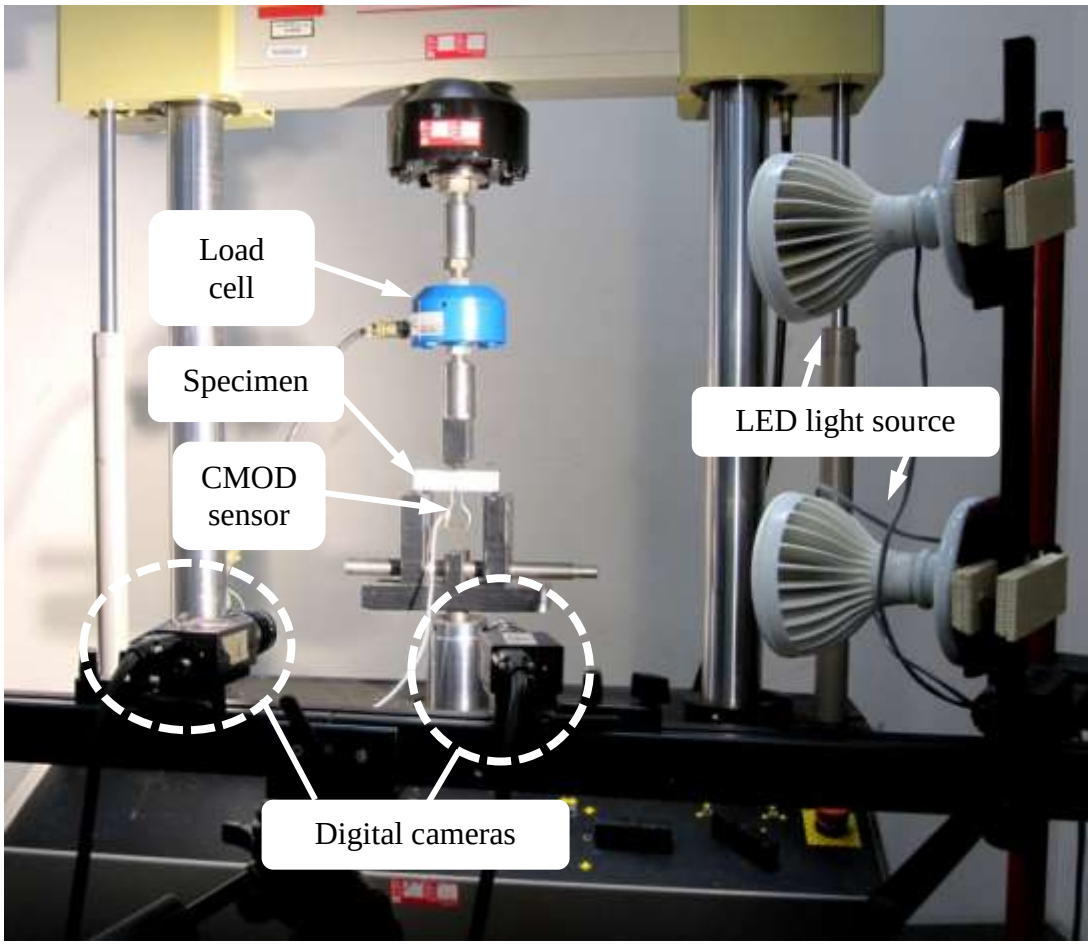

Figure 3.3 - Three-point bending test setup with DIC measurement equipment

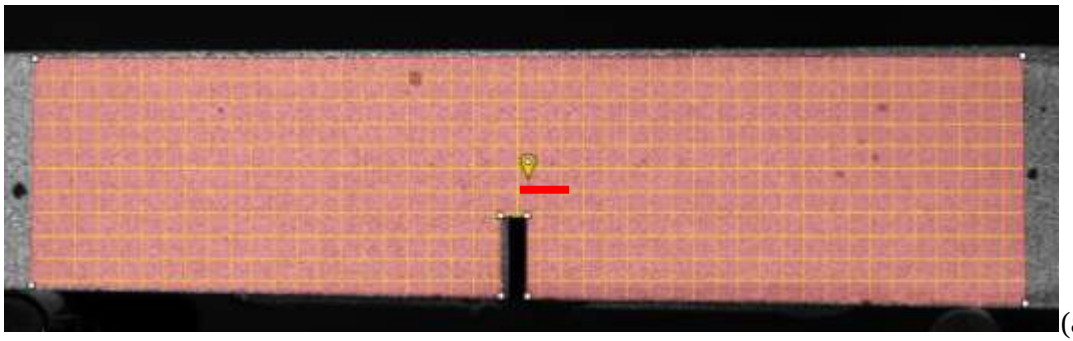

(a)

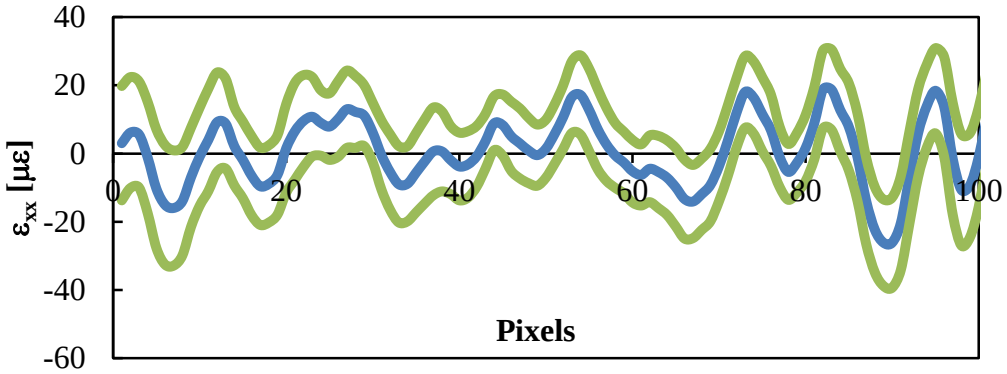

(b)

Figure 3.4 - (a) Subset size used in DIC analysis with respect to beam dimensions, (b) horizontal strain error at zero load along the red line above the notch corresponding with subset size of 49×49 pixels – Blue curve shows average error at different points and green curves show standard deviation values

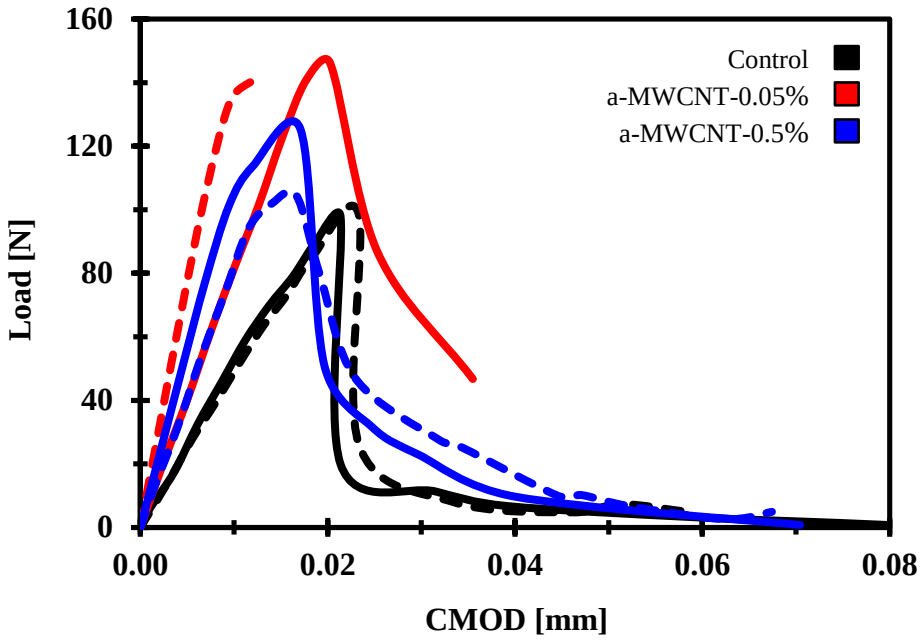

Figure 3.5 - Load-CMOD response curves for representative specimens of different groups

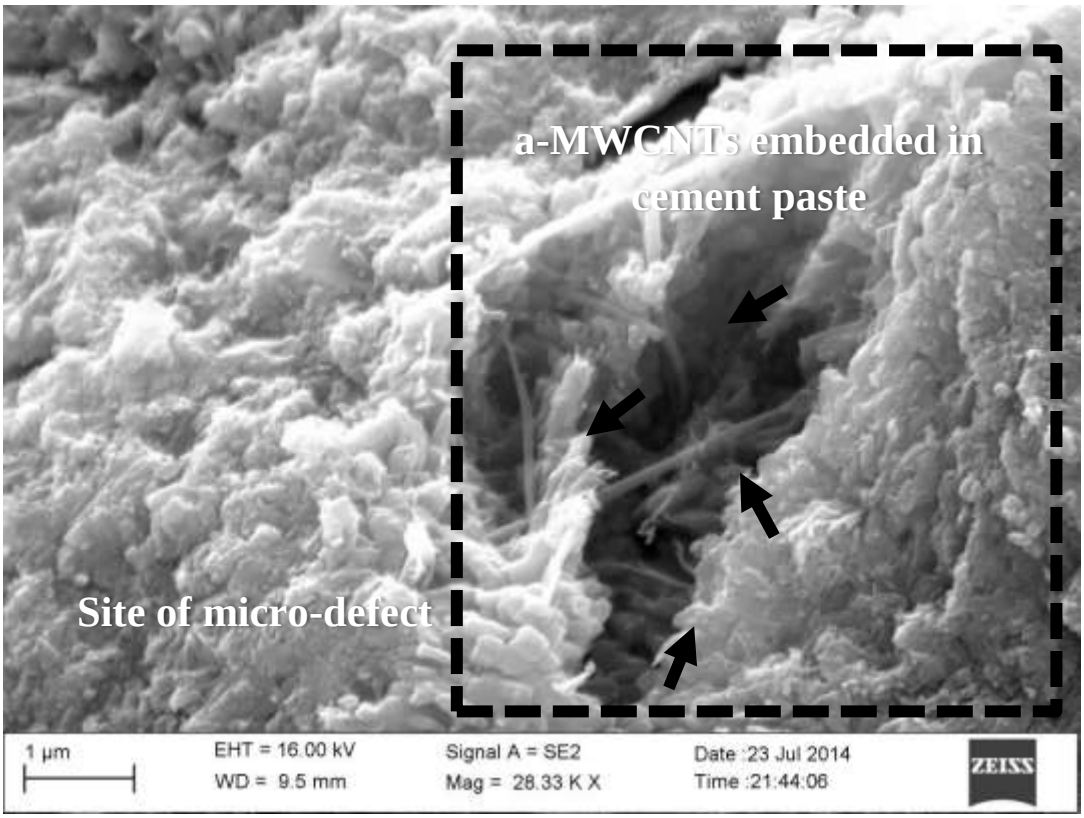

Figure 3.6 - Potential effect of a-MWCNTs on filling in micro-defects in cement paste – 0.05% concentration

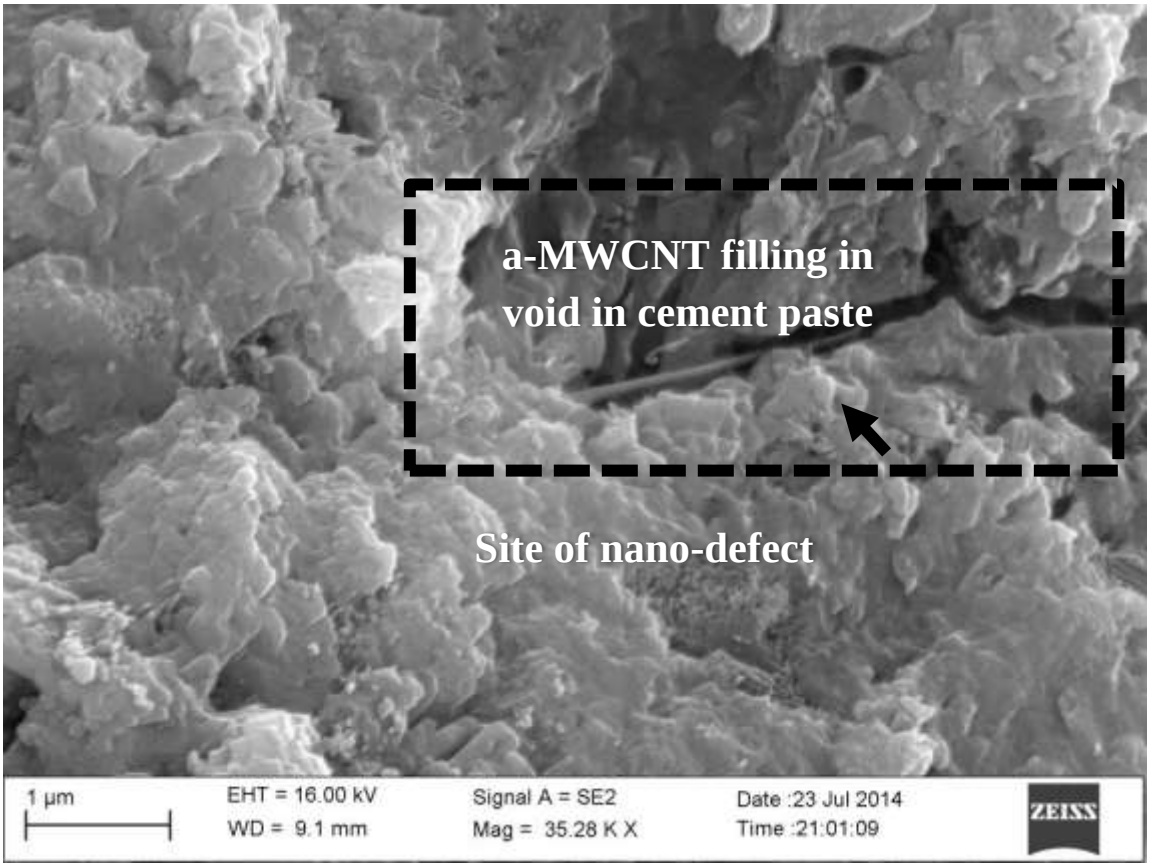

Figure 3.7 - Potential effect of a-MWCNT on filling in nano-defects – 0.5% concentration

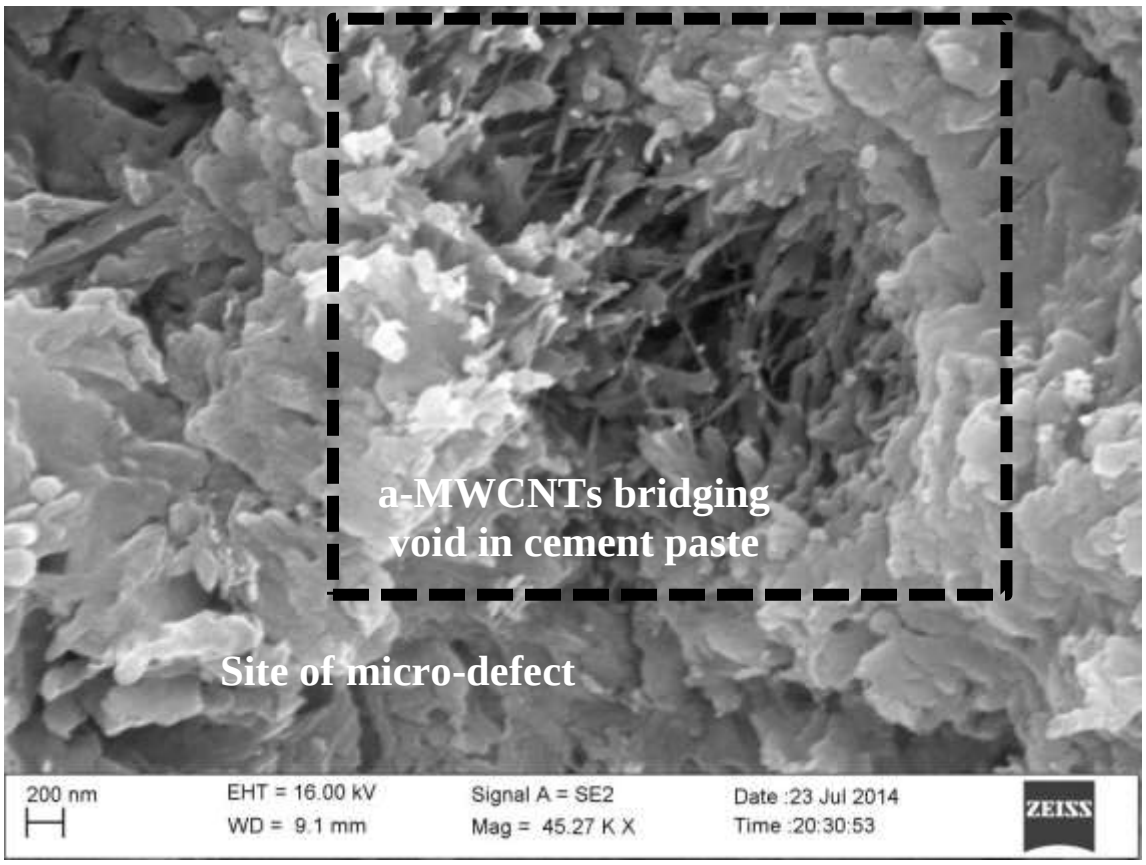

Figure 3.8 - a-MWCNTs bridging micro-size defect in cement paste

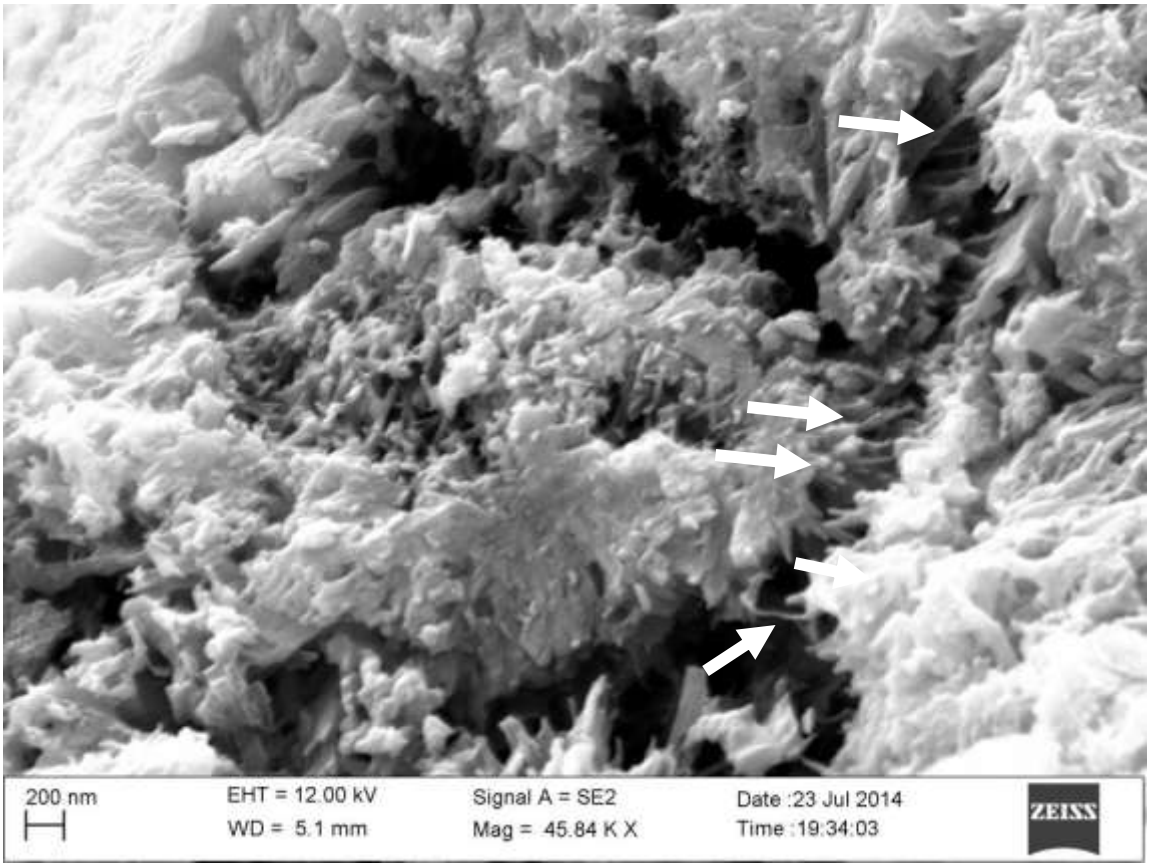

Figure 3.9- Potential crack-bridging effect of a-MWCNTs– obtained from cement paste reinforced with 0.5% a-MWCNTs

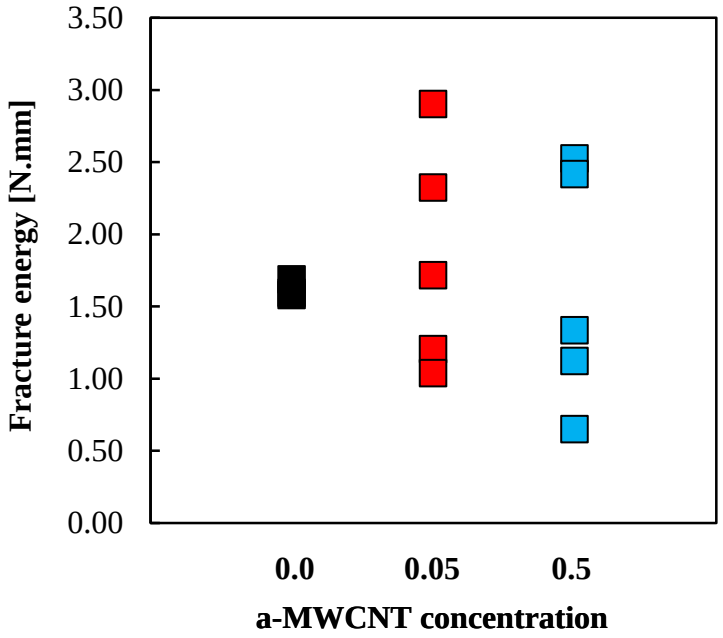

Figure 3.10 - Fracture energy for notched beam specimens containing 0.0, 0.05, and 0.5% a-MWCNTs

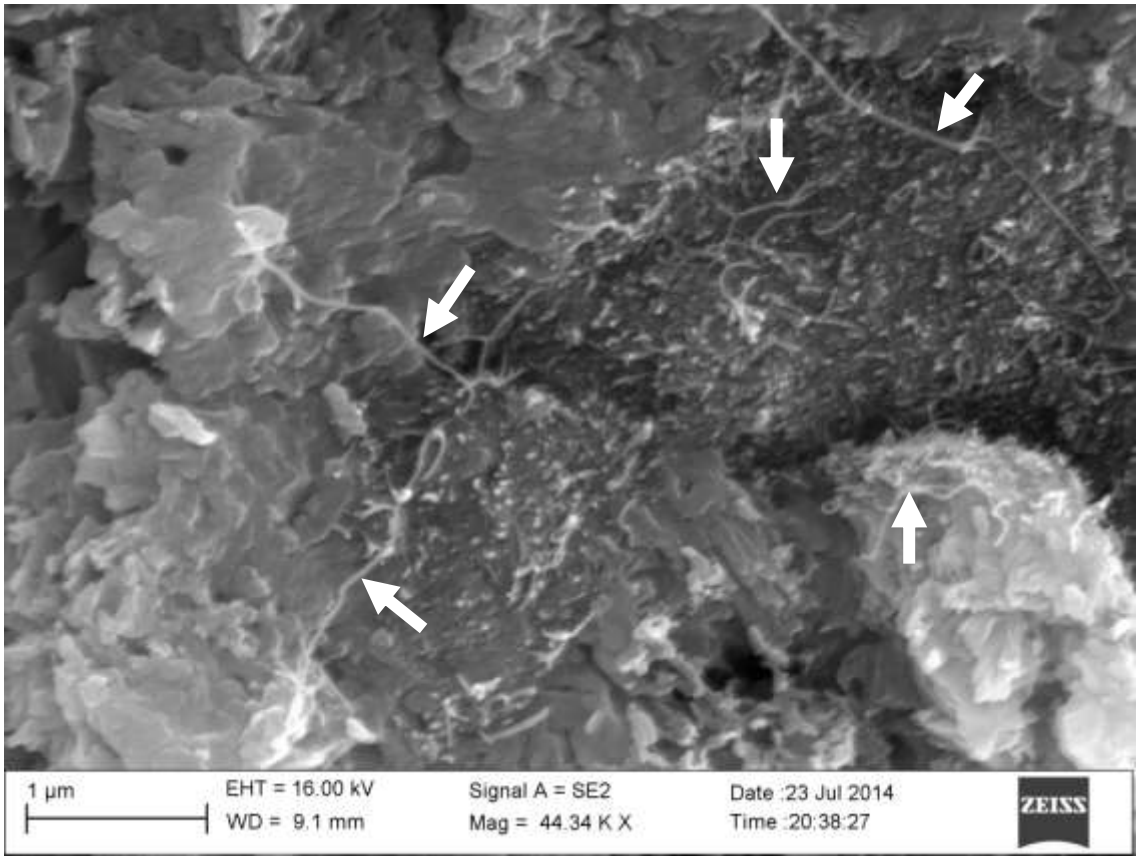

Figure 3.11 - SEM micrograph showing long MWCNTs passing through cement phases acting as long and stiff nano-ropes binding the cement paste phases tightly

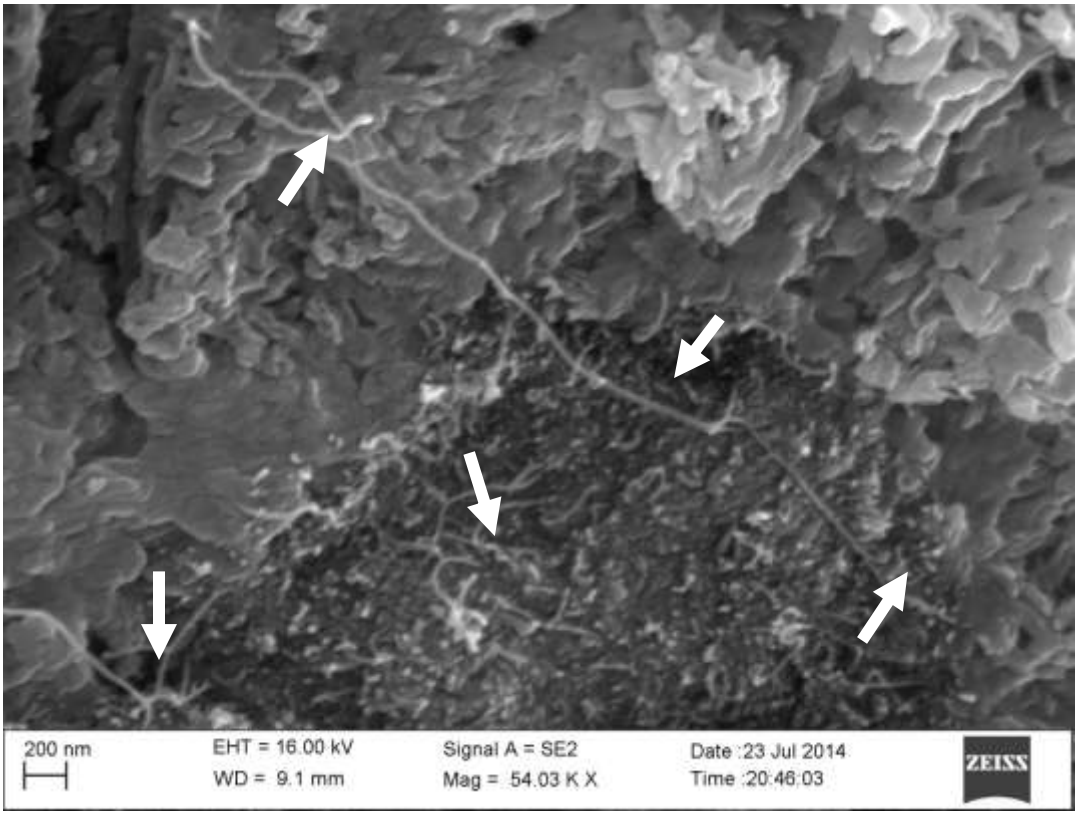

Figure 3.12 - SEM micrograph showing long MWCNTs passing through cement phases acting as long and stiff nano-ropes binding the cement paste phases tightly

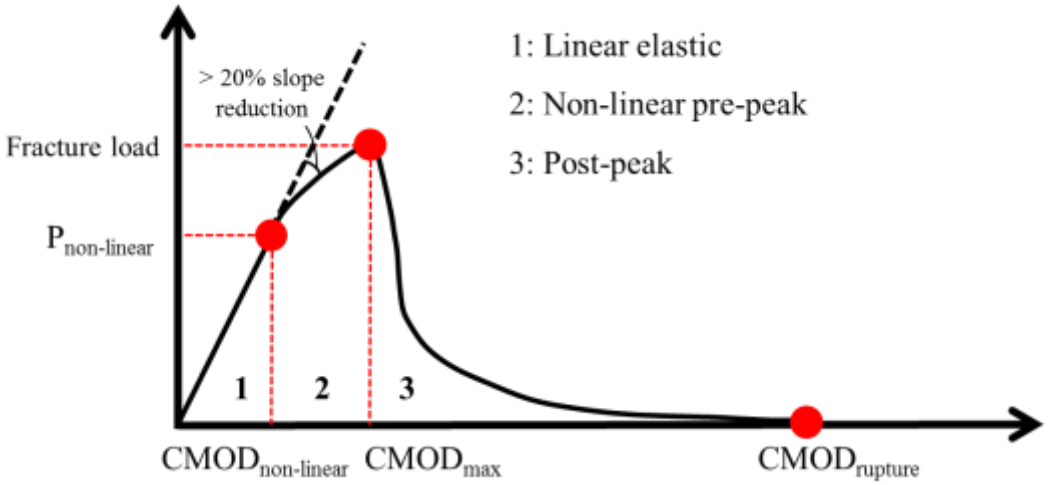

Figure 3.13 - Different loading stages in a typical load-CMOD response curve of cement paste notched beam: linear elastic, non-linear pre-peak, and post-peak

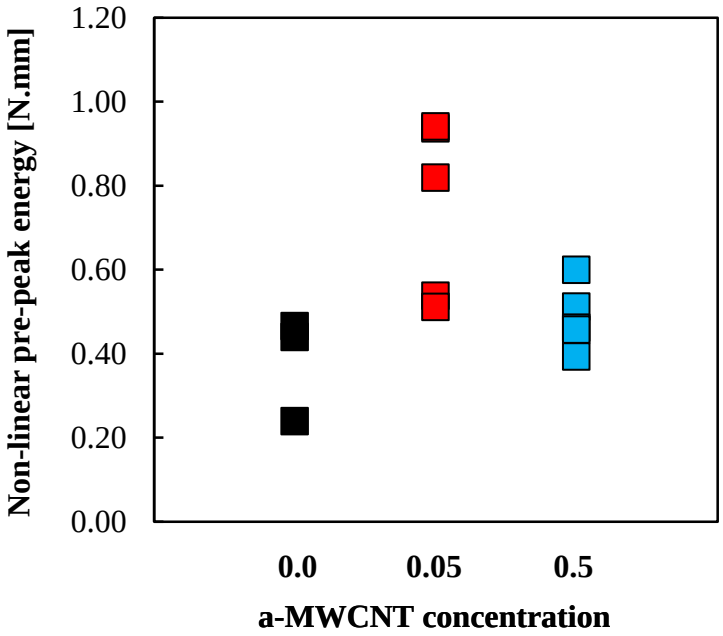

Figure 3.14 - Energy absorbed by notched beams specimens during non-linear pre-peak portion of load-CMOD response curves at 0.0, 0.05, and 0.5% a-MWCNTs

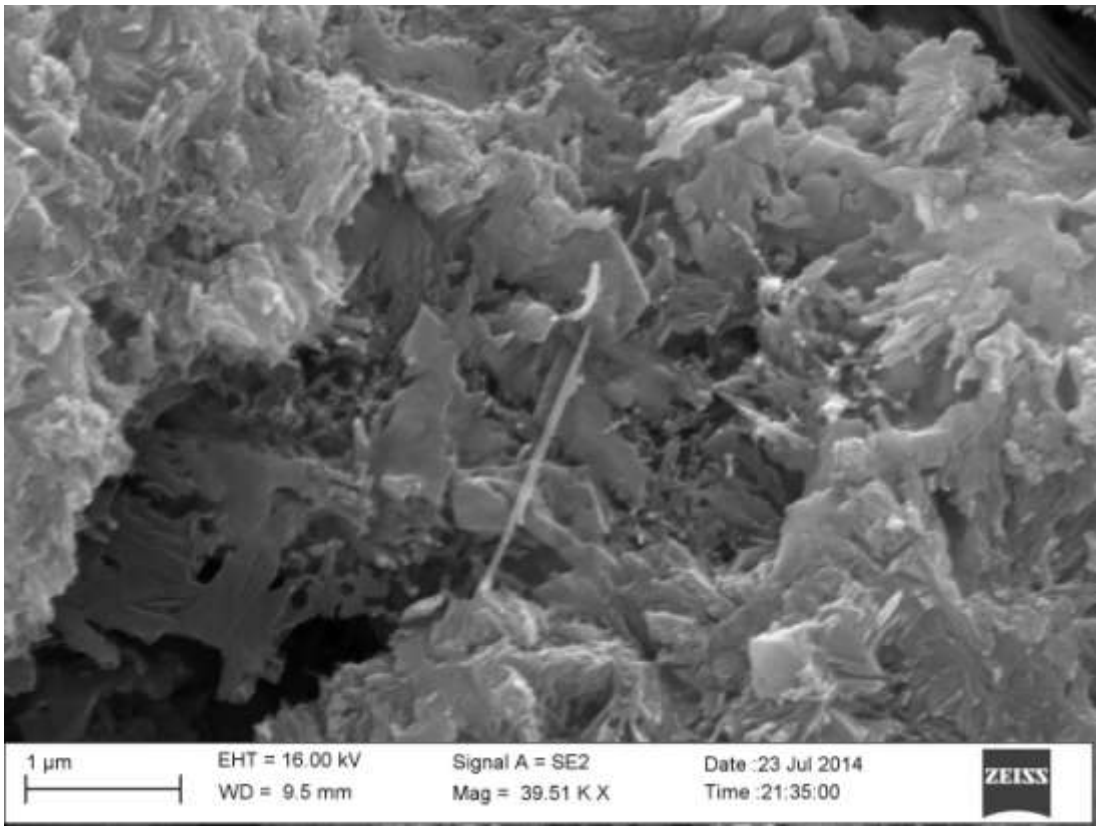

Figure 3.15 - Typical dispersion state of a-MWCNTs in cement paste at 0.05% concentration

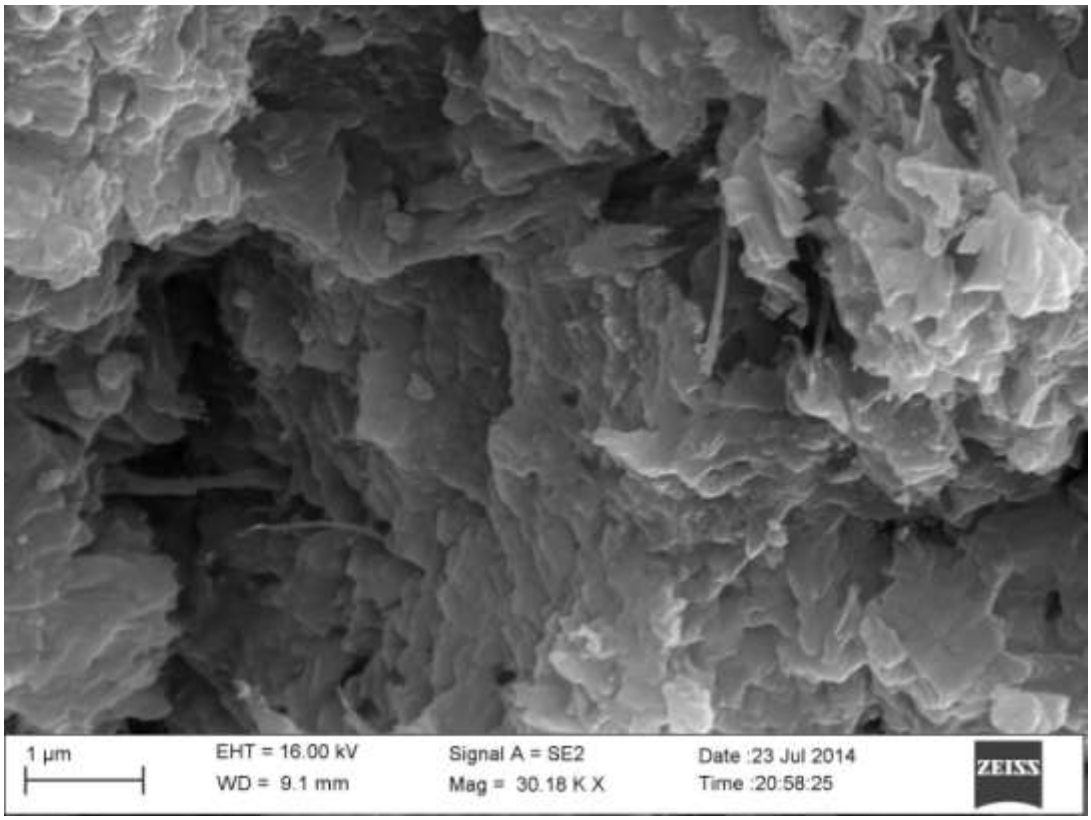

Figure 3.16 - Typical dispersion state of a-MWCNTs in cement paste at 0.5% concentration

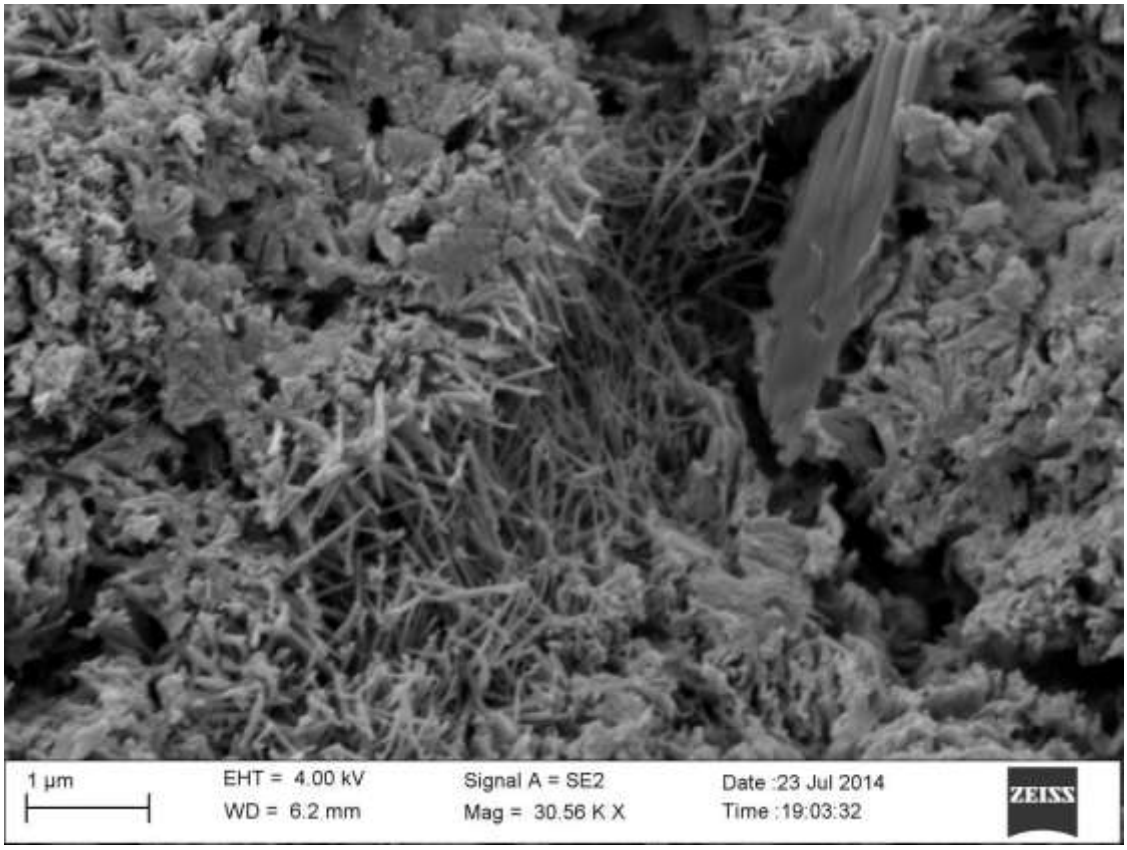

Figure 3.17- Example site of a-MWCNT cluster – obtained from notched beams reinforced with 0.05% a-MWCNTs

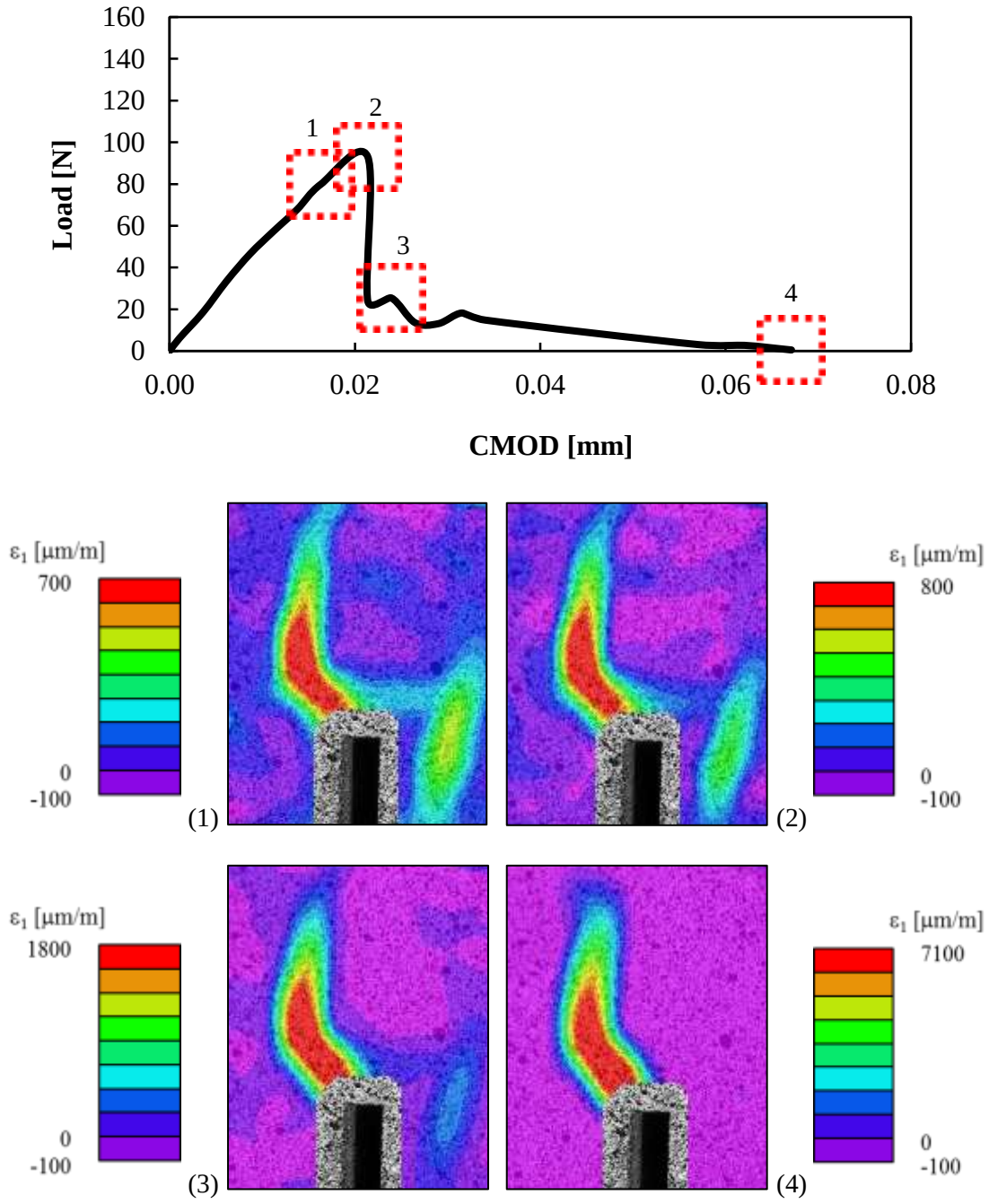

Figure 3.18 - DIC principal tensile strain maps at vicinity of notch at different stages of loading for representative unreinforced beam – coordinates for DIC maps are marked in the load-CMOD response curve of corresponding beam specimen

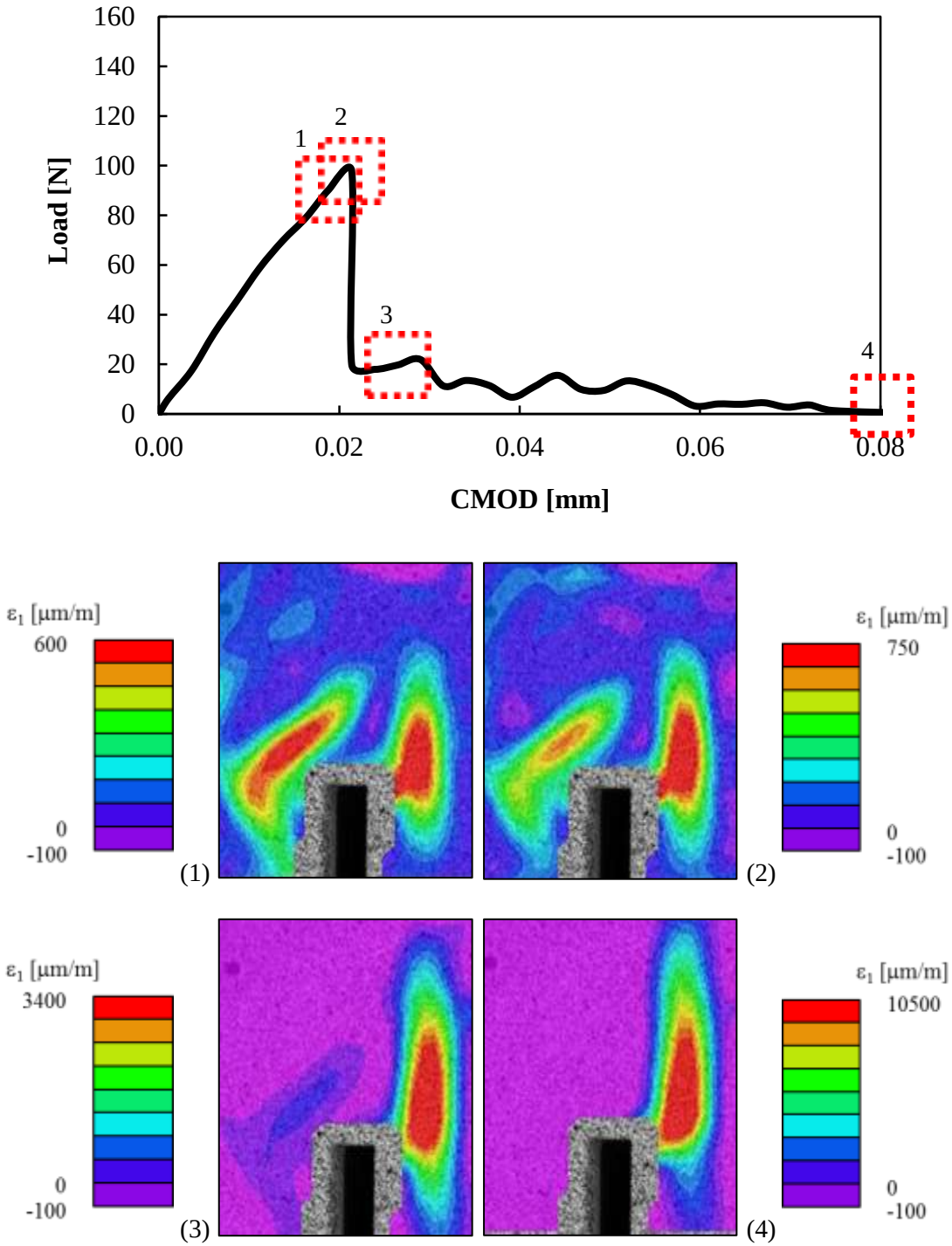

Figure 3.19 - DIC principal tensile strain maps at vicinity of notch at different stages of loading for representative unreinforced beam – coordinates for DIC maps are marked in the load-CMOD response curve of corresponding beam specimen

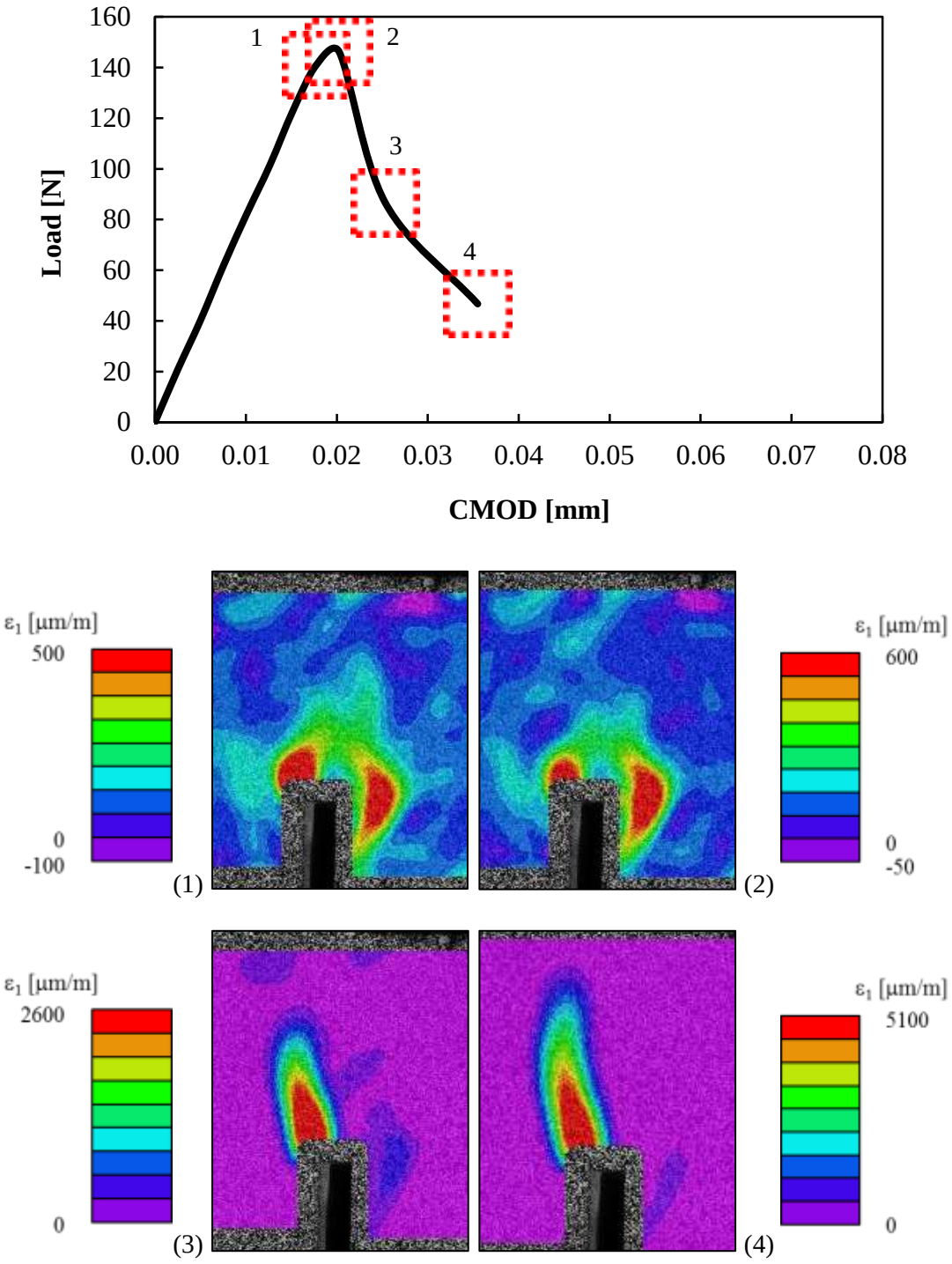

Figure 3.20 - DIC principal tensile strain maps at vicinity of notch at different stages of loading for representative nanoreinforced beam at 0.05% a-MWCNTs – coordinates for DIC maps are marked in the load-CMOD response curve of corresponding beam specimen

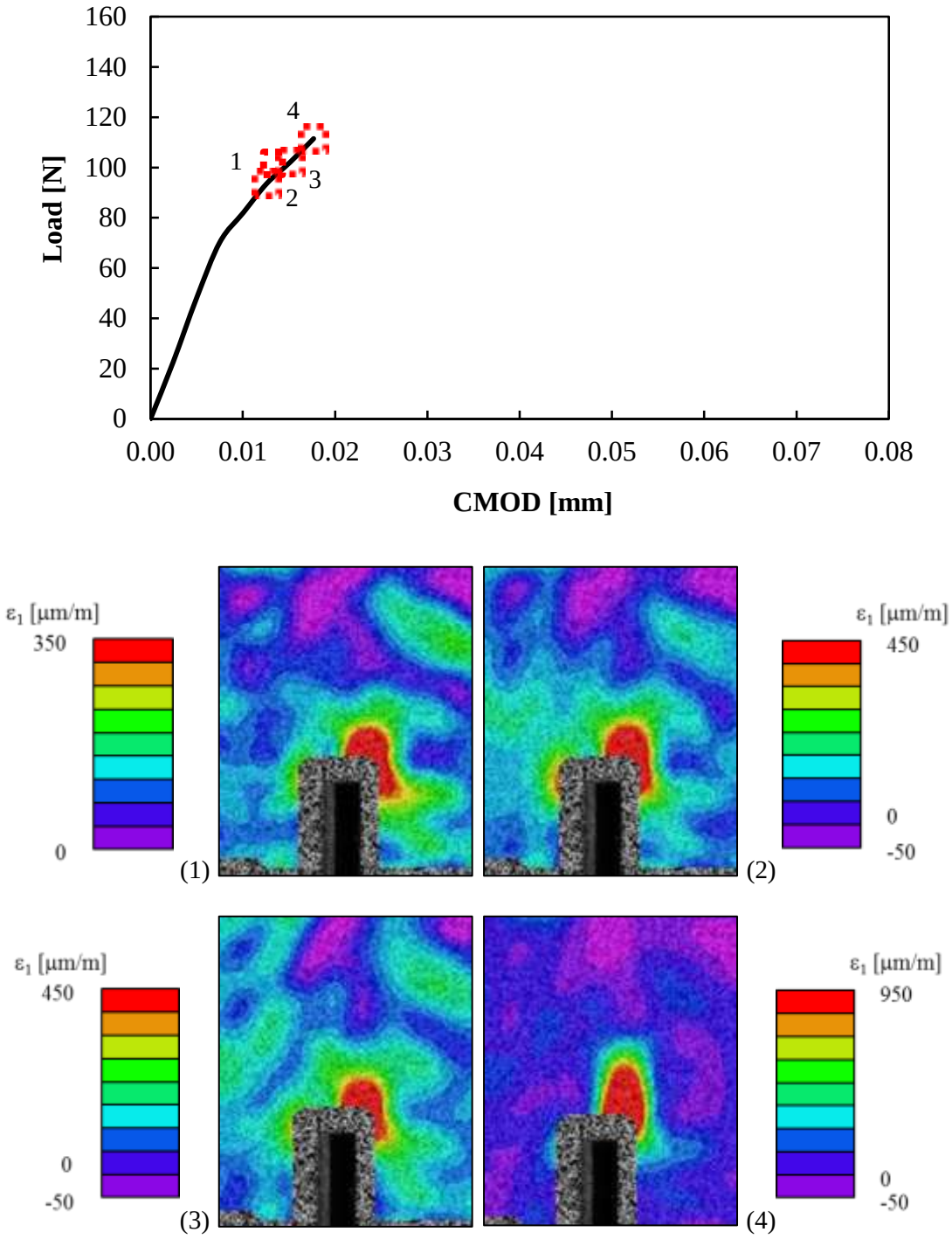

Figure 3.21 - DIC principal tensile strain maps at vicinity of notch at different stages of loading for representative nanoreinforced beam at 0.05% a-MWCNTs – coordinates for DIC maps are marked in the load-CMOD response curve of corresponding beam specimen

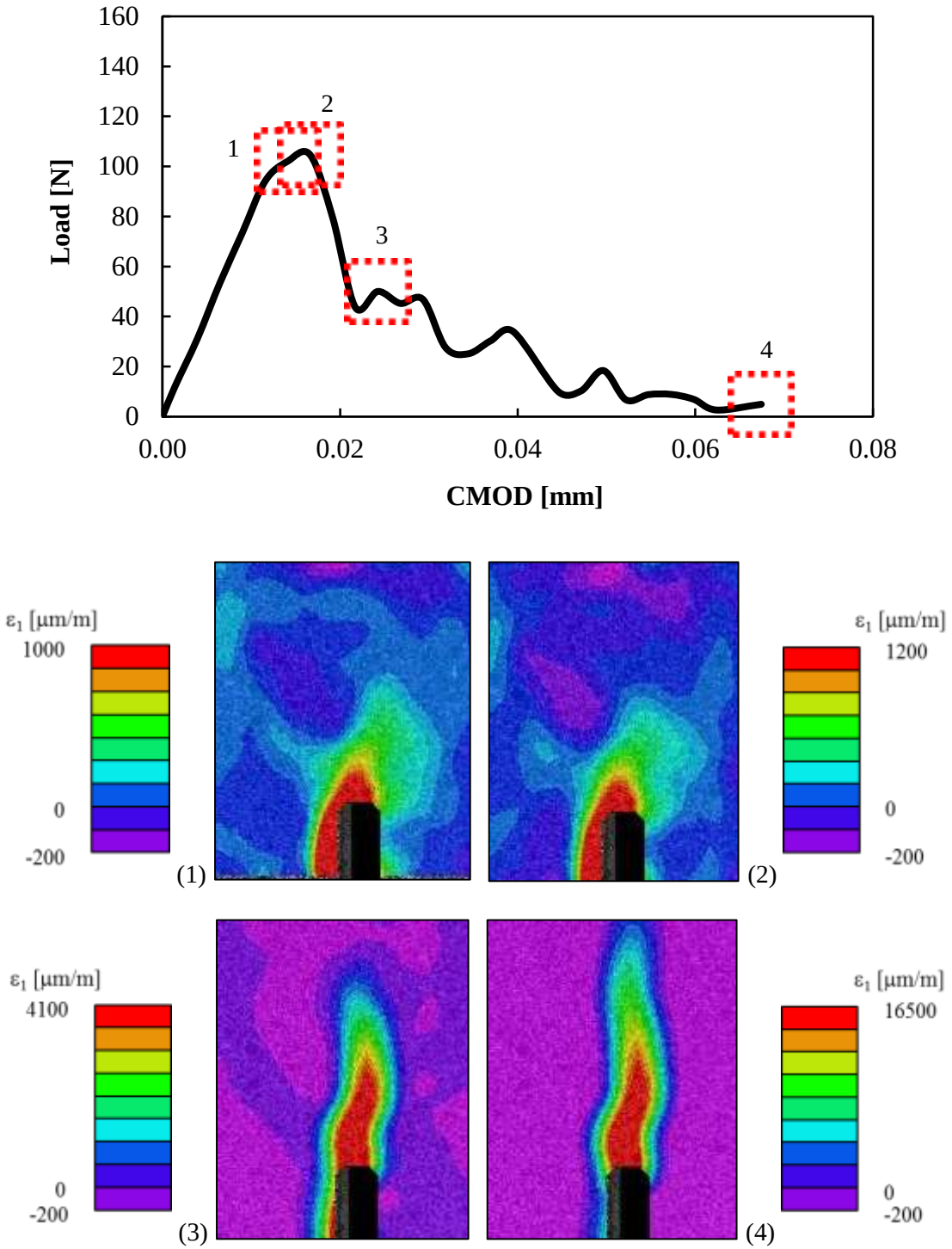

Figure 3.22 - DIC principal tensile strain maps at vicinity of notch at different stages of loading for representative nanoreinforced beam at 0.5% a-MWCNTs – coordinates for DIC maps are marked in the load-CMOD response curve of corresponding beam specimen

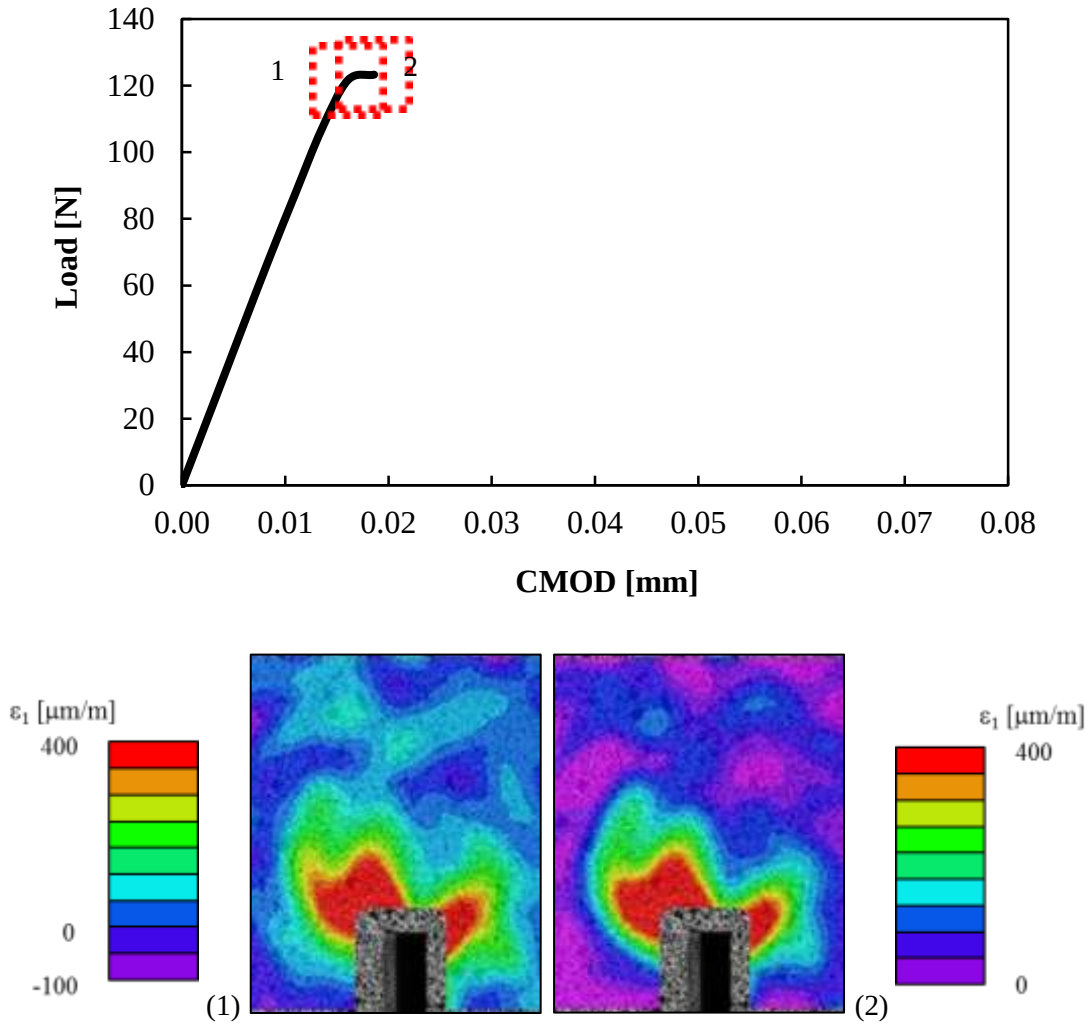

Figure 3.23 - DIC principal tensile strain maps at vicinity of notch at different stages of loading for representative nanoreinforced beam at 0.5% a-MWCNTs – coordinates for DIC maps are marked in the load-CMOD response curve of corresponding beam specimen

CHAPTER 4

GRAPHENE NANO-PLATELETS AS NANOREINFORCEMENT FOR CEMENT COMPOSITES

ABSTRACT

In this chapter, the effects of incorporating GNPs as nanoreinforcement for cement composites are investigated with respect to salient mechanical properties. Similar to MWCNTs, the two key requirements to exploit GNPs as nanoreinforcement are uniform dispersion and effective embedment in cement composite matrices. The effects of three dispersion techniques, namely, ultrasonication, surfactant-coating, and acid-etching on the compressive strength and microstructure of GNP-mortar cubes were investigated to devise a suitable technique to manufacture of GNP-reinforced cement composites. Effective acid-etching, i.e., attachment of carboxyl (-COOH) and hydroxyl (-OH) functional groups on the surface of GNPs, was verified using Raman and Fourier-transform infrared spectroscopy analysis. Dispersion in aqueous suspensions was evaluated using dynamic light scattering analysis. The compressive strength characterization of plain and GNP-reinforced cement mortar cubes served as a means to assess dispersion and chemical affinity of GNPs in the composite matrix. Dispersion and embedment of GNPs in mortar was further studied by means of SEM analysis of fracture surfaces in failed cubes. Surfactant-coating was selected as a suitable technique to manufacture of GNP-cement nanocomposites. It is shown that the incorporation of 0.05% of surfactant-coated GNPs (by weight of cement) resulted in an increase in the average compressive strength of mortar cubes of 28%. The effectiveness of the functionalization technique was further verified via three-point bending tests on cement paste notched beams. When using 0.05% of surfactant-coated GNPs, the flexural strength and stiffness increased on average by 39%, 109%, respectively, thus confirming the potential of surfactant-coating as a suitable functionalization technique for GNP reinforcement in cement composites.

4.1 Introduction

Due to their superior physical and mechanical properties graphitic nanoparticles in the form of carbon nanotubes (CNTs) and GNPs, hold promise as potential nanoreinforcement for cement matrices [Makar 2004, Lee 2008]. Previous research focused mainly on MWCNTs and considerable improvements in the properties of cement composites (including paste and mortar) were reported [Parveen 2013]. For example, the incorporation of MWCNTs concentrations in the range of 0.05-1% (by weight of cement) was found to improve the average compressive strength of cement paste blocks by 97% [Nasibulina 2012], the average flexural strength of cement paste beams by 30% [Luo 2009], and the average Young's modulus of cement paste (used in notched beams) by 45% [Konsta-Gdoutos 2010].

Little research has been reported on the use of graphene as nanoreinforcement for cement composites [Lv 2013, Alkhateb 2014, and Sedaghat 2014]. Graphene consists of a one atom-thick 2D sheet structure made of carbon atoms that are densely packed in a sp^2-bonded atomic-scale hexagonal pattern. GNPs exhibit extraordinary mechanical properties such as ultra-high Young's modulus (~1 TPa), tensile strength (130 GPa), light weight (0.77 mg/m^2, i.e., about 0.001% of the weight of 1 m^2 of standard paper sheets), thermal conductivity (~5000 $W.m^{-1}\cdot K^{-1}$, about five times higher than copper) and electrical conductivity (electron mobility of up to 200,000 $cm^2.V^{-1}.s^{-1}$) [Lee 2008]. In addition, GNPs possess a large ratio of exposed surface area to weight (see specific surface area in Table 8.1), thus lending themselves to interact with surrounding and chemically affine cement matrices. Similar to CNTs, GNPs exhibit a strong self-

aggregation tendency due to existence of attractive van der Waals forces among graphene sheets [Li 2008], which make their dispersion in cement matrices a major challenge. In addition, due to their small size, GNPs cannot be physically embedded with cement matrices through conventional mechanical anchorage such as for the case of steel fibers with hooked ends. Therefore, to create viable GNP-reinforced cement composites, measures must be devised to enable the formation of interfacial chemical bonds between GNPs and cement hydrates to facilitate load transfer (i.e., to provide crack- and defect-bridging capabilities that benefit damage tolerance).

Alkhateb et al. [2014] investigated the effects of pristine and acid-etched GNPs on the microstructure and the Young's and shear modulus of cement paste cubes. Pristine and acid-etched GNPs at 0.5% concentration (by weight of cement; it is noted that GNP concentrations are reported herein with respect to the cement content in weight) were dispersed in water via three-minute ultrasonication, and the resulting suspensions were used to fabricate 2-cm GNP-reinforced cement paste cubes. Molecular Dynamics (MD) analysis showed that the attachment of carboxyl (-COOH) and hydroxyl (-OH) groups (assuming that the functional groups cover about 18% of the GNP surface) produces an increase in the interfacial bond strength between GNPs and calcium silicate hydrate (C-S-H) by about 10 times. Resonant Ultrasound Spectroscopy (RUS) analysis performed on GNP-cement paste cubes showed that the addition of 0.5% of pristine and acid-etched GNPs resulted in increased longitudinal and shear moduli of cement paste by 6% and 21%, and 23% and 37%, respectively.

Sedaghat et al. [2014] studied the effects of adding pristine GNPs on the electrical conductivity and thermal diffusivity of cement paste. GNPs were incorporated in cement paste by simple mechanical mixing for three minutes. It was found that the addition of 1% and 10% of pristine GNPs resulted in an increase in electrical conductivity by three and six orders of magnitude, respectively, thus changing the electrical nature of cement paste from insulating to semi-conducting. In addition, the incorporation of 10% of GNPs determined an increase in thermal diffusivity by about 75% and 60% at a temperature of 25^{o}C and 400^{o}C, respectively.

Lv et al. [2013] investigated the effects of incorporating acid-etched GNPs on the compressive and flexural strength of cement mortar beams, and tensile strength of mortar dumbbell-shaped specimens. The GNPs were functionalized by exposure to sulfuric acid (H_2SO_4), potassium permanganate ($KMnO_4$), sodium nitrate ($NaNO_3$), and hydrogen peroxide (H_2O_2), increasing the relative oxygen content of GNPs by about 30%. The acid-etched GNPs were dispersed in water through ultrasonication for one hour. The tensile and flexural strength of cement mortar were enhanced as the GNP concentration was increased from 0.01 to 0.03%. However, further increasing the GNP concentration to 0.04 and 0.05% produced a decrease in strength. For example, adding 0.03% of GNPs resulted in higher average 28-day tensile and flexural strength by 78.6 and 60.7%, respectively. The compressive strength was enhanced by increasing the GNP concentration up to 0.05%. For example, adding 0.05% of GNPs resulted in an increase in the average 28-day compressive strength by 47.9%.

This chapter reports on research aimed at investigating the reinforcing effects of well-dispersed and chemically affine GNPs in cement paste and mortar. GNPs were introduced to the cement mixtures in dispersed phase in the form of aqueous suspensions. Three main-stream dispersion techniques that were also tested for MWCNT-reinforced cement composites (as reported in Chapters 2 and 3), namely, ultrasonication [Tyson 2011, Collin 2012], surfactant-coating [Luo 2009, Sobolkina 2012], and acid-etching [Li 2005, Musso 2009], were used to prepare GNP aqueous suspensions. Stable dispersion of GNPs as aqueous suspensions was assessed via dynamic light scattering (DLS) analysis. GNP-reinforced mortar cubes with 0.05 and 0.5% of GNPs were fabricated and tested under compression loading. The compressive strength and consistency thereof were used as an indirect measure of GNPs dispersion (and consistency thereof) within the cement matrix. The embedment of GNPs in the composite matrix was evaluated via scanning electron microscopy (SEM) analysis of fracture surfaces from failed cubes. Based on the experimental evidence obtained through compressive strength characterization and SEM analysis, surfactant-coating was selected as a suitable functionalization technique. In particular, the addition of 0.05% of surfactant-coated GNPs determined an increase in average compressive strength of mortar cubes of 28% compared with plain mortar counterparts. Then, the selected functionalization technique was verified with respect to the flexural strength and stiffness of cement paste notched beams tested in flexure. It was found that adding 0.05% of surfactant-coated GNPs resulted in an average increase in flexural strength and stiffness of 39% and 109%, respectively.

4.2 Materials and methods

4.2.1 Materials

The materials used in this study were Type I Ordinary Portland Cement (OPC) and standard silica sand. GNPs (Graphene Laboratories Inc., cat# SKU-NP-FL2, Calverton, NY) were used as-received. Salient physical properties of the as-received GNPs as provided by the supplier are summarized in Table 8.1. The morphology of as-received GNPs is illustrated in Figures 4.1 and 4.2.

4.2.2 Preparation of aqueous suspensions

To fabricate GNP-reinforced cement composites, GNP-aqueous suspensions were mixed with cement (and sand for the case of mortar mixtures, whereas no sand was used to prepare cement paste) in accordance with ASTM C305 [ASTM 2013]. The three dispersion techniques used are described in the following three sections.

4.2.2.1 Ultrasonication

GNPs were sonicated in deionized (DI) water at an energy rate of 22-25 W at amplitude of 50% for 20 minutes using an ultrasonic processor (S-4000 Ultrasonic Processor, Misonix, Inc., Farmingdale, NY). Ultrasonicated GNPs are herein referred to as u-GNPs.

4.2.2.2 Acid-etching

Ammonium persulfate, $(NH_4)_2S_2O_8$ (Sigma Aldrich, cat# 215589), and sulfuric acid, H_2SO_4 (Sigma Aldrich, cat# 339741), were dissolved in DI water using a magnetic

stirrer (VWR stirrer, Henry Troemner LLC., Thorofare, NJ). GNPs were then added to the aqueous solution and the resulting suspension was stirred until a clear solution was obtained. The aqueous solutions were then filtered through a 0.45 μm PVDF membrane filter (Millipore, Billerica, MA) to remove the undissolved ammonium persulfate. To facilitate the penetration of oxidants along the innermost GNP surfaces, the aqueous suspensions were sonicated for 10 minutes followed by magnetic stirring for 24 hours. The acid-etching process reduces the pH level of GNPs to about 1.0, which is not suitable for mixing with cement. Therefore, the acid-etched GNPs were washed with DI water to raise the pH level to a value of 7.0. Processed GNPs were then dried and stored as dry powder. The dried powder was added to DI water and sonicated for 20 minutes prior to incorporating the nanoreinforcement in the cement mixture. Acid-etched GNPs are herein referred to as a-GNPs.

4.2.2.3 Surfactant-coating

The surfactant used was anionic surfactant sodium deoxycholate, NaDC (Sigma Aldrich, cat# D6750). The surfactant was first dissolved in DI water by magnetic stirring at 1200 rpm until a clear solution was obtained. GNPs were then added to the solution, and the resulting suspension was sonicated for 20 minutes. A suitable surfactant/GNP weight ratio was determined by comparing the average hydrodynamic radius (AHR) of GNP aqueous suspensions prepared with different surfactant concentrations. The concentrations that were tested were selected based on the critical micelle formation concentration (CMC) of NaDC at room temperature, and the findings of Islam et al. [2003] who showed that the most suitable surfactant/CNT weight ratio for different

surfactant types was between 5 and 10. Five NaDC/GNP weight ratios, namely 1.92 (0.8 CMC), 2.40 (CMC), 3.60 (1.2 CMC), 7.00, and 10.00, were tested. Surfactant-coated GNPs are herein referred to as s-GNPs.

4.2.3 Methods

4.2.3.1 Dynamic light scattering analysis

GNP-aqueous suspensions were assessed using DLS analysis. The AHR value was used to compare the dispersion quality in GNP aqueous suspensions. DLS analysis was performed using an ALV/CGS-3 compact goniometer system (ALV-Laser Vertriebsgesellschaft m-bH, Langen/Hessen, Germany). The DLS system was equipped with a 22 mW HeNe Laser at 632 nm wavelength and high QE APD detector with photomultipliers of 1:25 sensitivity. 2 mL samples of GNP aqueous suspension were vortex-mixed prior to be examined in the DLS vat chamber. Measurements were collected at 15-second intervals for up to 10 minutes with the laser operating at full exposure level and scattering data collected at a 90^{o} scattering. Each measurement was the average of 50 runs.

4.2.3.2 Raman spectroscopy

Raman spectroscopy analysis was used to verify the creation of active sites on the surface of a-GNPs. Raman spectroscopy analysis was performed using a LabRam Confocal Raman spectrophotometer (JY Horiba, HORIBA Instruments Inc., CA) equipped with a liquid nitrogen-cooled CCD detector and He/Ne laser operating at 632

nm. Each resulting Raman spectrum was an average of five scans with integration time of 90 seconds.

4.2.3.3 FT-IR spectroscopy analysis

FT-IR analysis was used to verify the attachment of carboxyl (-COOH) and hydroxyl (-OH) functional groups on the surface of a-GNPs. FT-IR analysis was performed using a Nicolet Nexus 470 spectrometer equipped with a MCT-B detector for FT-IR analysis. Samples of pristine and a-GNPs were mixed with FT-IR grade KBr, and pressed in the form of pellets. Measurements were taken at transmission mode in a wavenumber range of 4000-1200 cm^{-1} with 4 cm^{-1} resolution. Each resulting FT-IR spectrum is the average of 16 scans.

4.2.3.4 TEM analysis

TEM analysis was used to characterize the morphology of GNPs. GNP powder was dissolved in ethanol and examined using an H-9500 HRTEM (Hitachi High Technologies America, Inc, Pleasanton, CA) following the methodology describe elsewhere [Aich 2012].

4.2.3.5 SEM analysis

SEM analysis was performed on cement composite samples extracted from fracture surfaces to collect visual evidence on the microstructure of GNP-reinforced cement composites. SEM micrographs were acquired using a Zeiss Ultra Plus Field

Emission Scanning Electron Microscope (FESEM). The test samples were oven-dried at 60^{o}C for 24 hours and gold-sputtered prior to SEM examinations.

4.2.3.6 Compression tests

GNP-aqueous suspensions were mixed with cement and sand per ASTM C305 [ASTM 2013], with mixing proportions of cement:sand:water of 1:2.75:0.5. Three GNPs concentrations, namely 0.05, 0.5 and 1%, were used. Three 50-mm mortar cubes were made for each GNP concentration in addition to three plain mortar cubes that were used as benchmark. It is noted that only the 0.05% u-GNP concentration was tested since at higher concentrations u-GNPs appeared mainly as large aggregates in water. The cube specimens were moist-cured for 24 hours, demolded and stored in saturated lime water until the age of 28 days. The compression strength tests were performed using a test frame (MTS 810 Material Testing System, MTS systems Inc., Eden Prairie, Minnesota) under displacement control mode with a displacement rate of 0.625 mm/min.

4.2.3.7 Notched beam tests

Based on the outcomes of compressive strength tests and SEM analysis, surfactant-coating was selected as the most suitable functionalization technique among the three methods tested, as discussed in Section 4.3.3. Functionalization by means of surfactant-coating was further tested to investigate the flexural strength and stiffness of GNP-reinforced cement paste beams. Three-point bending tests were performed on 20×20×80 mm single-edge notched beam specimens. Three specimens per group (0, 0.05 and 0.5% of s-GNPs) were cast following the mixing protocol described previously, moist-cured

for 24 hours, demolded, and stored in saturated lime water until the age of 28 days. A water-cooled diamond saw was used to cut a 6×2 mm notch at the mid-span section of each specimen. A clip gage was used to measure the crack mouth opening displacement (CMOD). The tests were performed using a test under a displacement rate of 0.01 mm/minute.

4.3 Results and discussion

In this section, first the most suitable surfactant/GNP weight ratio is selected by comparing the AHR values of s-GNP aqueous dispersions prepared with different surfactant concentrations. This surfactant/GNP weight ratio was used to fabricate s-GNP-reinforced mortar cubes. The compression test results for different dispersion techniques are then discussed, and representative SEM micrographs illustrating the typical dispersion state and embedment of GNPs in cement mortar for different dispersion techniques are shown. The formation of the necessary (-COOH) and (-OH) functional groups on the surface of GNPs is verified using Raman and FT-IR spectroscopy analysis. Surfactant-coating was selected as the most suitable functionalization technique among those tested, and was further verified through notched beam tests. The notched beam test results are then presented, and the effects of the addition of s-GNPs on the flexural strength and stiffness of cement paste are discussed.

4.3.1 Surfactant/GNP weight ratio

The surfactant/GNP weight ratio was selected by comparing the AHR values of GNP aqueous suspensions containing different surfactant concentrations. AHR values for

GNP aqueous suspensions with different surfactant concentrations are presented in Figure 4.3. The highest level of dispersion is associated with the minimum AHR value. Increasing the surfactant concentration until a surfactant/GNP weight ratio of 7.0 resulted in a progressive decrease in the AHR value to a minimum of 102.51 ± 12.59 nm. Therefore a surfactant/GNP weight ratio of 7.0 was selected for s-GNP-reinforced cement composites.

4.3.2 DLS characterization of GNP-aqueous suspensions

The effectiveness of the different dispersion techniques were compared based on the AHR values of their corresponding GNP aqueous suspension. Figure 4.4 compares the AHR values for u-GNP, a-GNP, and s-GNP. Before the application of ultrasonication the majority of GNPs particles were larger than the largest particle detectable via DLS. The AHR values of aqueous suspensions containing u-GNP, a-GNP, and s-GNP were 215 ± 25 nm (average ± standard deviation), 166 ± 22 nm, and 55 ± 1 nm, respectively. The highest level of dispersion was achieved through surfactant-coating. In addition, the standard deviation value for s-GNPs was significantly smaller than that for u-GNPs and a-GNPs, highlighting the effectiveness of surfactant-coating in improving the homogeneity of the s-GNP aqueous suspensions.

4.3.3 Compressive strength and microstructure of cement mortar

The effect of dispersion technique and GNPs concentration on the compressive strength of cement mortar was investigated via compression tests on 50-mm cubes. The test results for different functionalization techniques and GNP concentrations are

presented in Figure 4.5. Compression test results for all specimens of different groups are shown in Table C-2.

4.3.3.1 Ultrasonication

The average compressive strength for unreinforced and u-GNP-reinforced mortar cubes was 23.3 ± 3.76 MPa (average ± standard deviation) and 20.3 ± 0.52 MPa, respectively. The standard deviation parameter is used as a measure of data variation between samples of a given group. Standard deviation values for all GNP-reinforced cubes were close to that of the plain mortar specimens. The incorporation of 0.05% of u-GNPs produced a decrease in the average compressive strength by 13% (Figure 4.5). A SEM micrograph showing the typical microstructure of u-GNP-reinforced mortar is presented in Figure 4.6. GNPs were typically found as large agglomerates, indicating that a poor dispersion was achieved through ultrasonication. The majority of the graphene sheets in a GNP agglomerate have minimal contact with cement hydrates, hindering nanoreinforcement-cement matrix bonding (Figure 4.6). It is concluded that poorly dispersed u-GNPs with minimal exposure to cement paste act as sites of discontinuity or "defects", facilitating crack development under mechanical stress and, consequently, reducing the compressive strength of the nanoreinforced mortar.

4.3.3.2 Surfactant-coating

The average compressive strength for s-GNP-reinforced mortar cubes with 0.05, 0.5, and 1% of s-GNPs was 29.9 ± 3.55 MPa (average ± standard deviation), 14.7 ± 4.23 MPa, and 3.9 ± 0.53 MPa, respectively. The incorporation of s-GNPs at 0.05%

concentration resulted in an average increase in compressive strength of 28%. Conversely, further increasing the GNP concentration to 0.5 and 1% resulted in a decrease in the average compressive strength of 37% and 83%, respectively, compared with control samples.

The typical microstructure of s-GNP-reinforced mortar at 0.05, 0.5, and 1% concentration is illustrated in Figure 4.7 through Figure 4.9. It is noted that using high voltages (denoted as electron high tension (EHT) in SEM micrographs), for example 19.00 kV made some GNPs (most likely GNPs with fewer number of graphene sheets) to appear as translucent sheets in the SEM images. s-GNPs were typically found as individual GNPs indicating that a good dispersion was obtained for all GNP concentrations. However, s-GNPs agglomerates were found more frequently on the fracture surfaces of samples containing 0.5 and 1% of s-GNPs. At 0.05% of s-GNPs the majority of s-GNPs were coated by or embedded in cement paste, suggesting that some interfacial bonding developed between GNPs and cement hydrates. To better illustrate this aspect, another SEM micrograph obtained from the fracture surface of a sample containing 0.05% of s-GNPs is presented in Figure 4.10. A potential effect of s-GNPs in bridging across nano- and micro-scale defects is illustrated in Figure 4.11.

The presence of high amounts of needle like-structures was noted on the fracture surfaces of mortar cubes containing 0.5 and 1% of s-GNPs (Figures 4.8 and 4.9). These needle-like structures were mostly found in the vicinity of s-GNPs, obstructing contact between GNPs and cement paste. The formation of these structures at higher s-GNP

concentrations can be attributed to amount of surfactant embedded in these samples. Although the surfactant/GNP weight ratio was constant at all s-GNP concentrations, the absolute amount of surfactant introduced in the mixture increased by 10 and 20 times for 0.5 and 1% s-GNPs concentrations, respectively, compared with the 0.05% concentration. It is hypothesized that at 0.5 and 1% s-GNP concentrations, the amount of surfactant added to the mixture served to coat GNPs but also participated in undesired reactions that resulted in the formation of the needle-like structures observed in Figures 4.8 and 4.9. This phenomenon may hinder the cement hydration process by consuming the water required for hydration, or disturb the integrity of the matrix by introducing sites of discontinuity (defects). In fact, it was noted during the fabrication of s-GNP-reinforced mortar cubes that increasing the s-GNP concentration (i.e., the absolute amount of surfactant) was associated with a significant reduction of the workability, such that a proper compaction was more difficult to achieve. Therefore, the strength loss can also be attributed to defects resulting from a less effective compaction due to a reduced workability.

The significant strength loss observed for higher s-GNP concentrations was further investigated by evaluating the sole effect of surfactant on the compressive strength of mortar. A summary of the test results are presented in Table 4-1. Test results for all specimens of different groups are shown in Table 8-3. The average compressive strength for mortar cubes containing surfactant amounts of 0, 2.5, 25, and 50 g were 45.5 ± 0.95 MPa (average ± standard deviation), 29.21 ± 2.77 MPa, 22.75 ± 1.35 MPa, and 16.38 ± 1.94 MPa, respectively. In the absence of GNPs, the addition of surfactant led to

strength drops similar to those observed for samples having s-GNPs, thus confirming the negative effect of high surfactant contents.

4.3.3.3 Acid-etching

The average compressive strength for mortar cubes with 0.05, 0.5, and 1% concentration of a-GNPs was 16.3 ± 5.28 MPa (average ± standard deviation), 16.4 ± 3.30 MPa, and 12.8 ± 0.58 MPa, respectively. The incorporation of a-GNPs at 0.05, 0.5, and 1% concentration produced a decrease in compressive strength of 30%, 30%, and 45%, respectively, compared with that of plain mortar. The typical dispersion state of a-GNPs at 0.05, 0.5, and 1% concentrations are illustrated in Figure 4.12 through Figure 4.14. a-GNPs were mostly found as large agglomerates with minimal contact with cement hydrates. It is concluded that similar to u-GNPs, a-GNPs are not effective as they introduce defect sites in the composite matrix.

4.3.3.4 Formation of functional groups on a-GNPs

The formation of necessary carboxyl (-COOH) and hydroxyl (-OH) functional groups on the surface of a-GNPs was verified using Raman and FT-IR spectroscopy analysis. Functional groups attach to the surface of GNPs from sites of carbon atoms with free electrons (active carbons or defects), which are capable of forming new reactions. Mixing GNPs with strong acids during the etching process is expected to damage some of the covalent bonds between carbon atoms on the GNP surface, and increase the amount of chemically active carbon atoms . The creation of active carbon sites through acid-etching was verified using Raman spectroscopy analysis. Figure 4.15 compares the

Raman spectra of pristine and a-GNPs. The peaks near 1580 cm^{-1} (G band) are the signature of graphitic materials and represent C-C bonds. The peaks near 1350 cm^{-1} (D band, associated with defects) represent C-O stretches. The ratio between the intensity of the two peaks, or I(D)/I(G), is typically used to compare the amount of defects between two samples. As shown in the inset plot in Figure 4.15, the I(D)/I(G) ratio was marginally increased from 0.19 for pristine GNPs to 0.21 for a-GNPs, indicating that the acid-functionalization scheme was ineffective in creating of active carbon sites.

To corroborate the results from Raman spectroscopy analysis, the attachment of (-COOH) and (-OH) groups on the surface of a-GNPs was verified using FT-IR spectroscopy analysis. FT-IR spectra of pristine and a-GNP are presented in Figure 4.16. The peaks near 1580 cm^{-1} correspond to C-C bonds and peaks near 1725 cm^{-1} correspond to C-O stretches present in the functional groups. No peaks associated with (-COOH) or (-OH) groups were detected through FT-IR analysis, indicating that functional groups were not attached to the surface of a-GNPs, and thus confirming the findings from Raman spectroscopy analysis. It can be concluded that acid-etching was ineffective in enabling the formation of functional groups on the surface of a-GNPs. This explains the poor dispersion of a-GNPs in cement mortar (Figures 4.12-4.14), and the associated reduction of compressive strength compared with plain mortar cubes (Figure 4.5).

4.3.4 Effect of s-GNPs and flexural strength and stiffness of cement paste

The effect of well-dispersed and chemically-affine s-GNPs on the flexural strength and stiffness of cement paste was evaluated by performing three-point bending

tests on notched beams. Salient test results are summarized in Table 4.3. Notched beam test results for all specimens of different groups are shown in Table X. Representative examples of load-CMOD curves for plain and s-GNP-reinforced beams are presented in Figure 4.17. The average failure load (flexural strength) for s-GNP concentrations of 0.0, 0.05, and 0.5% was 110.9 ± 3.33 N (average ± standard deviation), 153.8 ± 12.6 N, and 133.0 ± 9.36 N, respectively. The addition of 0.05 and 0.5% of s-GNPs resulted in increased average failure load (flexural strength) by 39% and 20%, respectively, compared with plain cement paste beams. The flexural stiffness, which is estimated as the slope of the linear (elastic) portion of the load-CMOD curve, was more affected by the addition of s-GNPs. The flexural stiffness of cement paste beams with 0.0, 0.05, and 0.5% concentration of s-GNP was 5476 ± 561 N/mm (average ± standard deviation), 11454 ± 2529 N/mm, and 9920 ± 1660 N/mm, respectively. Therefore, the incorporation of 0.05 and 0.5% of s-GNPs resulted in an average increase in stiffness of 109% and 81%, respectively.

The improvements in flexural strength and stiffness can be attributed to different possible mechanisms including composite action, porosity reduction, and possible contribution of crack-bridging effect of GNPs. Due to their high Young's modulus (~ 1TPa), the incorporation of small amounts of GNPs can lead to an increase in the stiffness of nanoreinforced cement paste. In addition, due to their small size (see Table 8.1), GNPs can fill in micro- (<2nm) and meso-pores (2-50 nm) and reduce porosity. For example, it was shown that the incorporation of MWCNTs can result in a decrease in the porosity of cement paste [Konsta-Gdoutos 2010] and mortar [Li 2005]. Porosity

reduction can determine a significant increase in the Young's modulus of cement composites. For example, Kendall et al. [1983] showed that reducing the porosity volume fraction from 25% to 7.5% nearly doubled the Young's modulus of cement paste beams. The observed enhancements can also be partially attributed to a crack-arrest effect of GNPs. In fact, GNPs may contribute to controlling the growth of smaller cracks through mechanisms similar to those observed for conventional fibers at larger scales. Further research is required to evaluate the contribution of different possible mechanisms responsible for the improvements in flexural strength and stiffness observed for the nanoreinforced notched beams.

4.4 Conclusions

In the research presented in this chapter, the effect of different dispersion techniques, namely, ultrasonication, surfactant-coating, and acid-etching, on the mechanical properties and microstructure of GNP-reinforced cement mortar and paste was investigated. The following conclusions are drawn:

(1) Ultrasonication, in the absence of surface functionalization, leads to poor dispersion of GNPs in cement mortar. Poorly dispersed u-GNPs have poor affinity with cement hydrates and introduce defect sites, resulting in reduced compressive strength.

(2) Surfactant-coating of GNPs leads to uniform dispersion irrespective of the s-GNPs concentration. However, increasing the s-GNPs concentration results in an increased number of s-GNP agglomerates. s-GNPs exhibited chemical affinity

with cement hydrates. The addition of 0.05% of s-GNPs produced an increase in the average compressive strength of cement mortar of 28% compared with plain mortar. The same s-GNPs concentration produced an average increase in the flexural strength and stiffness of cement paste notched beams of 39% and 109%, respectively.

(3) In addition to the surfactant/GNP weight ratio, the absolute amount of surfactant introduced in the cement composite mixture plays a role on the final properties of the composites. The incorporation of excess NaDC resulted in a reduced workability of the cementitious mixture. The formation of areas with numerous surfactant crystals was associated with a reduced compressive strength.

(4) Acid-etching was ineffective in creating carboxyl (-COOH) and hydroxyl (-OH) functional groups on the surface of GNPs. As a result, the incorporation of a-GNPs leads to a poor dispersion in mortar. a-GNPs had poor chemical affinity with cement hydrates and produced defect sites decreasing the compressive strength of cement mortar.

4.5 References

Aich N., Zohhadi N., Khan I.A., Matta F., Ziehl P., and Saleh N.B., Applied TEM apprach for micro/nanostructural characterization of carbon nanotube reinforced cementitious composites. Journal of Research Updates in Polymer Science 2012: 1: 14-23.

ASTM Standard C305, 2013, "Standard practice for mechanical mixing of hydraulic cement pastes and mortars of plastic consistency" ASTM International, West Conshohocken, PA, 2013, DOI: 10.1520/C0305, www.astm.org

Bentur A., and Mindess S., Fibre reinforced cementitious composites. CRC Press, 2006.

Collins F., Lambert J., and Duan W.H., The influences of admixtures on the dispersion, workability, and strength of carbon nanotube–OPC paste mixtures, Cement Concrete Comp. 2012: 34: 201-207.

Islam M.F., Rojas E., Bergey D.M., Johnson A.T., and Yodh A.G., High weight fraction surfactant solubilization of single-wall carbon nanotubes in water, Nano. Lett. 2003: 3: 269-273.

Konsta-Gdoutos M.S., Metaxa Z.S., and Shah S.P., Highly dispersed carbon nanotube reinforced cement based materials, Cement Concrete Res 2010: 40: 1052-1059.

Kowald T., and Trettin R., Influence of surface-modified carbon nanotubes on ultrahigh performance concrete, In Proceedings of the International Symposium on Ultra High Performance Concrete: 2004: pp. 195-202.

Lee C., Wei X., Kysar J.W., and Hone J., Measurement of the elastic properties and intrinsic strength of monolayer graphene, SCIENCE 2008: 321: 385-388.

Li D., Müller M.B., Gilje S., Kaner R.B., and Wallace G.G., Processable aqueous dispersions of graphene nanosheets, Nat Nanotechnol 2008: 3: 101-105.

Li G.Y., Wang P.M., and Zhao X., Mechanical behavior and microstructure of cement composites incorporating surface-treated multi-walled carbon nanotubes, Carbon 2005: 43: 1239-1245.

Luo J., Duan Z., and Li H., The influence of surfactants on the processing of multi-walled carbon nanotubes in reinforced cement matrix composites, Phys Status Solidi (a): 2009: 206: 2783-2790.

Lv S., Ma Y., Qiu C., Sun T., Liu J., and Zhou Q., Effect of graphene oxide nanosheets of microstructure and mechanical properties of cement composites, Const Build Mat 2013: 49: 121-127.

Makar J.M., and Beaudoin J.J., Carbon nanotubes and their application in the construction industry, Special Publication-Royal Society of Chemistry 2004: 292: 331-342.

Manzur T., and Yazdani N., Strength enhancement of cement mortar with carbon nanotubes, Transp. Res. Record: Journal of the Transportation Research Board 2010: 2142: 102-108.

Nasibulina L.I., Anoshkin I.V., Nasibulin A.G., Cwirzen A., Penttala V., and Kauppinen E.I., Effect of carbon nanotube aqueous dispersion quality on mechanical properties of cement composite, J Nanomater 2012: 169262.

Parveen S., Rana S., and Fangueiro R., A review on nanomaterial dispersion, microstructure and mechanical properties of carbon nanotube and nanofiber reinforced cementitious composites, J Nanomater 2013: 80.

Raki L., Beaudoin J., Alizadeh R., Makar J., and Sato T., Cement and concrete nanoscience and nanotechnology, Materials 2010: 3: 918-942.

Sedaghat A., Ram M.K., Zayed A., Kamal R., and Shanahan N., Investigation of physical properties of graphene-cement composite for structural applications, Open J Comp Mats 2014: 4:12-21.

Sobolkina A., Mechtcherine V., Khavrus V., Maier D., Mende M., Ritschel M., and Leonhardt A., Dispersion of carbon nanotubes and its influence on the mechanical properties of the cement matrix, Cement Concrete Comp 2012: 34:1104-1113.

Strano M.S., Moore V.C., Miller M.K., Allen M.J., Haroz E.H., Kittrell C., Hauge R.H., and Smalley R.E., The role of surfactant adsorption during ultrasonication in the dispersion of single-walled carbon nanotubes, J Nanosci Nanotechno 2003: 3: 81-86.

Tyson B.M., Abu Al-Rub R.K., Yazdanbakhsh A., and Grasley Z., Carbon nanotubes and carbon nanofibers for enhancing the mechanical properties of nanocomposite cementitious materials, J Mater Civil Eng 2011: 23: 1028-1035.

4.6 Tables

Table 4.1 - Compression test results for mortar cubes containing different surfactant (NaDC) amount

NaDC amount [g]	Compressive strength [MPa]
0.0	45.5 ± 0.95
2.5	29.2 ± 2.77
25.0	22.7 ± 1.35
50.0	16.4 ± 1.94

Table 4.2 - Notched beam test results

Group	Failure load [N]	Stiffness [N/mm]
Control (0%)	110.9 ± 3.33	5476 ± 560
s-GNP-0.05%	153.8 ± 12.59	11454 ± 2529
s-GNP-0.5%	133.0 ± 9.36	9920 ± 795

4.7 Figures

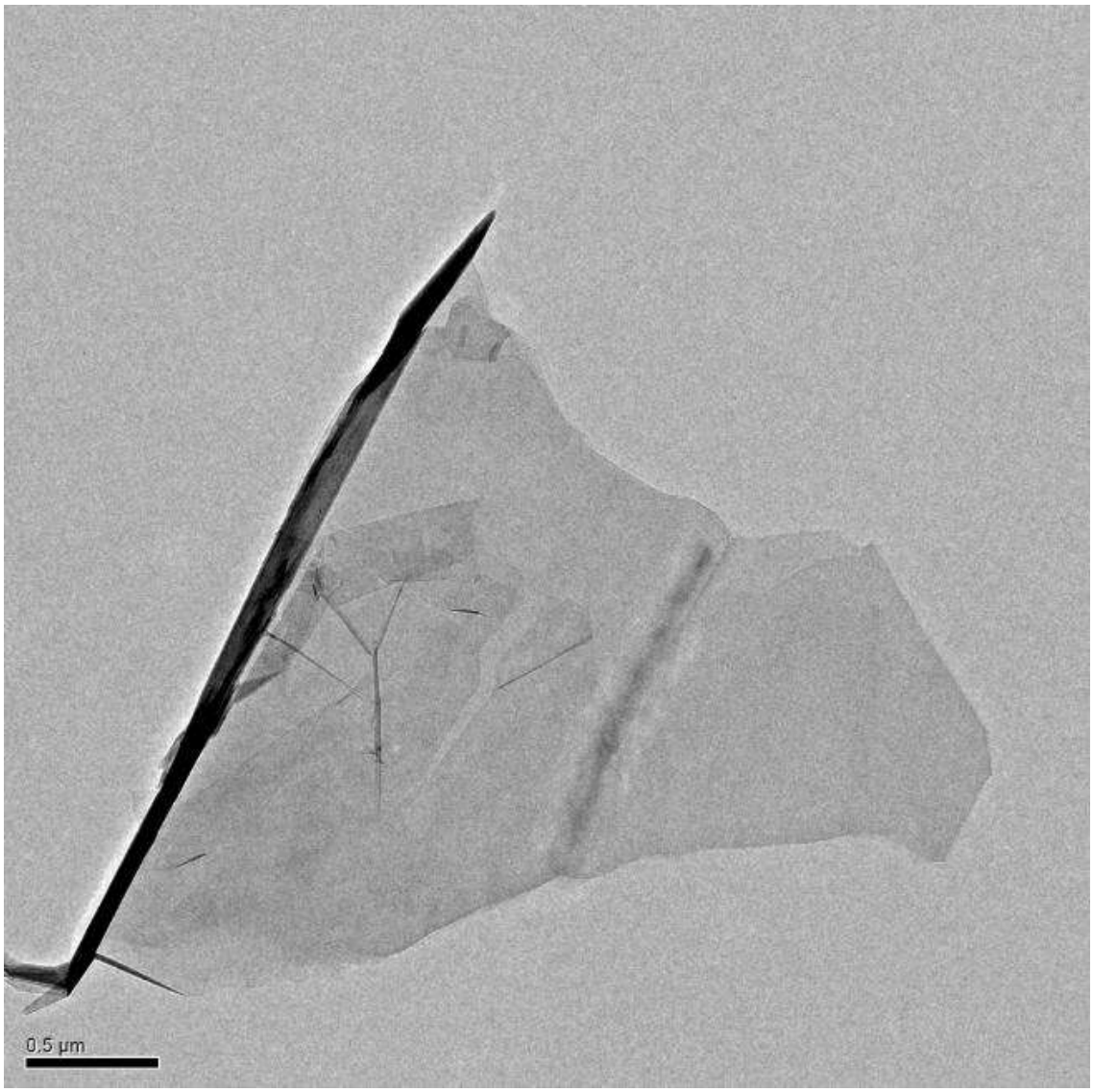

Figure 4.1 - TEM micrograph illustrating morphology of individual as-received GNPs

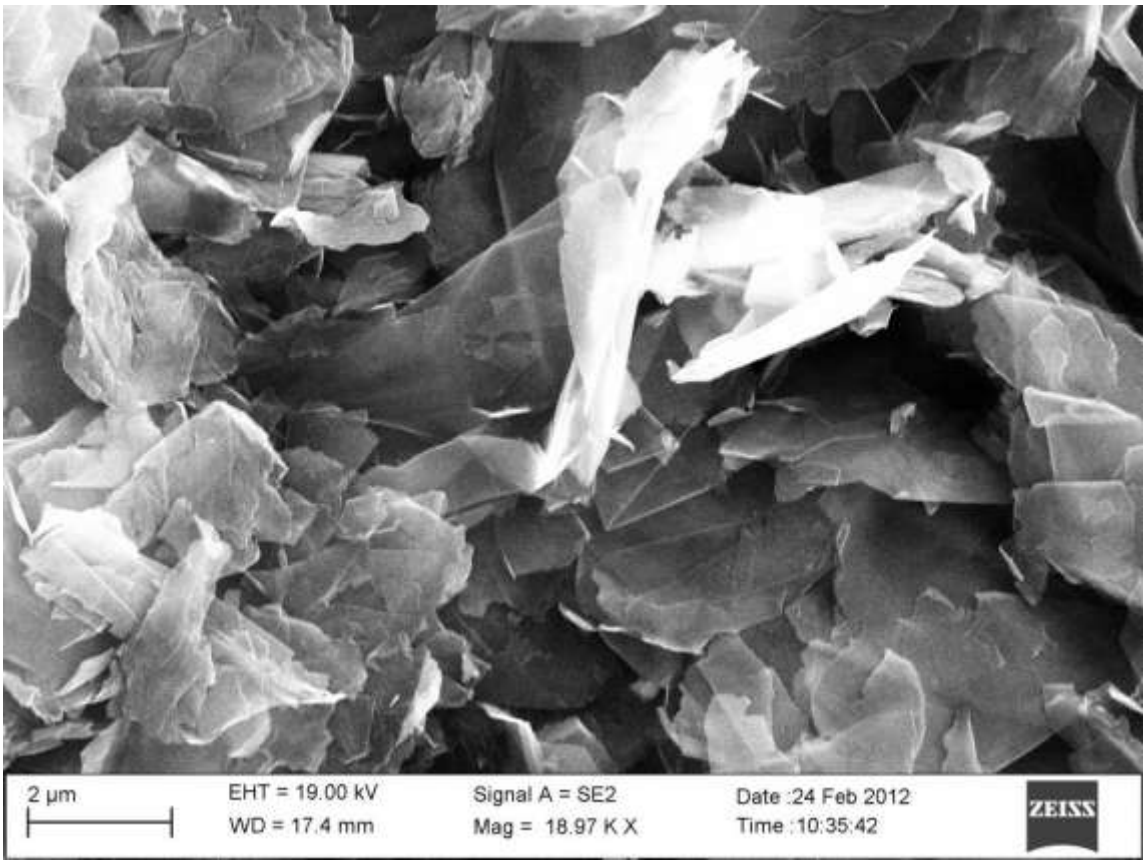

Figure 4.2 - SEM micrograph illustrating morphology of aggregates of as-received GNPs

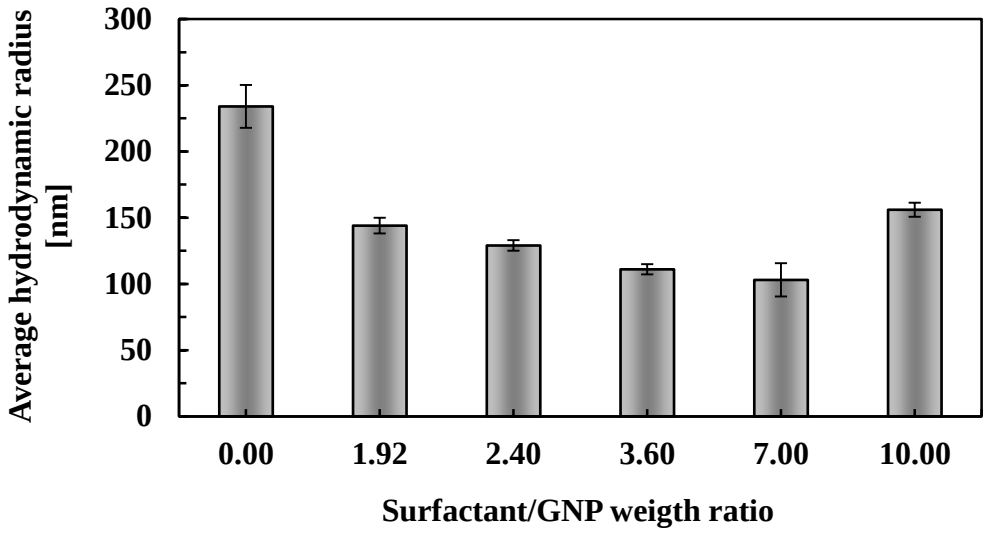

Figure 4.3 - AHR values for s-GNP aqueous suspensions containing different surfactant concentrations

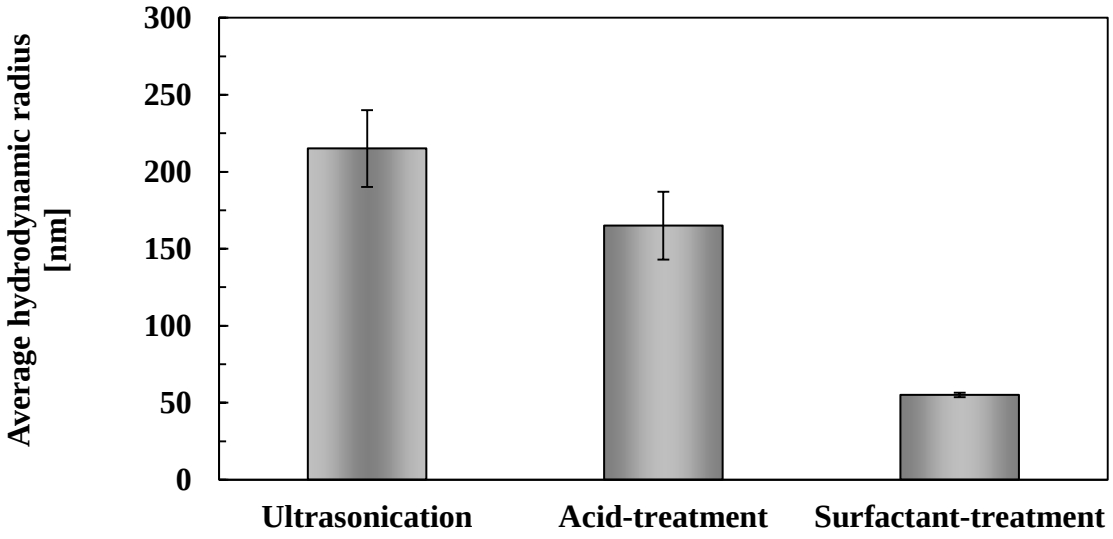

Figure 4.4 - AHR values for aqueous dispersions of u-GNPs, a-GNPs, and s-GNPs

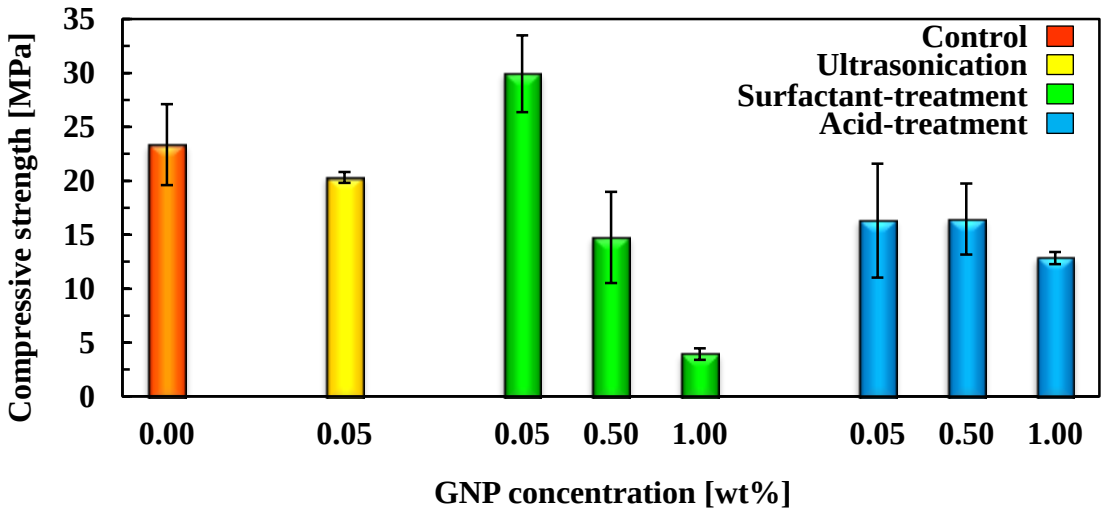

Figure 4.5 - Compression test results for unreinforced and GNP-reinforced mortar cubes

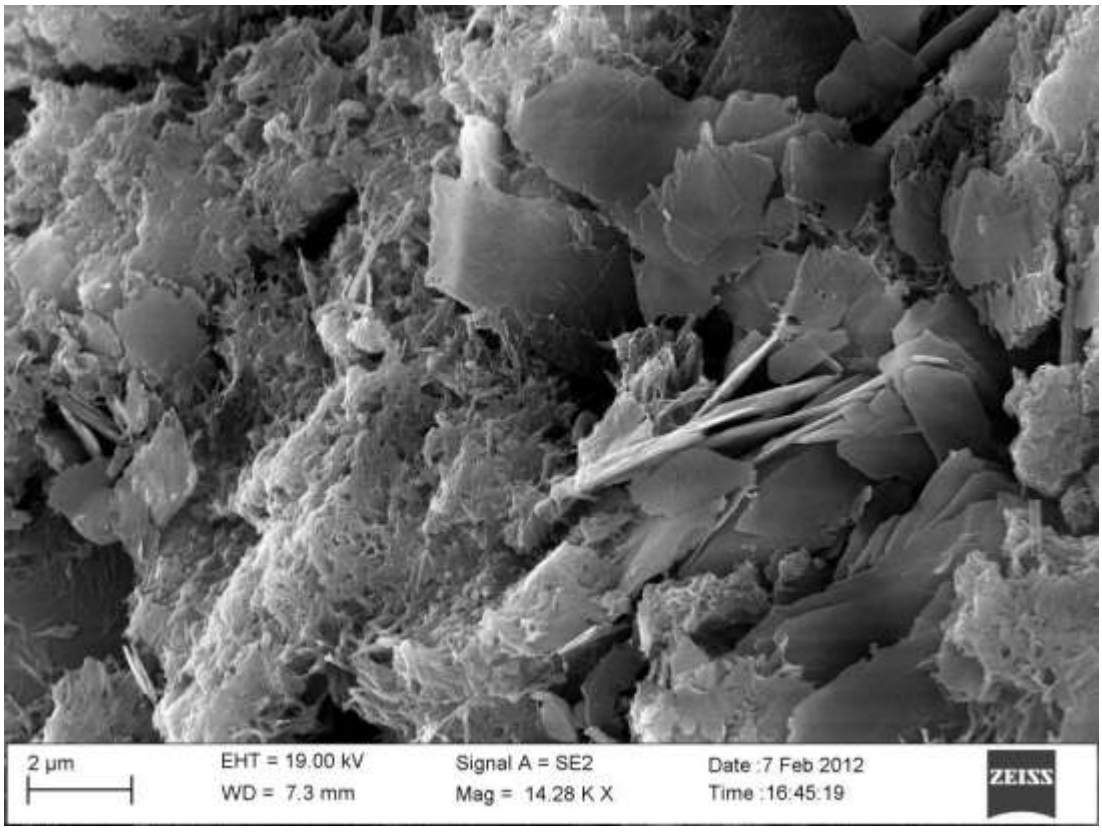

Figure 4.6 - Typical microstructure of mortar containing 0.05% u-GNP

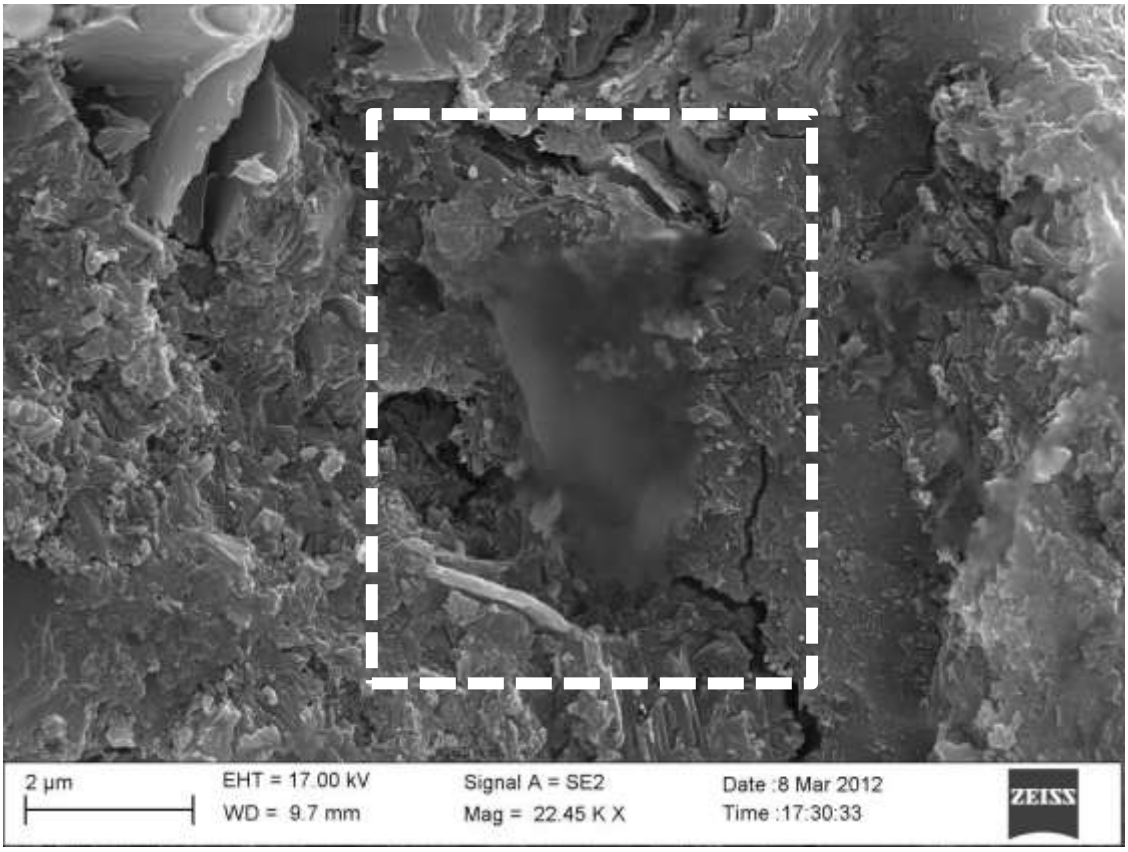

Figure 4.7 - Typical dispersion state of s-GNPs in mortar matrix at 0.05% concentration

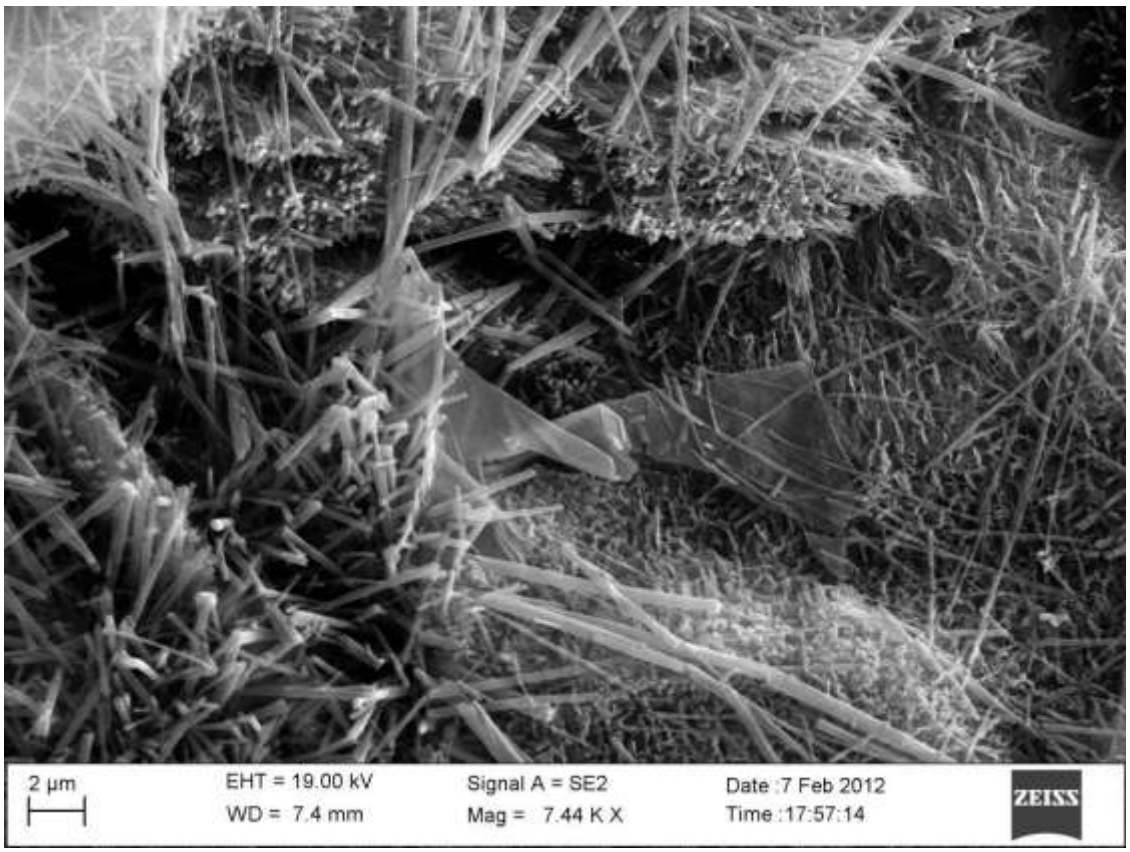

Figure 4.8 - Typical dispersion state of s-GNPs in mortar matrix at 0.5% concentration

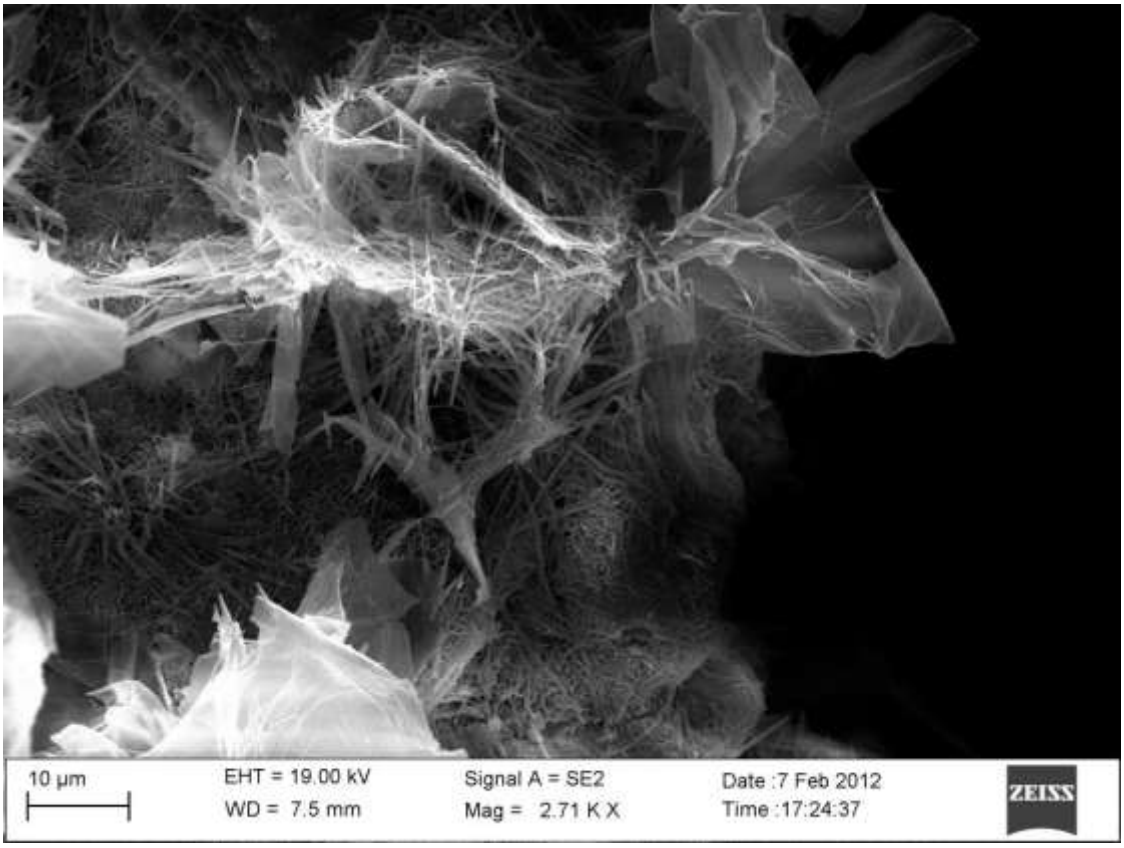

Figure 4.9 - Typical dispersion state of s-GNPs in mortar matrix at 1% concentration

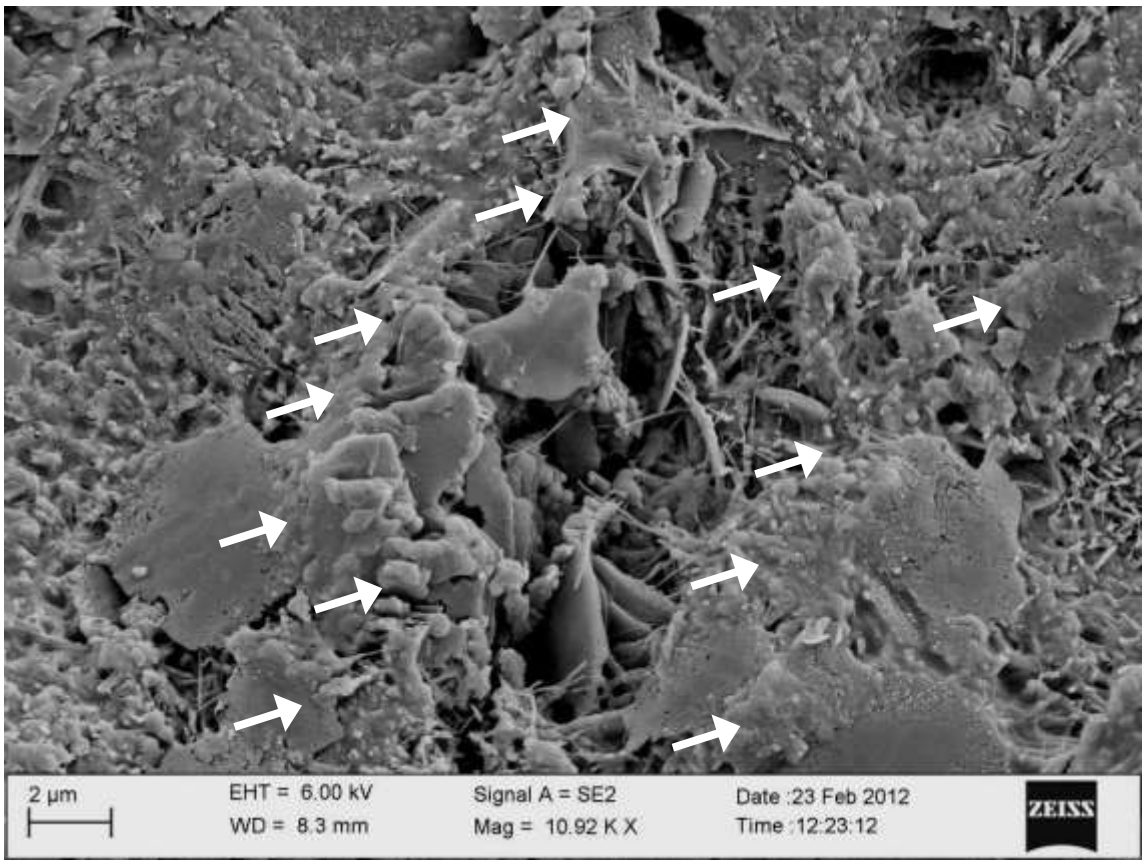

Figure 4.10 - Enhanced chemical affinity of s-GNPs and cement hydrates in microstructure of mortar containing 0.05% s-GNP; residual cement paste on s-GNP surface is marked with white arrows

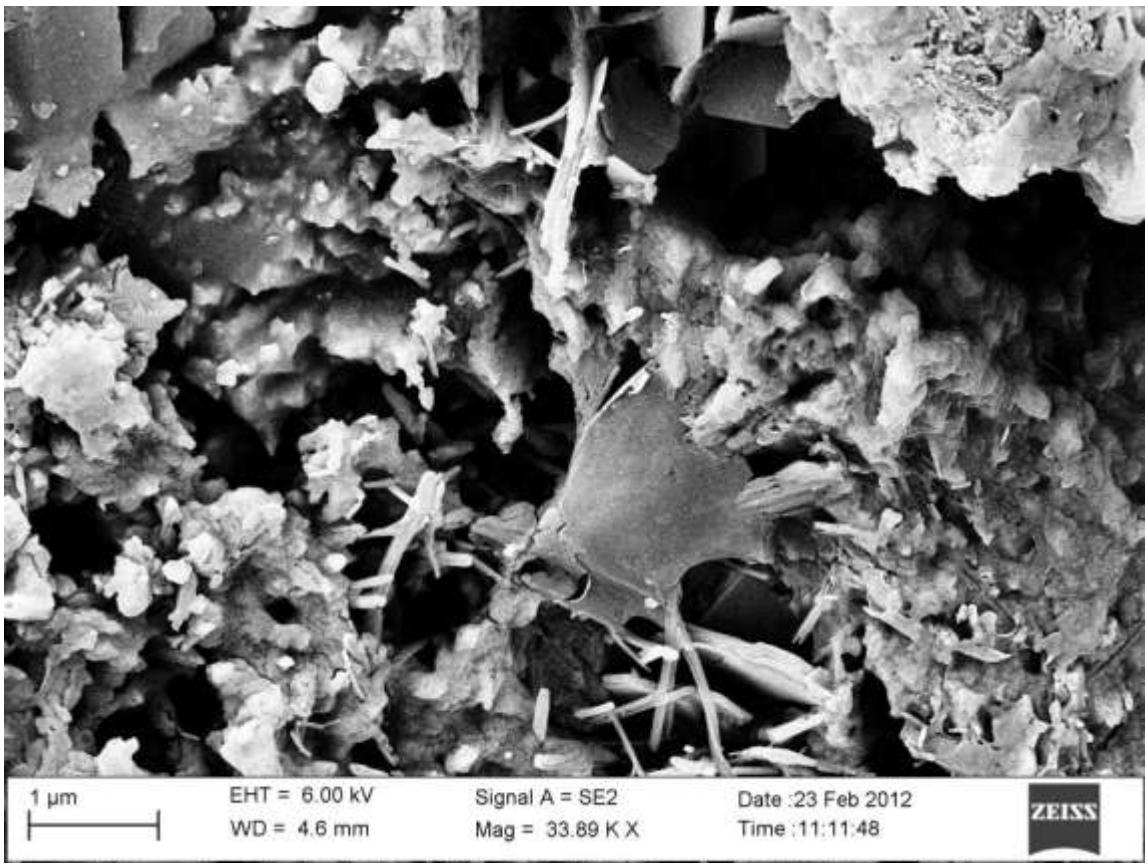

Figure 4.11 - Possible crack-bridging mechanism of well-bonded s-GNPs in mortar matrix at 0.05%

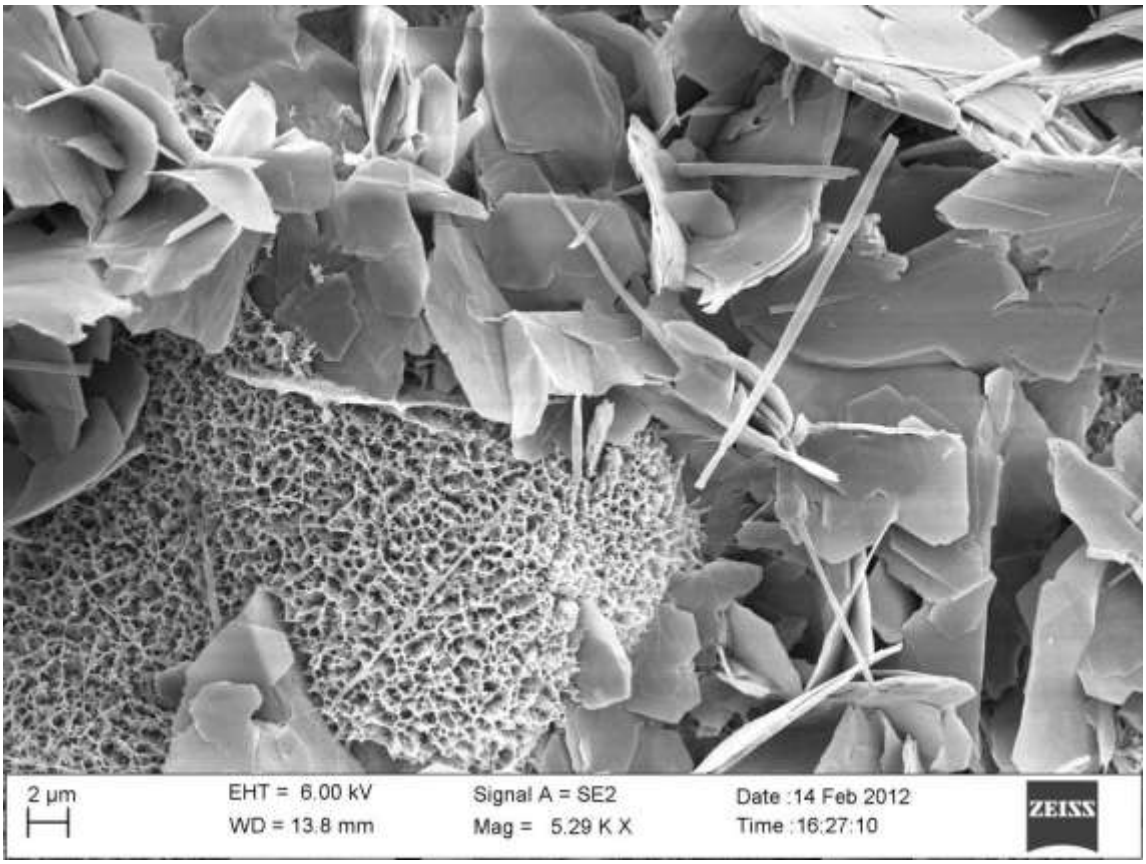

Figure 4.12 - Typical dispersion state of a-GNPs in mortar matrix at 0.05% concentration

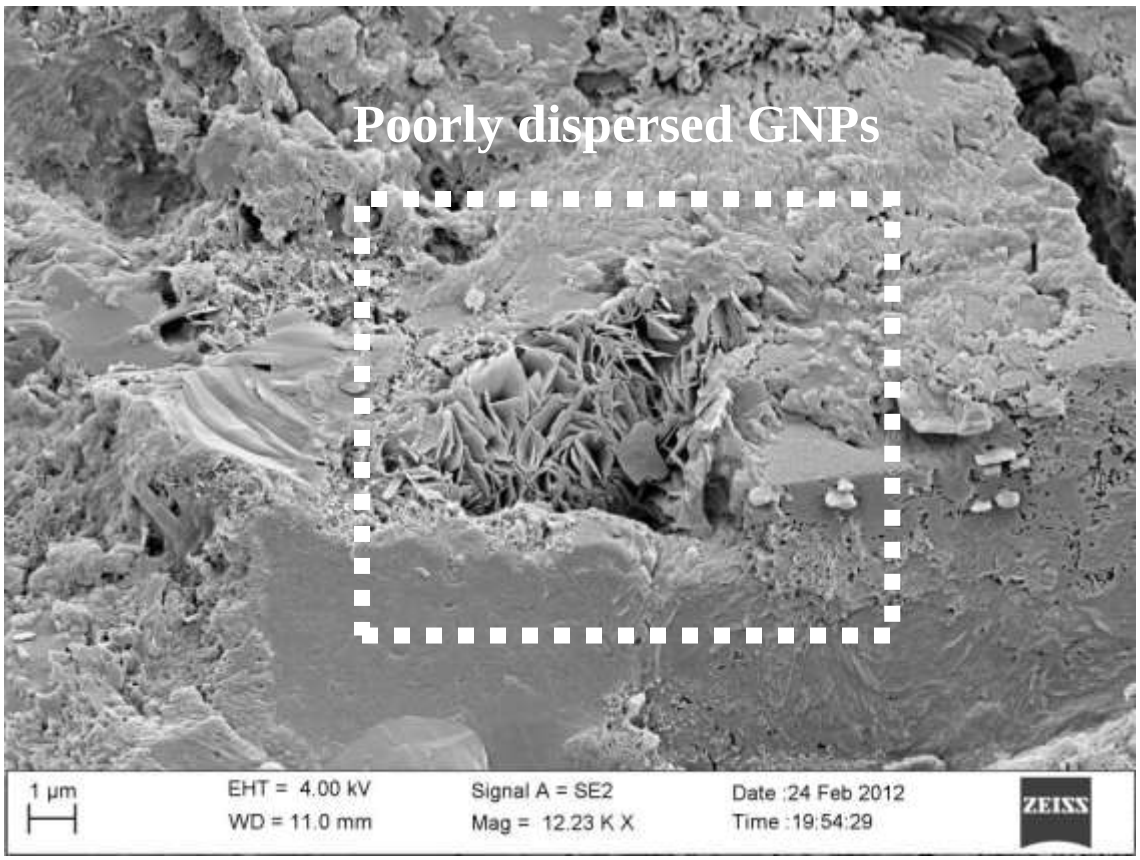

Figure 4.13 - Typical dispersion state of a-GNPs in mortar matrix at 0.5% concentration

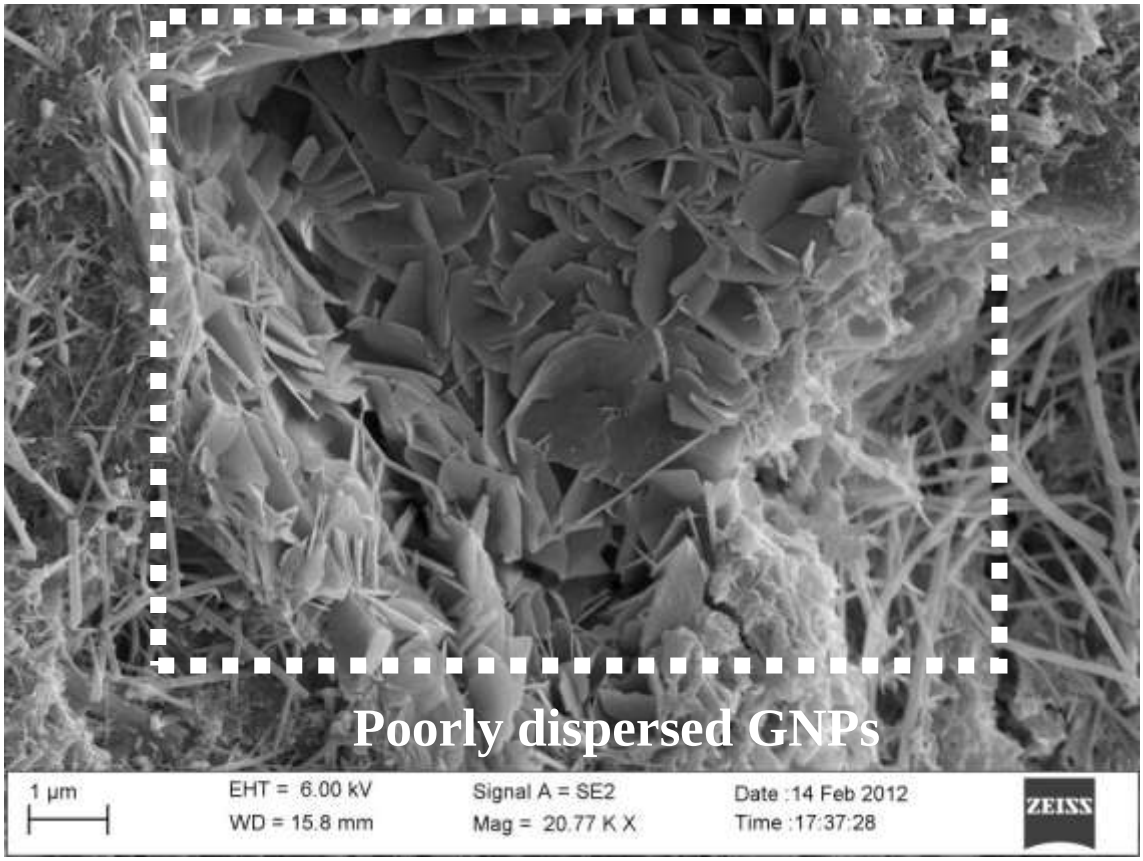

Figure 4.14 - Typical dispersion state of a-GNPs in mortar matrix at 1% concentration

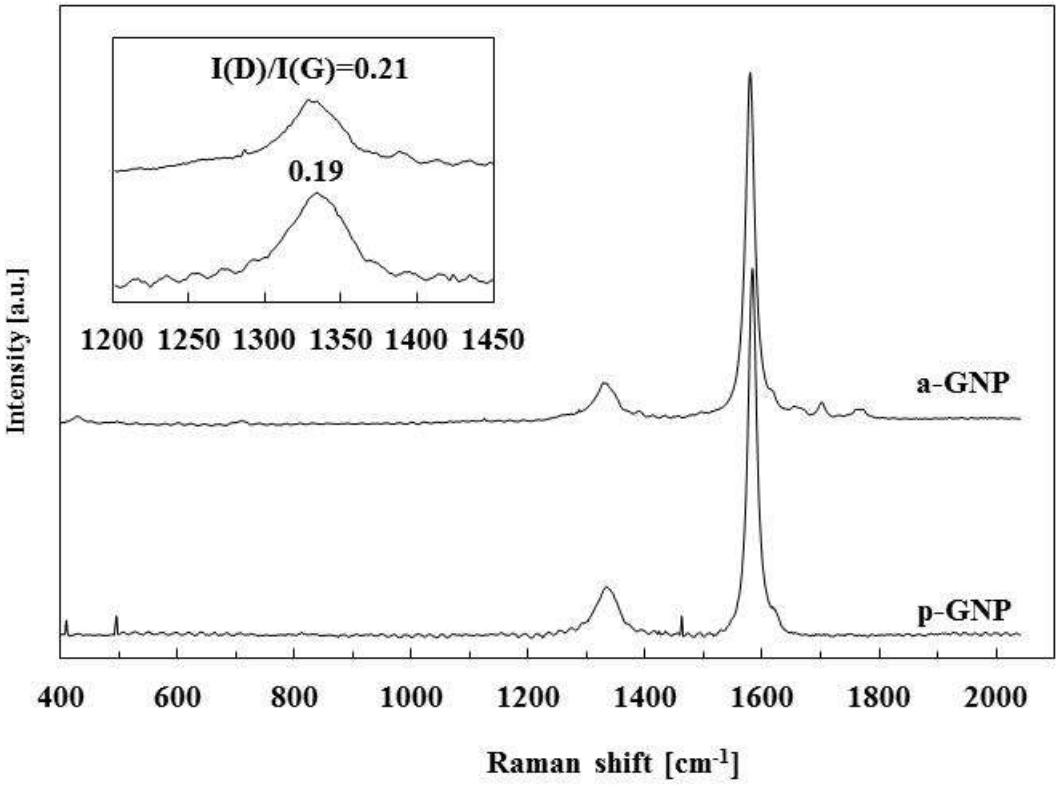

Figure 4.15 - Raman spectra for pristine and a-GNPs; inset plot compares D bands at higher magnification

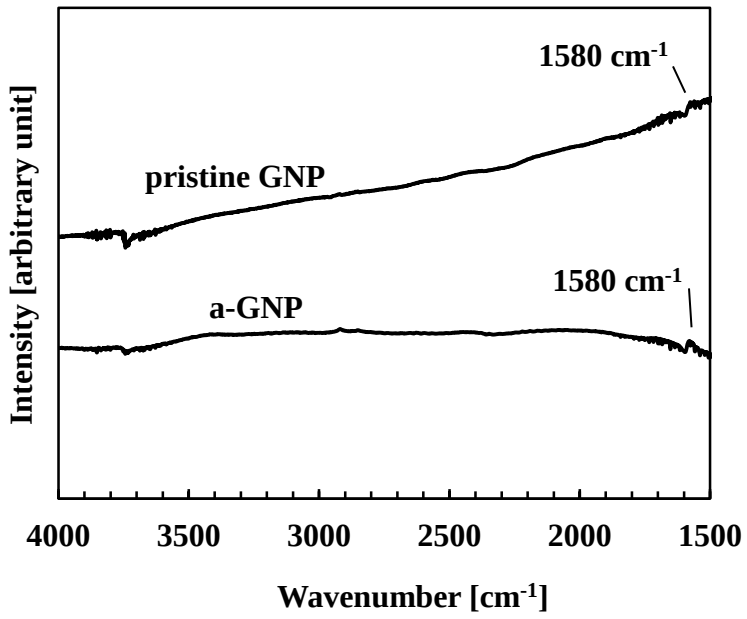

Figure 4.16 - FT-IR absorption spectra pristine and a-GNPs

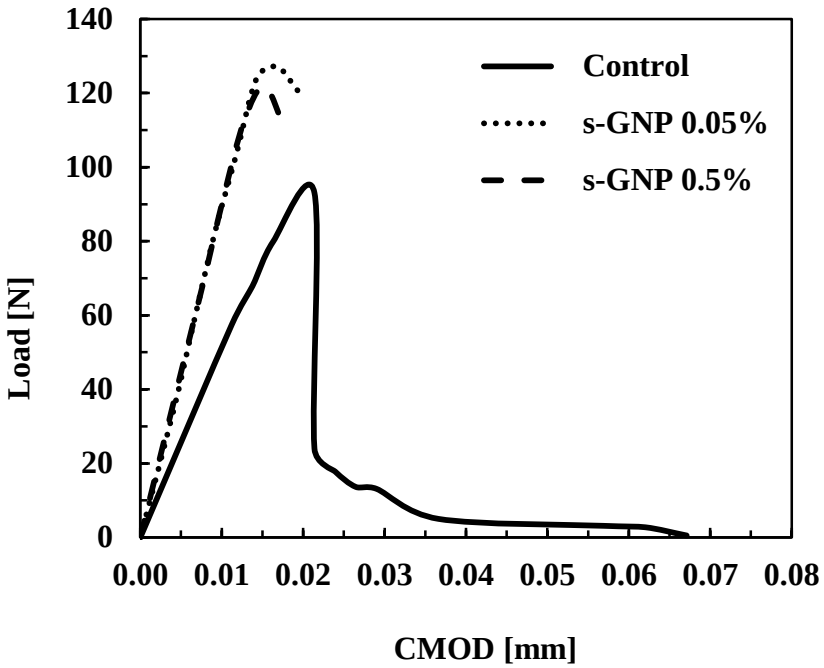

Figure 4.17 - Representative load-CMOD response curves of unreinforced and s-GNP-reinforced cement paste notched beams

CHAPTER 5

CONCLUSIONS AND RECOMMENDATION

5.1 Conclusions

This study was set out to explore the reinforcing effects of multi-walled carbon nanotubes (MWCNTs) and graphene nano-platelets (GNPs) in cement composites. The first objective was to identify a suitable functionalization technique to attain a high level of dispersion of MWCNTs and GNPs in cement mortar and paste, and improve the chemical affinity with cement hydrates. To this end, the effects of three techniques, namely, ultrasonication, acid-etching, and surfactant-coating, on selected mechanical properties and the microstructure of nanoreinforced cement composites were evaluated.

Effective acid-etching was verified using Raman spectroscopy, Fourier-transform infrared spectroscopy (FT-IR), and X-ray photoelectron spectroscopy (XPS). The MWCNT-and GNP-aqueous dispersions were assessed using dynamic light scattering (DLS) analysis, while compressive strength characterization served as an indirect measure of dispersion and chemical affinity of MWCNTs and GNPs. Dispersion and embedment of MWCNTs and GNPs in cement paste and mortar were evaluated via scanning electron microscopy (SEM) analysis of fracture surfaces. Based on the experimental evidence obtained, surfactant-coating and acid-etching were selected for MWCNTs and GNPs, respectively. Selected techniques were verified through three-point bending tests on single-edge notched beams containing acid-etching MWCNTs and surfactant-coated GNPs.

The effects of well-dispersed and well-bonded acid-etched MWCNTs on the fracture properties of cement paste were studied by means of three-point bending tests on single-

edge notched beams. Different parameters obtained from load-CMOD data were used to describe the fracture behavior of nanoreinforced beams at different stages of loading. Through DIC measurements, the morphology and evolution of the fracture process zone in MWCNT-reinforced cement paste was studied. The salient conclusions of this study are summarized as follows:

(1) Ultrasonication in absence of proper surface functionalization leads to poor dispersion of GNPs and MWCNTs in the composite matrix. Poorly dispersed GNPs and MWCNTs have poor affinity with cement paste and introduce defect sites reducing the compressive strength of mortar.

(2) Acid-etching created carboxyl (-COOH) and hydroxyl (-OH) groups on the surface of MWCNTs, which are necessary to obtain a uniform dispersion and interfacial covalent bonds. Acid-etched MWCNTs were well dispersed in cement mortar matrix irrespective of the concentration of MWCNTs in the mixture, and showed enhanced chemical affinity with cement hydrates. However, the number of MWCNT clusters increased at increasing MWCNT concentrations. The incorporation of 0.5% of acid-etched MWCNTs resulted in increased compressive strength of mortar by 41% on average. The strength data of MWCNT-reinforced mortar cubes had comparable standard deviation with respect to control (plain mortar) samples, highlighting the consistency of the results.

(3) Acid-etching was ineffective in enabling the creation of carboxyl (-COOH) and hydroxyl (-OH) functional groups on the surface of GNPs. As a result, the incorporation of acid-etched GNPs led to a poor dispersion in mortar. Acid-etched GNPs had poor chemical affinity with cement hydrates and produced defect sites, decreasing the mortar compressive strength.

(4) Surfactant-coating of MWCNTs using sodium deoxycholate (NaDC) led to their uniform dispersion at a MWCNT concentration of 0.05%. Increasing the MWCNT concentration to 0.5% and 1% resulted in reduced dispersion in mortar. It was found that in addition to the surfactant/MWCNT weight ratio, the absolute amount of surfactant introduced to the mixture plays a role on the properties of the mortar. The incorporation of excess NaDC resulted in a reduced workability of the mixture and formation of undesired crystals, reducing the compressive strength of mortar.

(5) Surfactant-coating of GNPs using NaDC led to their uniform dispersion irrespective of the GNPs concentration. However, increasing the GNPs concentration produced an increase in the number of GNP agglomerates. NaDC-coated GNPs exhibited chemical affinity with cement hydrates. The addition of 0.05% of NaDC-coated GNPs resulted in increased mortar compressive strength by 28% on average. The same GNP concentration was associated with an increase in the flexural strength and stiffness of cement paste notched beams on average by 39% and 109%, respectively.

(6) The incorporation of 0.05% and 0.5% of acid-etched MWCNTs resulted in an increase in the fracture load and elastic stiffness of cement paste notched beams on average by 37% and 24%, and 108% and 93%, respectively. The incorporation of acid-etched MWCNTs also improved the post-peak behavior of notched beams. Nanoreinforced beams had higher post-peak residual strength compared with unreinforced beams.

(7) The fracture energy was improved by adding acid-etched MWCNTs. Due to high variability observed between the nanoreinforced notched beams, the average fracture energy value did not reflect the potential effect of a-MWCNTs on the fracture energy. The incorporation of acid-etched MWCNTs resulted in a maximum increase in the fracture energy of 79% and 56% for 0.05 and 0.5% MWCNT concentrations, respectively.

(8) The fracture process zone in unreinforced (plain) cement paste notched beams consisted of areas of concentrated damage around and ahead the crack tip, with a sharp transition between the areas of larger and smaller deformation. The fracture process zone in nanoreinforced beams consisted of larger zones of distributed damage at the vicinity of the notch, with a relatively smooth transition between the areas of larger and smaller deformation, attesting to the potential of acid-etched MWCNTs to contribute to enhancing damage tolerance.

(9) SEM micrographs collected from fracture surfaces of cement paste notched beams reinforced with acid-etched MWCNTs offered visual evidence of the potential effect of MWCNTs in filling in micro- and meso-pores, and bridging across voids and (possibly) cracks.

5.2 Recommendations for future research

Our knowledge on reinforcing effects of GNPs and MWCNTs and the underlying mechanisms is still in its infancy. This study has offered an evaluative perspective on the promising potential of GNPs and MWCNTs as nanoreinforcement for cement-based composites. However, due to the scale of this subject and limitations of the adopted methodology, new research questions have been encountered in the course of this study, which need further research. Exploring the following as future research strategies can facilitate the attainment of a deeper knowledge on the reinforcing effects of GNPs and MWCNTs:

- Effects of graphitic nanoreinforcement on cement hydration: the incorporation of graphitic nanoreinforcement in cement composites was reported to yield a denser microstructure and promote formation of higher quality (i.e., denser and stiffer) cement hydrates. Further research is needed to identify the underlying mechanisms.

- Contribution of porosity reduction: the incorporation of MWCNTs can lead to a reduction and refinement of the porosity of cement paste and mortar. Porosity

reduction results in improvements in Young's modulus, compressive and flexural strength, and fracture toughness. Further research is needed to understand the contribution of porosity reduction to the mechanical performance of cement composites.

- Identification and characterization of interfacial bonding mechanisms: the type of bonds formed at the interface of cement hydrates and MWCNTs and GNPs greatly affects the physical and mechanical properties of GNP- and MWCNT-cement composites. Therefore, identifying and characterizing the interfacial bonding mechanisms is of great importance.

- Refinement of composite mixture design: the formation of strong interfacial bonds between the nanoreinforcement and cement hydrates is a key attribute of MWCNT- and GNP-cement nanocomposites. Reducing the water/cement (w/c) ratio may contribute to decreasing the pore volume and facilitate interfacial bonding. Superplasticizers may be used to ensure workability.

- Stability measurement of aqueous dispersions: the colloidal stability of GNP- and MWCNT-aqueous dispersions can play a significant role on the dispersion of GNPs and MWCNTs in cement matrix. Further research is needed to understand the relationship between stability of the aqueous dispersions and dispersion of nanoreinforcement in hardened cement composites.

REFERENCES

Aich N., Zohhadi N., Khan I.A., Matta F., Ziehl P., and Saleh N.B., Applied TEM approach for micro/nanostructural characterization of carbon nanotube reinforced cementitious composites. Journal of Research Updates in Polymer Science 2012: 1: 14-23.

Banthia N., and J. Sheng. Fracture toughness of micro-fiber reinforced cement composites. Cement and Concrete Comp 1996: 18(4): 251-269.

Bentur A., and Mindess S., Fibre reinforced cementitious composites. CRC Press, 2006.

Brandt A.M., Fibre reinforced cement-based (FRC) composites after over 40 years of development in building and civil engineering. Compos Struct 2008: 86(1): 3-9.

Collins F., Lambert J., and Duan W.H., The influences of admixtures on the dispersion, workability, and strength of carbon nanotube–OPC paste mixtures. Cement Concrete Comp 2012: 34(2): 201-207.

Cwirzen A., Habermehl-Cwirzen K., and Penttala V., Surface decoration of carbon MWCNTs and mechanical properties of cement/carbon nanotube composites. Adv Cem Res 2008: 20(2): 65-73.

Cwirzen A., Habermehl-Cwirzen K., Nasibulin A.G., Kaupinen E.I., Mudimela P.R., and Penttala V., SEM/AFM studies of cementitious binder modified by MWCNT and nano-sized Fe needles. Mater Charact 2009: 60(7): 735-740.

Datsyuk V., Kalyva M., Papagelis K., Parthenios J., Tasis D., Siokou A., Kallitsis I., and Galiotis C., Chemical oxidation of multi-walled carbon MWCNTs. Carbon 2008: 46(6): 833-840.

Hilding J., Grulke E.A., Zhang Z.G., and Lockwood F. Dispersion of carbon MWCNTs in liquids. J Disper Sci Technol 2003: 24(1): 1-41.

Ishibashi A., and Nakashima N., Individual Dissolution of Single-Walled Carbon Nanotubes in Aqueous Solutions of Steroid or Sugar Compounds and Their Raman and Near-IR Spectral Properties. Chem-Eur J 2006: 12(29): 7595-7602.

Islam M.F., Rojas E., Bergey D.M., Johnson A.T., and Yodh A.G., High weight fraction surfactant solubilization of single-wall carbon MWCNTs in water. Nano Lett 2003: 3(2): 269-273.

Khan I.A., Afrooz A.N., Flora J.R.V., Schierz P.A., Ferguson P.L., Sabo-Attwood T., and Saleh N.B., "Chirality affects aggregation kinetics of single-walled carbon nanotubes. Environ Sci Technol 2013: 47(4): 1844-1852.

Konsta-Gdoutos M.S, Metaxa Z.S., and Shah S.P., Multi-scale mechanical and fracture characteristics and early-age strain capacity of high performance carbon nanotube/cement nanocomposites. Cement and Concrete Comp 2010: 32(2): 110-115.

Konsta-Gdoutos M.S., Metaxa Z.S., and Shah S.P., Highly dispersed carbon nanotube reinforced cement based materials. Cement Concrete Res 2010: 40(7): 1052-1059.

Kuilla T., Bhadra S., Yao D., Kim N.H., Bose S., and Lee J.H., Recent advances in graphene based polymer composites. Prog Polym Sci 2010: 35(11): 1350-1375.

Lee C., Wei X., Kysar J.W., and Hone J., Measurement of the elastic properties and intrinsic strength of monolayer graphene, SCIENCE 2008: 321: 385-388.

Li D., Müller M.B., Gilje S., Kaner R.B., and. Wallace G.G, Processable aqueous dispersions of graphene nanosheets, Nat Nanotechnol 2008: 3: 101-105.

Li G.Y., Wang P.M., and Zhao X., Mechanical behavior and microstructure of cement composites incorporating surface-treated multi-walled carbon MWCNTs. Carbon 2005: 43(6): 1239-1245.

Luo J., Duan Z., and Li H., The influence of surfactants on the processing of multi-walled carbon MWCNTs in reinforced cement matrix composites. Phys Status Solidi (a) 2009: 206(12): 2783-2790.

Luo J.L., Duan Z., Xian G., Li Q., and Zhao T., Fabrication and fracture toughness properties of carbon nanotube-reinforced cement composite. Eur Phys J Appl Phys 2011: 53: 30402.

Lv S., Ma Y., Qiu C., Sun T., Liu J., and Zhou Q., Effect of graphene oxide nanosheets of microstructure and mechanical properties of cement composites, Const Build Mats 2013: 49: 121-127.

MacGregor B., Grierson J., Wight J.K., Teng S., and Irawan P.. Reinforced concrete: mechanics and design. Vol.3. Upper Saddle River, NJ: Prentice Hall, 1997.

Makar J.M., and Beaudoin J.J., Carbon MWCNTs and their application in the construction industry. Special Publication-Royal Society of Chemistry 2004: 292: 331-342.

Manzur T., and Yazdani N., Strength Enhancement of Cement Mortar with Carbon MWCNTs. Transp Res Record: Journal of the Transportation Research Board 2010; 2142(1): 102-108.

Mehta P.K., and Monteiro P.J.M., Concrete: microstructure, properties, and materials. Vol.3. New York: McGraw-Hill, 2006.

Mi Y., Zhang X., Zhou S., Cheng J., Liu F., Zhu H., Dong X., and Jiao Z., Morphological and mechanical properties of bile salt modified multi-walled carbon nanotube/poly (vinyl alcohol) nanocomposites. Compos Part A-Appl S 2007: 38(9): 2041-2046.

Morsy M.S., Alsayed S.H., and Aqel M., Hybrid effect of carbon nanotube and nano-clay on physico-mechanical properties of cement mortar. Constr Build Mater 2011: 25(1): 145-149.

Musso S., Tulliani J.M., Ferro G., and Tagliaferro A., Influence of carbon MWCNTs structure on the mechanical behavior of cement composites. Compos Sci Technol 2009: 69(11): 1985-1990.

Nagasawa S., Yudasaka M., Hirahara K., Ichihashi T., and Iijima S., Effect of oxidation on single-wall carbon MWCNTs. Chem Phys Lett 2000: 328(4): 374-380.

Nasibulina L.I., Anoshkin I.V., Nasibulin A.G., Cwirzen A., Penttala V., and Kauppinen E.I., Effect of carbon nanotube aqueous dispersion quality on mechanical properties of cement composite. J Nanomater 2012; 169262.

Nochaiya T., and Chaipanich A., Behavior of multi-walled carbon MWCNTs on the porosity and microstructure of cement-based materials. Appl Surf Sc 2011: 257(6): 1941-1945.

Nochaiya T., Tolkidtikul P., Singjai P., and Chaipanich A., Microstructure and characterizations of Portland-carbon MWCNTs pastes. Adv Mat Res 2008: 55: 549-552.

Parveen S., Rana S., and Fangueiro R., A review on nanomaterial dispersion, microstructure and mechanical properties of carbon nanotube and nanofiber reinforced cementitious composites, J. Nanomater. 2013: 80.

Raki L., Beaudoin J., Alizadeh R., Makar J., and Sato T., Cement and concrete nanoscience and nanotechnology. Materials 2010: 3(2): 918-942.

Rastogi R., Kaushal R., Tripathi S.K., Sharma A.L., Kaur I., and Bharadwaj L.M., Comparative study of carbon nanotube dispersion using surfactants. J Colloid Interf Sci 2008: 328(2): 421-428.

Saez de Ibarra Y., Gaitero J.J., Erkizia E., and Campillo I., Atomic force microscopy and nanoindentation of cement pastes with nanotube dispersions, Phys. Status Solidi (a) 2006: 203: 1076-1081.

Saleh N.B., Pfefferle L.D., and Elimelech M., Aggregation kinetics of multiwalled carbon nanotubes in aquatic systems: measurements and environmental implications, Environ Sci Technol 2008: 42(21): 7963-7969.

Saleh N.B., Pfefferle L.D., and Elimelech M., Influence of biomacromolecules and humic acid on the aggregation kinetics of single-walled carbon nanotubes. Environ Sci Technol 2010: 44(7), 2412-2418.

Sanchez F., and Sobolev K., Nanotechnology in concrete – A review, Constr Build Mater 2010: 24: 2060-2071.

Sedaghat A., Ram M.K., Zayed A., Kamal R., and Shanahan N., Investigation of physical properties of graphene-cement composite for structural applications, Open J Comp Mats 2014: 4:12-21.

Sobolkina A., Mechtcherine V., Khavrus V., Maier D., Mende M., Ritschel M., and Leonhardt A., Dispersion of carbon MWCNTs and its influence on the mechanical properties of the cement matrix. Cement Concrete Comp 2012: 34:1104-1113.

Sobolkina A., Mechtcherine V., Khavrus V., Maier D., Mende M., Ritschel M., and Leonhardt A., Dispersion of carbon MWCNTs and its influence on the mechanical properties of the cement matrix. Cement Concrete Comp 2012: 34:1104-1113.

Stankovich S., Dikin D.A., Dommett G.H.B., Kohlhaas K.M., Zimney E.J., Stach E.A., Piner R.D., Nguyen S.T., and Ruoff R.S., Graphene-based composite materials. Nature 2006: 442(7100): 282-286.

Strano M.S., Moore V.C., Miller M.K., Allen M.J., Haroz E.H., Kittrell C., Hauge R.H., and Smalley R.E., The role of surfactant adsorption during ultrasonication in the dispersion of single-walled carbon MWCNTs. J Nanosci Nanotechno 2003: 3(1-2): 81-86.

Thostenson E.T., Ren Z., and Chou T.W., Advances in the science and technology of carbon MWCNTs and their composites: a review. Compos Sci Technol 2001: 61(13): 1899-1912.

Tyson B.M., Abu Al-Rub R.K., Yazdanbakhsh A., and Grasley Z., Carbon MWCNTs and carbon nanofibers for enhancing the mechanical properties of nanocomposite cementitious materials. J Mater Civil Eng 2011: 23(7): 1028-1035.

Vaisman L., Wagner H.D., and Marom G., The role of surfactants in dispersion of carbon MWCNTs. Adv Colloid Interfac 2006: 128: 37-46.

Wang B., Han Y., and Liu S., Effect of highly dispersed carbon MWCNTs on the flexural toughness of cement-based composites. Constr Build Mater 2013: 42: 8-12.

Wang Y., Wu J., and Wei F., A treatment method to give separated multi-walled carbon MWCNTs with high purity, high crystallization and a large aspect ratio. Carbon 2003: 41(15): 2939-2948.

Yang Y., Grulke A., Zhang G.Z., Wu G., Thermal and rheologic al properties of carbon nanotube-in-oil dispersions, J Appl Phys 2006: 99(11): 114307.

Zaib Q., Khan I.A., Yoon Y., Flora J.R.V., Park Y.G., and Saleh N.B., Ultrasonication study for suspending single-walled carbon nanotubes in water, J Nanosci Nanotechno 2012: 12(5): 3909-3917.

Zollo R.F., Fiber-reinforced concrete: an overview after 30 years of development. Cement and Concrete Comp 1997: 19(2): 107-122

APPENDIX A

SUPPORTING MATERIAL FOR CHAPTER 2

Table A.1 – Specifications of as-received MWCNTs (reported by the manufacturer)

Outside diameter	Inside diameter	Specific surface area	Length	Purity
< 8 nm	2 – 5 nm	500 m^2/g	10 – 30 μm	> 95 wt. *%

* By the weight of carbon.

Table A.2 - Compression test results for all specimens of different groups with different surfactant amount

SAA amount [g]	Compressive strength [MPa]
0.0	45.04
0.0	44.91
0.0	46.93
0.0	45.13
2.5	30.21
2.5	25.14
2.5	31.33
2.5	30.17
25.0	21.59
25.0	21.60
25.0	23.67
25.0	24.13
50.0	16.36
50.0	14.04
50.0	16.32
50.0	18.80

Table A.3 - Compression test results for all specimens of different groups

Specimen	Compressive strength [MPa]
Control	35.59
Control	33.52
Control	29.83
Control	27.24
u-MWCNT-0.05%	19.38
u-MWCNT-0.05%	20.18
u-MWCNT-0.05%	27.69
a-MWCNT-0.05%	39.91
a-MWCNT-0.05%	38.71
a-MWCNT-0.05%	38.85
a-MWCNT-0.5%	48.95
a-MWCNT-0.5%	45.14
a-MWCNT-0.5%	39.17
a-MWCNT-1%	39.20
a-MWCNT-1%	39.75
a-MWCNT-1%	42.54
s-MWCNT-0.05%	27.31
s-MWCNT-0.05%	24.33
s-MWCNT-0.05%	23.07
s-MWCNT-0.5%	14.76
s-MWCNT-0.5%	11.31
s-MWCNT-0.5%	13.97
s-MWCNT-1%	8.35
s-MWCNT-1%	7.03
s-MWCNT-1%	8.19

APPENDIX B

SUPPORTING MATERIAL FOR CHAPTER 3

Table B.1 - Fracture mechanics properties for all specimens of different groups

Specimen	Fracture load [N]	Stiffness [N/mm]	P_{non} [N]	$CMOD_{non-linear}$ [mm]	$CMOD_{rupture}$ [mm]
Control	98.61	4830	84.56	0.018	0.059
Control	93.06	5761	79.85	0.016	0.067
Control	97.80	5836	90.33	0.019	0.085
a-MWCNT-0.05%	111.47	9215	70.28	0.008	0.018
a-MWCNT-0.05%	146.20	8296	131.88	0.016	0.035
a-MWCNT-0.05%	108.79	11295	101.31	0.010	0.038
a-MWCNT-0.05%	155.29	12484	134.28	0.011	0.017
a-MWCNT-0.05%	140.98	15530	120.20	0.008	0.012
a-MWCNT-0.5%	125.33	11142	113.70	0.012	0.070
a-MWCNT-0.5%	104.62	8545	94.08	0.012	0.067
a-MWCNT-0.5%	123.30	8052	114.26	0.015	0.019
a-MWCNT-0.5%	125.57	10236	110.62	0.011	0.015
a-MWCNT-0.5%	117.62	14973	84.20	0.006	0.010

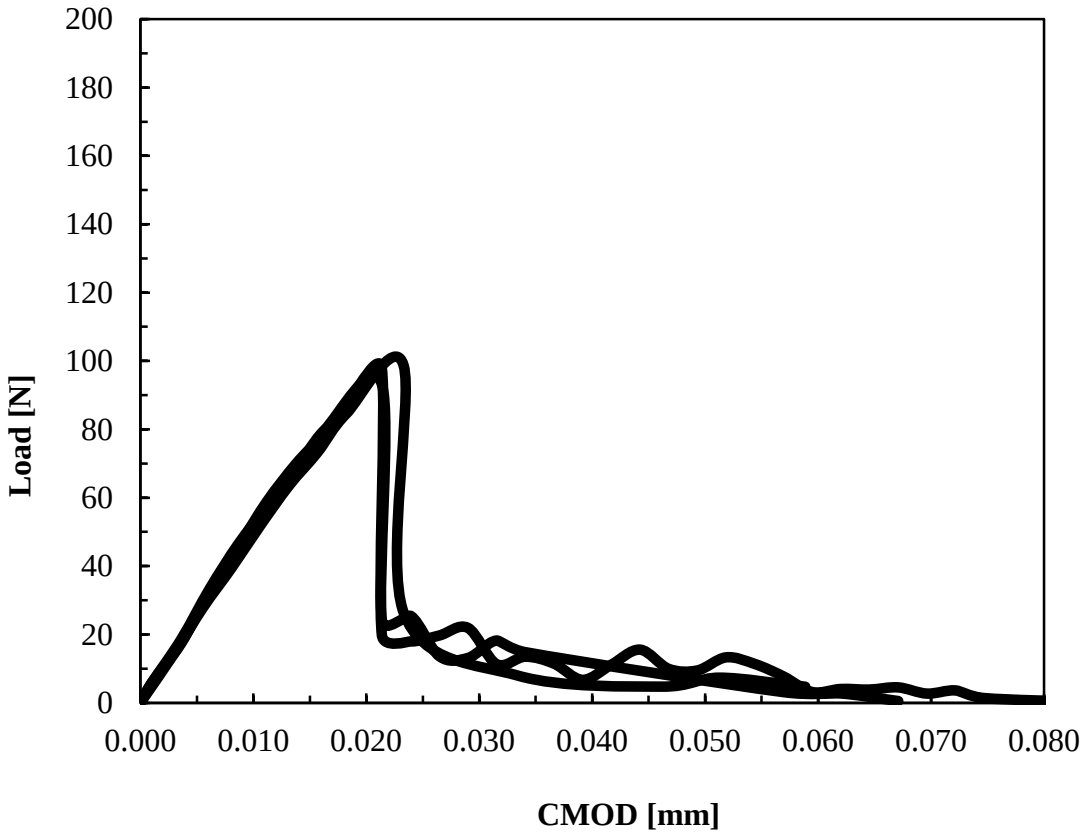

Figure B.1 - Load-CMOD response curves of unreinforced notched beams

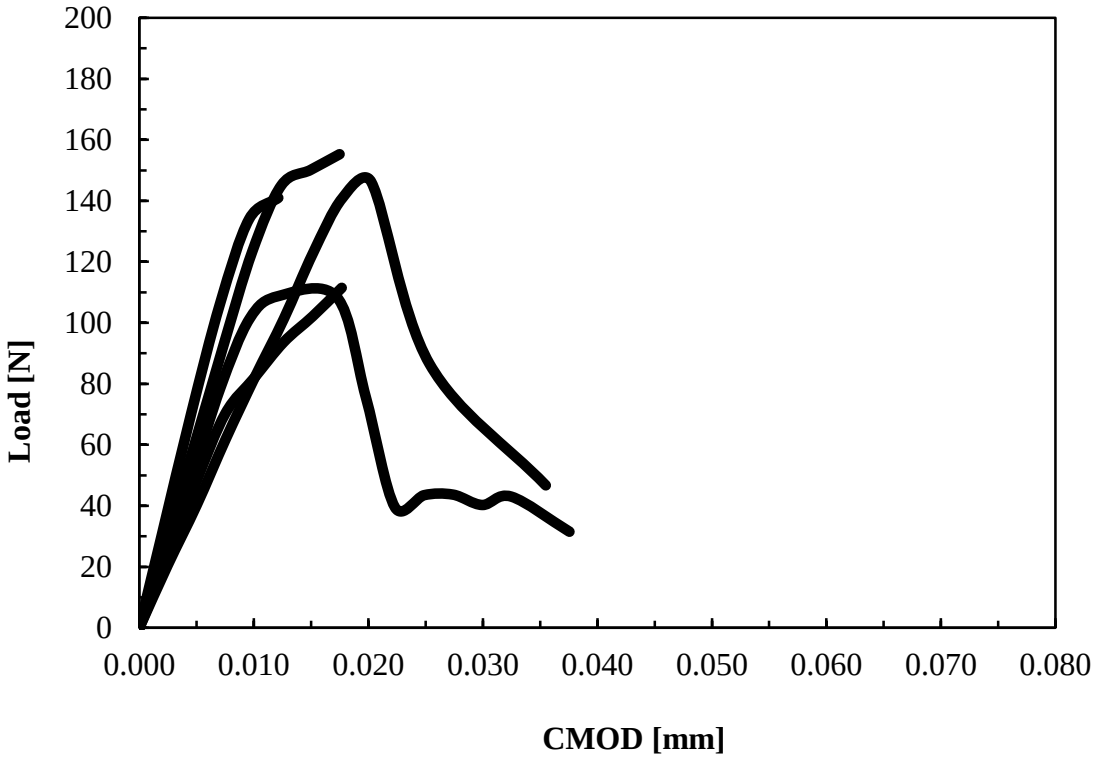

Figure B.2 - Load-CMOD response curves of a-MWCNT-reinforced notched beams at 0.05% a-MWCNTs concentration

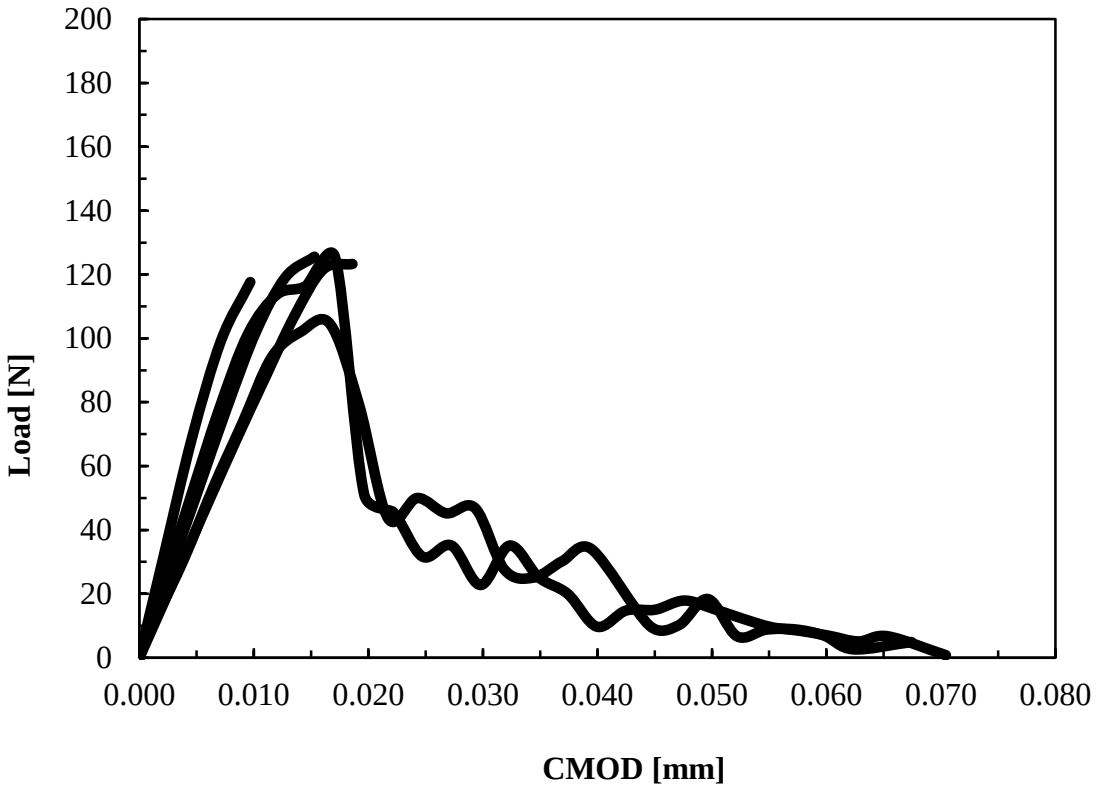

Figure B.3 - Load-CMOD response curves of a-MWCNT-reinforced notched beams at 0.5% a-MWCNTs concentration

APPENDIX C

SUPPORTING MATERIAL FOR CHAPTER 4

Table C.1 - Specifications of as-received GNPs (reported by the manufacturer)

Average flake thickness	Average particle size	Average particle lateral size	Specific surface area	Purity
8 nm	550 nm	150 – 3000 nm	100 m^2/g	99.9 wt.*%

* By the weight of carbon.

Table C.2 - Compression test results for all specimens of different groups

Specimen	Compressive strength [MPa]
Control	18.16
Control	27.37
Control	21.02
Control	26.10
Control	24.07
u-GNP-0.05%	20.26
u-GNP-0.05%	20.85
u-GNP-0.05%	19.82
s-GNP-0.05%	25.89
s-GNP-0.05%	32.58
s-GNP-0.05%	31.31
s-GNP-0.5%	10.52
s-GNP-0.5%	14.72
s-GNP-0.5%	18.98
s-GNP-1%	4.47
s-GNP-1%	3.92
s-GNP-1%	3.41
a-GNP-0.05%	21.15
a-GNP-0.05%	17.09
a-GNP-0.05%	10.68
a-GNP-0.5%	16.01
a-GNP-0.5%	19.94
a-GNP-0.5%	13.39
a-GNP-1%	12.78
a-GNP-1%	13.44
a-GNP-1%	12.29

Table C.3 - Notched beam test results for all specimens of different groups

Specimen	Fracture load [N]	Stiffness [N/mm]
Control	107.04	4830
Control	113.18	5761
Control	112.36	5836
s-GNP-0.05%	140.37	9496
s-GNP-0.05%	155.64	14309
s-GNP-0.05%	165.35	10557
s-GNP-0.5%	123.00	9990
s-GNP-0.5%	134.41	10678
s-GNP-0.5%	141.57	9093